A Control Systems Perspective to Condition Monitoring and Fault Diagnosis

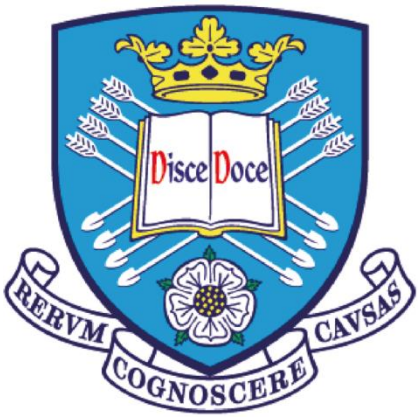

Shenal Rajintha Alexander Samarathunge Gunawardena

Department of Automatic Control and Systems Engineering

The University of Sheffield

Thesis submitted for the degree of MPhil

14/07/2018

Acknowledgements

To God our Father, Jesus our Saviour and Holy Spirit our Redeemer.

To my parents, friends and my supervisor

Abstract

Modern industrial processors, engineering systems and structures, have grown significantly in complexity and in scale during the recent years. Therefore, there is an increase in the demand for automatic processors, to avoid faults and severe break downs, through predictive maintenance. In this context, the research into nonlinear systems analysis has attained much interest in recent years as linear models cannot be used to represent some of these systems. In the field of control systems, the analysis of such systems is conducted in the frequency domain using methods of Frequency Response Analysis. Generalised Frequency Response Functions (GFRFs) and the Nonlinear Output Frequency Response Functions (NOFRFs) are Frequency Response Analysis techniques used for the analysis of nonlinear dynamical behaviour in the frequency domain. The problem of Condition Monitoring and Fault Diagnosis has been investigated in the perspective of modelling, signal processing and multivariate statistical analysis, data-driven methods such as neural networks have gained significant popularity. This is because possible faulty conditions related to complex systems are often difficult to interpret. In such a background, recently, a new data-driven approach based on a systems perspective has been proposed. This approach uses a controls systems analysis method of System Identification and Frequency Response Analysis and has been shown before as a potential technique. However, this approach has certain practical concerns regarding real-world applications. Motivated by these concerns in this thesis, the following contributions are put forward:

1. The method of evaluating NOFRFs, using input-output data of a nonlinear system may experience numerical errors. This is a major concern, hence the development of a method to overcome these numerical issues effectively.

2. Frequency Response Analysis cannot be used in its current state for nonlinear systems that exhibit severe nonlinear behaviour. Although theoretically, it has been argued that this is possible, even though, it has been impossible in a practical point of view. Therefore, the possibility and the manner in which Frequency Response Analysis can be conducted for these types of systems is presented.

3. Development of a System Identification methodology to overcome the issues of inadequately exciting inputs and appropriately capturing system dynamics under general circumstances of Condition Monitoring and Fault Diagnosis.

In addition to the above, the novel implementation of a control systems analysis approach is implemented in characterising corrosion, crack depth and crack length on metal samples. The approach is applied to the data collected, using a newly proposed non-invasive Structural Health Monitoring method called RFID (Radio Frequency IDentification) wireless eddy current probing. The control systems analysis approach along with the RFID wireless eddy current probing method shows the clear potential of being a new technology in non-invasive Structural Health Monitoring systems.

Contents

Abbreviations ..... **iv**

Nomenclature ..... **vi**

Chapter 1 Introduction **8**

1.1 Background 8

1.2 Motivation 9

1.3 Aims and objectives 11

1.4 Thesis overview 12

1.5 Summary of contributions and research outputs 13

Chapter 2 Condition Monitoring and Fault Diagnosis – Brief Overview and a Control Systems Approach **15**

2.1 Introduction 15

2.2 A brief overview of Fault Diagnosis, isolation and condition monitoring 16

2.3 Outline of different types of Condition Monitoring and Fault Diagnosis schemes 18

2.4 A control systems analysis approach to Condition Monitoring and Fault Diagnosis 21

2.5 Summary 25

Chapter 3 Introduction to System Identification **26**

3.1 Introduction 26

3.2 The dynamic nature of linear and non-linear systems 27

3.3 The procedure of System Identification 28

3.4 Model structure representation 29

3.4.1 Linear black-box models 29

3.4.2 Non-linear black-box models 31

3.5 Parameter estimation 32

3.5.1 Least squares 34

3.5.2 Recursive least squares 35

3.6 Model structure detection 36
3.6.1 Linear regression 37
3.6.2 Criteria for model structure selection and model structure detection algorithms 38
3.6.3 Non-linear regression 39
3.7 Model selection 40
3.7.1 Bias-variance trade-off in models 40
3.8 Model validation 41
3.9 Summary 42
Chapter 4 Frequency Response Analysis of Dynamic Systems 43
4.1 Introduction 43
4.2 Analysis of linear systems in the frequency domain 44
4.3 Analysis of non-linear systems in the frequency domain 45
4.3.1 Output frequency response of non-linear systems 46
4.3.2 Generalised Frequency Response Functions 48
4.3.3 Non-linear Output Frequency Response Functions 49
4.4 Summary 56
Chapter 5 An Effective Least Squares Method of Evaluating Nonlinear Output Frequency Response Functions of Nonlinear Systems 57
5.1 Introduction 57
5.2 The Modified Least Squares method for the evaluation of Nonlinear Output Frequency Response Functions 59
5.3 Comparison of the Least Squares and Modified Least Squares based methods of Nonlinear Output Frequency Response Functions evaluation 63
5.3.1 Comparison for the case of a general input 63
5.3.2 Comparison for the case of a harmonic input 67
5.4 Convergence analysis of Volterra series representation of Duffing's oscillator 70
5.4.1 NOFRF based local approximation of severe non-linear oscillator exhibiting the jump phenomena 71
5.5 Summary 84

Chapter 6 Data-driven Condition Monitoring and Fault Diagnosis Using System Identification and Frequency Response Analysis 86

6.1 Introduction 86

6.2 Sampling time, System Identification and nonlinearity detection 87

6.3 Model term selection criterion and model building 89

6.3.1 Choice of maximum dynamic order 89

6.3.2 Reduced set of candidate model terms 90

6.3.3 PEM and SEM approach to model term selection 90

6.4 A new method to System Identification based on SEM and iFRO 91

6.4.1 Obtaining a reduced set of candidate model terms using the S-iFRO algorithm 95

6.5 CM-FD methodology based on SI and FRA optimised for practical implementation 99

6.6 Summary 100

Chapter 7 Low-Frequency RFID Based Eddy Current Probing and Defect Characterisation Using System Identification and Frequency Response Analysis 102

7.1 Introduction 102

7.2 Experimental rig used for LF RFID based SHM 104

7.3 The Reader-Tag-Metal system 107

7.4 Analysis of the Reader-Tag-Metal system using the SI and FRA approach with metal samples of various defects 109

7.4.1 Corrosion characterisation 112

7.4.2 Crack length and crack depth progressions 113

7.5 Summary 117

Chapter 8 Conclusions 118

8.1 Conclusions and summary 118

8.2 Future work 119

References 122

Abbreviations

AR	Auto-Regressive
ARMAX	Auto-Regressive Moving Average with eXogenous input
ARX	Auto-Regressive with eXogenous input
BJ	Box-Jenkins
CM	Condition Monitoring
CM-FD	Condition Monitoring and Fault Diagnosis
ERR	Error Reduction Ratio
FD	Fault Diagnosis
FDI	Fault Diagnosis and Isolation
FDIA	Fault Diagnosis, Isolation and Analysis
FFT	Fast Fourier Transform
FRF	Frequency Response Function
FT	Fourier Transform
GFRF	Generalised Frequency Response Function
LF	Low Frequency
LS	Least Squares
LTI	Linear Time-Invariant
M-LS	Modified Least Squares
MSS	Model Structure Space
NAR	Nonlinear Auto-Regressive

NARMAX	Non-linear Auto-Regressive Moving Average with eXogenous input
NARX	Non-linear Auto-Regressive with eXogenous input
NDE&T	Non-Destructive Evaluation and Testing
NOFRF	Non-linear Output Frequency Response Function
PEC	Pulse Eddy Current
PEM	Prediction Error Minimisation
RFID	Radio Frequency IDentification
RLS	Recursive Least Squares
SEM	Simulation Error Minimisation
SI	System Identification
SRR	Simulation error Reduction Ratio

Nomenclature

t	Time
τ	Time delay index
$u(t)$	Input signal to a system
$y(t)$	Output response of a system
$\hat{y}(t)$	Model Predicted or model generated output
$e(t)$	Residual or error between $y(t)$ and $\hat{y}(t)$
n_y	The maximum lag order or the dynamic order of the output $y(t)$
n_u	The maximum lag order or dynamic order of the input $u(t)$
n_c	The maximum lag order or the dynamic order of the residuals $e(t)$
n_p	The total number of terms in the polynomial model
N	The highest order of nonlinearity to be considered
N_p	The highest nonlinear polynomial order
T_s	Sampling time
$y_n(t)$	Output response of the n^{th} order nonlinearity
$h(t)$	Impulse response of a linear system
$h_n(t_1,\cdots,t_n)$	n^{th} order Volterra kernel
z	Forward shift operator
z^{-1}	Backward shift operator
f_{Y_n}	Possible output frequency range contributed by the n^{th} order nonlinearity

f_Y	Possible output frequency range of the complete output of a nonlinear system
$G_n(j\omega)$	n^{th} order Volterra kernel
$Y_n(j\omega)$	Output frequency response of the n^{th} order nonlinearity
L	Number of observations or the data length

Chapter 1

Introduction

1.1 Background

Fault Diagnosis (FD) and Condition Monitoring (CM) is a vital aspect of mechanical systems, electrical systems and structures. The significance of timely identifying the occurrence of faults, its type, location and severity in engineering systems is immense and vital. This is due to the high costs that are to be carried from severe damages owing to ill-timed maintenance due to not being able to identify faults beforehand [1].

This is done mainly for the aid of safe and optimal operation of systems, as well as its components without overstressing. Most systems are set to function within bounded limits or functional conditions. Thus increasing its lifetime and efficiency [2]. At the same time Condition Monitoring and defect detection in systems and structures is of key importance to avoid any severe incidents and losses that can be experienced by carrying out well-timed upkeep.

The process of Condition Monitoring and Fault Diagnosis involves collecting specific information from a system and evaluation of the precise condition of a system. Through this process, an assessment of the true confidence of the system and its operations is the main criteria of Condition Monitoring and Fault Diagnosis. This provides a certain level of assurance to the operator in the application of safety-critical purposes. Fault Diagnosis is, the accurate detection and isolation of faults, while Condition Monitoring is, the observation of a system for the development of faults [2], [3]. Through Condition Monitoring, an assessment of the system state in relation to the progress towards faults and information about the system safety or its optimum operating level can be determined. This information can be utilized to conduct predictive maintenance to avoid faults and occurrence of severe break downs [2]. Fault-tolerant functioning and avoidance of off-spec operations in mission and safety-critical applications are achieved using on-line Condition Monitoring and Fault Diagnosis. While off-line diagnosis and monitoring are used for complete maintenance of systems and structures [4]. Essentially, there is an important need for online, as well as off-line Condition Monitoring and Fault Diagnosis.

Many Condition Monitoring and Fault Diagnosis (CM-FD) methods that fall under different types or schemes have been formulated. These different categories of CM-FD methods exhibit various advantages and disadvantages. Hence, depending on the needs of the application, a suitable framework should be chosen [3,5,6,8,9]. From the different CM-FD schemes, the analytical type and knowledge-based schemes are the most popular in industry and research. This is due to the advantages these schemes possess [6]–[8].

However, analytical schemes, which are data-driven and model-based methods, are most widely used in practice [5], [7]. This is mainly due to its advantage over knowledge-based schemes regarding the amount of prior expert knowledge required and the complexity involved in designing knowledge-based schemes.

The use of black-box models, particularly time-series analysis models and the data-driven identification of these models for Fault Diagnosis has gained particular interest [9]–[11]. This is in reason to not requiring much prior information about the physical characteristics of the system under consideration, as these can be obtained from the system input-output data itself [12].

In recent advancements of System Identification based FD methods, in particular to autoregressive time-series models. Some researchers have taken a control systems approach to the CM-FD problem. In regard to both linear and nonlinear systems, the authors of [13]–[19] have used the method of Frequency Response Analysis (FRA) through the Frequency Response Function (FRF) for linear systems. While in the case of nonlinear systems, the Generalised Frequency Response Functions (GFRFs) or the Nonlinear Output Frequency Response Functions (NOFRFs) of the identified system model is used to extract frequency response based features for CM-FD. The current status of the system dynamics is captured through System Identification and the dynamics of the model are analysed using Frequency Response Analysis methods. Faults, or a change in system conditions that induce dynamical changes, thus can be isolated and recognised. This is the essence behind CM-FD through the method of System Identification and Frequency Response Analysis. This approach stems from the well-established methodology of analysing system dynamics in the field of control systems engineering, for the purpose of designing controllers and compensators to achieve desired system responses and system stability in the frequency domain.

1.2 Motivation

The field of CM-FD has been driven towards constant development in order to keep in pace with the development of more complex and large-scale systems and structures. This is also motivated by the effort to minimise the disadvantages incurred by currently available techniques for CM-FD. The recently proposed method of using a control systems approach of System Identification and Frequency Response Analysis has been one such effort for CM-FD of engineering systems and structures. Especially, in the case of nonlinear systems. This is because in the case of nonlinear systems, the currently available model-based techniques are mostly based on linear systems Fault Diagnosis [20], [21] thus cannot be easily applied and is a relatively difficult task [22]. In order to overcome these issues with model-based methods, techniques based on multivariate statistics and expert systems have been under study [4], [23]. However, these techniques usually do not consider the dynamical behaviour of the system. Therefore, overlooking features that could be used potentially for additional insight into the dynamical characteristics of faults.

In this context, the approach of System Identification of black-box time-series models avoid the requirement of much prior knowledge of the system and overcomes the issue when phenomenological modelling is difficult. Furthermore, through the Frequency Response Analysis of these identified time-series models, the dynamic nature of the faults can be interpreted in the frequency domain. Thus, obtaining credible fault features.

System Identification (SI) strategies for nonlinear systems time-series models is well established and thus have been used in various real-world applications [24]. The Frequency Response Analysis (FRA) of these nonlinear models using the GFRFs and NOFRFs have been under the subject of several studies [13], [18]. In comparison, with regard to CM-FD, the NOFRFs are preferred to the GFRFs, because of its one-dimensional nature compared to the multi-dimensional GFRFs. This is because the NOFRFs can be interpreted and evaluated with ease compared to the GFRFs [19]. Therefore, the NOFRFs are more practical in embedded implementations. However, in the previous studies conducted on the SI and FRA approach to CM-FD, in both linear and nonlinear systems, some practical concerns involved have been overlooked.

In order to capture the system dynamics, appropriately using System Identification, the system usually has to be persistently excited. However, inadequate inputs which do not persistently excite the system are commonly present and at times nothing can be done about this. This is because CM-FD has to be carried out without interrupting normal operations of the system by feeding different inputs [25]. Furthermore, the dynamic model resulting from the System Identification procedures; should be able to dynamically reconstruct the system from the data, in order for the model to be analysed in the frequency domain accurately. The accurate dynamical reconstruction of a system from its data, especially in the nonlinear case, depends on certain specifics of a suitable choice, sampling time and the order of the model [26]–[28]. Such concerns are related to System Identification explicitly have not been considered in previous studies in the context of CM-FD using System Identification.

In the context of Frequency Response Analysis of nonlinear systems, using the NOFRFs, the algorithm for extracting NOFRFs using input and output data of the system or a model of the system [29] has numerical inaccuracies [30]. Therefore, the NOFRFs evaluation has to be done using appropriately chosen gains in the input data. This will hinder the process of automatic CM-FD. Furthermore, when considering nonlinear systems that exhibit severe nonlinear behaviour, Volterra series based methods, such as, the GFRFs or the NOFRFs were not able to be applied. This is because the Volterra series does not have a convergent solution around severe nonlinear behaviour. However, it has been argued that in theory, a truncated solution should exist given the use of a very high order of nonlinearity [31]. The GFRFs cannot be used because of the computational effort concerning higher-order nonlinearities and the NOFRFs cannot be used because of numerical inaccuracies attained when using higher order nonlinearities, thus causing a limitation.

The SI and FRA approach to CM-FD has shown to be of clear potential in the previous studies. However, the concerns mentioned, limits the use of this approach in wider CM-FD applications. The present study is concerned with overcoming these practical

concerns, that are present in the method and to establish the SI and FRA method to CM-FD. Additionally, an embedded application of NDE&T (Non-Destructive Evaluation and Testing) or non-invasive technique for SHM (Structural Health Monitoring) will be undertaken. The SI and FRA method to CM-FD will be applied to a recently proposed NDE&T technique of wireless eddy current probing for non-invasive SHM through the use of RFID (Radio Frequency Identification) technology [32], [33].

In [32], [33], the respective authors used features from the time-series signal of the RFID system to distinguish between different stages of corrosion and different progressions of cracks. Even though time-domain features were able to be used in a controlled laboratory environment, these time-domain features are highly susceptible to even very low noise levels and other external disturbances [34]. Furthermore, the circuitry in RFID systems is vulnerable to noise when operated in the outside environment [35]. Therefore, to overcome this issue in the practicality of applying this NDE&T method is of importance thus the proposition of applying a SI and FRA approach.

Through this implementation of the SI and FRA method to CM-FD in the context of SHM through wireless eddy current probing via RFID technology, a novel SHM technique is presented.

1.3 Aims and objectives

The main aim of the research undertaken is to optimise the SI and FRA approach to CM-FD in relation to the concerns mentioned in the previous section. Thus, facilitating the use of this approach generally in the wider CM-FD problems. Consequently, applying the optimised method to RFID based wireless eddy current probing approach for non-invasive SHM to result in a new method of corrosion and crack detection in metallic structures. To accomplish this the key objectives will be perused:

1. Examine the concept of NOFRFs and address the issues of numerical inaccuracy present in the current method of evaluating NOFRFs using input-output data of a system or a model.

2. Investigate severe nonlinear behaviour and the method in which the concept of NOFRFs can be applied for the analysis of these types of nonlinear systems.

3. Develop a System Identification methodology addressing the concerns of inadequate inputs and dynamical reconstruction. Thus, in combination with Frequency Response Analysis, a widely applicable CM-FD methodology.

    - Realise the specifics that can be used for accurate dynamical reconstruction of system behaviour in the form of time-series black-box models.
    - The approach to System Identification that needs to be taken to overcome the issue of inadequate excitation inputs.

4. Develop a novel method to SHM by the implementation of the RFID NDE&T technique coupled with SI and FRA approach to CM-FD for the characterisation of corrosion and cracks in metals.

1.4 Thesis overview

The thesis is organised into 8 chapters in the following manner;

- Chapter 2: provides a brief overview of common terminology used in the field of CM-FD and introduces the recently proposed approach of a controls systems analysis approach of System Identification and Frequency Response Analysis. The chapter briefly overlooks the advantages and disadvantages of different types of CM-FD methodologies while highlighting the significance of hybrid approaches.

- Chapter 3: provides an overview of System Identification procedures. A description of linear and nonlinear systems in the time-domain is introduced and model structures that can be used with these systems are reviewed. The main steps in System Identification are reviewed with different methods used in each step. Two of the commonly used model structure selection criteria are discussed.

- Chapter 4: introduces the theory of Frequency Response Analysis of linear and nonlinear systems. The description of both linear and nonlinear systems is provided and the characterisations of the output frequency response in relation to these systems are reviewed. The FRF used in characterising linear system frequency response and the GFRFs and NOFRFs which can be used to describe nonlinear systems in the frequency domain is discussed. The concept of NOFRFs has been discussed in detail because of the use of this method in the CM-FD of nonlinear systems in this thesis.

- Chapter 5: focuses on a new effective method of extracting NOFRFs that can be used with ease with just the input-output data of nonlinear systems. This new method is named as the M-LS method for evaluating NOFRFs. The M-LS method is shown to extract NOFRFs with significant numerical accuracy than the original method. The accuracy of the new method is demonstrated under two cases of inputs, general bandlimited and harmonic instances. This chapter also demonstrated, the existence of a truncated convergent Volterra series, of extremely high order around severe nonlinear behaviour that was previously only argued theoretically and was deemed impossible or impractical to achieve practically. This was shown using the NOFRFs, which is based on the Volterra series, evaluated using the M-LS method. This is a significant manifestation of the numerical accuracy in the M-LS method and

the efficiency of using the NOFRFs for nonlinear systems analysis now possible in the case of severe nonlinear behaviour.

- Chapter 6: presents an identification methodology, based on other previous works that can be used in CM-FD mitigating the concerns mentioned earlier in Chapter 1 Section 1.2. Therefore, a new identification methodology which is an extension to an already existing method is proposed to produce models that tend to be dynamically optimum. Furthermore, some steps that need to be considered when using System Identification is introduced, in order to address the issues mentioned in Chapter 1 of this thesis.

- Chapter 7: presents a novel implementation of System Identification and Frequency Response Analysis, on a recently proposed new technology called Low Frequency (LF) RFID wireless eddy current probing, for non-invasive SHM. It is shown through characterisation of defects on metal samples, LF RFID wireless eddy current probing technology coupled with System Identification and Frequency Response Analysis has the clear potential of being a new technology in SHM.

- Chapter 8: provides concluding remarks for the work presented in this study and the future direction of research heading from the work are highlighted.

1.5 Summary of contributions and research outputs

Novel contributions that stem from the work conducted in the current study are listed below:

1. Chapter 5: A new and effective method that mitigates the numerical inaccuracies of the original method of evaluating NOFRFs using just the system input-output data has been developed. The numerical accuracy achieved by this method is demonstrated under the instance of two different types of inputs; general bandlimited and harmonic inputs. It is shown that the new method (M-LS method) evaluates NOFRFs with significant accuracy. Therefore, the NOFRFs can be used to decompose the output of a nonlinear system to its respective output nonlinearities, in the frequency domain. Hence to facilitate practical nonlinear system analysis with applications including engineering system Fault Diagnosis and SHM. The chapter also presents for the first time, the existence of a convergent Volterra series, around the regions of severe nonlinear behaviour. Such an existence was only theoretically argued in the literature and was considered impossible or impractical to achieve. This is, because of the extremely high order required to reach such a convergence, due to the computational efforts needed. Therefore, in previous studies, the regions of severe nonlinear behaviour were not possible to be studied in a pure Frequency Response Analysis

framework. However, explicitly, because of the numerical accuracy attained by the M-LS method and the NOFRFs being one-dimensional Volterra series based frequency functions. It was demonstrated practically, that a convergent Volterra series indeed exists in severe nonlinear cases because of the convergence achieved by the NOFRFs. This enables the study of severe nonlinear behaviour, in a Frequency Response Analysis framework and the analysis, design and Fault Diagnosis of such systems.

2. Chapter 6: This chapter proposes a novel method to System Identification, in the form of extending an already existing method, in order to achieve models that tend to be dynamically optimum. Furthermore, in a CM-FD point of view, a novel System Identification methodology is proposed in considering previous work done in the field of System Identification, to address the concerns mentioned in Chapter 1 of this thesis. These concerns specifically relate to using System Identification for CM-FD. Addressing these concerns facilitates; the use of a control systems analysis based approach to CM-FD through System Identification and Frequency Response Analysis.

3. Chapter 7: In this chapter, the initial investigation of potential new technology in SHM is presented. Data on metal samples are collected, using a recently proposed technology on non-invasive SHM called LF RFID based wireless eddy current probing. The data is processed and features are obtained using System Identification and Frequency Response Analysis. The results obtained illustrate a clear indication of this new implementation being a potential new technology in the field of SHM.

Based on the work conducted in Chapter 5; on the formulation of the M-LS method. A conference paper has been accepted and published.

- S. R. A. S. Gunawardena and Z. Q. Lang, "*An Effective Method for Evaluation of the Nonlinear Output Frequency Response Functions from System Input-Output Data*," 2018 UKACC 12th International Conference on Control (CONTROL)*, Sheffield, 2018, pp. 134-139.*

Furthermore, on the work presented in this chapter regarding the use of NOFRFs on the analysis of severe nonlinear systems will be presented in a journal in the future.

Chapter 2

Condition Monitoring and Fault Diagnosis – Brief Overview and a Control Systems Approach

2.1 Introduction

Throughout the developments in the field of CM-FD, basic terminology and concepts have been introduced to categorise different types of faults and the different stages involved in Condition Monitoring and Fault Diagnosis. The chapter briefly overlooks at the different terminology used and various approaches to Fault Diagnosis and introduces the recently proposed control systems analysis approach to CM-FD. The main focus on the work undertaken in the current study is this new approach. Advantages and disadvantages of the currently available and the industry standard methods to CM-FD are reviewed in brief and the use of hybrid versions of these approaches are highlighted. The control systems analysis based approach of System Identification and Frequency Response Analysis could be looked at in the perspective of being one such hybrid approach, in which being a purely data-driven, model-based signal processing method.

The clear potential of the new approach is highlighted, especially with regard to the dynamic nature of faults. Faults and off-spec conditions induce dynamic changes to the system concerned. As such, these dynamic changes can be observed and analysed using a systems perspective in which the system is considered in its entirety as a black-box. This systems perspective to CM-FD is the motivation behind the use of a control systems analysis approach to diagnosing faults and the monitoring of the current condition of engineering systems.

2.2 A brief overview of Fault Diagnosis, isolation and Condition Monitoring

The process of diagnosing faults can be generally broken down into three important steps [1], [5], [7].

1) **Fault detection.**
   The stage at which it is detected whether a problem has arisen or is about to arise. In this particular stage, the root cause of the fault is not established.
2) **Fault isolation.**
   Using the information collected from the system, the procedure of classification of what individual faults that have occurred is determined in this stage.
3) **Fault analysis or identification.**
   The procedure of identifying the root cause of the fault is carried out where either preventive or remedial measures could be taken. It is in this stage the type of fault, its severity and location are determined.

In particular to what functions a Fault Diagnosis system provides, the process is known as Fault Detection, Fault Detection and Isolation (FDI) or Fault Detection, Isolation and Analysis (FDIA) [7]. In the literature, however, at times both FDI and FDIA are commonly referred to as FDI.

Faults that affects a system as a whole, can be categorically separated into two main types;

- **Additive faults.**
  These type of faults affects a system as an addition to the system output by an external influence. Essentially the fault signal is added to the system, for example, a sensor fault.
- **Multiplicative faults.**
  This type of fault acts as parameter changes in the system, where the fault influences a variable as a multiplication. This can be translated into an internal component of the system being affected.

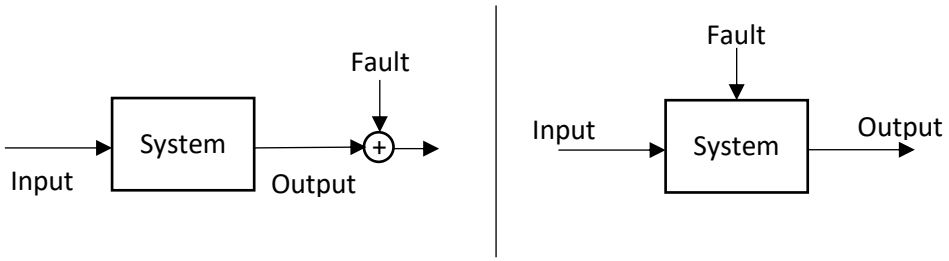

Figure 2.1: Example of an additive fault (left) and a multiplicative fault (right).

Faults are further categorised within the above mentioned two types according to the time dependency of a fault [8] as follows.

- **Abrupt fault**: Fault takes the form as a stepwise function. It affects the monitoring fault feature as a bias.
- **Incipient fault**: Fault increases in a linear manner as time increases, such as a ramp. Brings about a drift effect on the monitoring feature.
- **Intermittent fault**: A collection of impulses with different amplitudes.

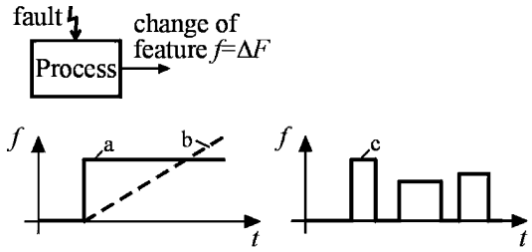

Figure 2.2: Illustration of the effect of the time-dependent behaviour of faults on the monitoring fault feature f. (a) abrupt fault, (b) incipient fault and (c) intermittent fault [36].

Throughout the literature [1], [4], [7], [36]–[41] the performance of CM-FD schemes are determined by the concepts of *fault detectability* and *fault isolability*;

- **Fault detectability**: Detectability of faults in the presence of noise, uncertainties and unknown disturbances.
- **Fault isolability (ability to isolate a fault)**: Clear identification and classification of a fault that has occurred, even in the presence of other fault occurrences.

Expanding upon these two concepts the respective authors of [1] and [4] have outlined the desirable qualities that should be expected from a fault diagnostic system. A complete CM-FD framework should possess these qualities to be considered as a good CM-FD method [4]. These qualities are reflected throughout every stage of the Condition Monitoring and Fault Diagnosis process. The significant ones that generally apply to most techniques are summarised below.

- **Quick detection and diagnosis:** Ability to detect and diagnose faults in a timely fashion.
- **Precise isolation:** Ability to clearly distinguish between the occurred faults.
- **Robustness:** Accuracy of diagnosis in the presence of noise and uncertainties.
- **Novelty identifiability:** Identification and classification of unknown or new faults.
- **Classification error estimate:** Ability to identify the reliability of decisions given.
- **Adaptability:** Identifying and easy adaptation to changing environments that could change operating conditions.
- **Explanation facility:** Capability to clarify the reason for the faults that have arisen.

- **Multiple fault identifiability:** Identification of multiple faults that occurred simultaneously.

2.3 Outline of different types of Condition Monitoring and Fault Diagnosis schemes

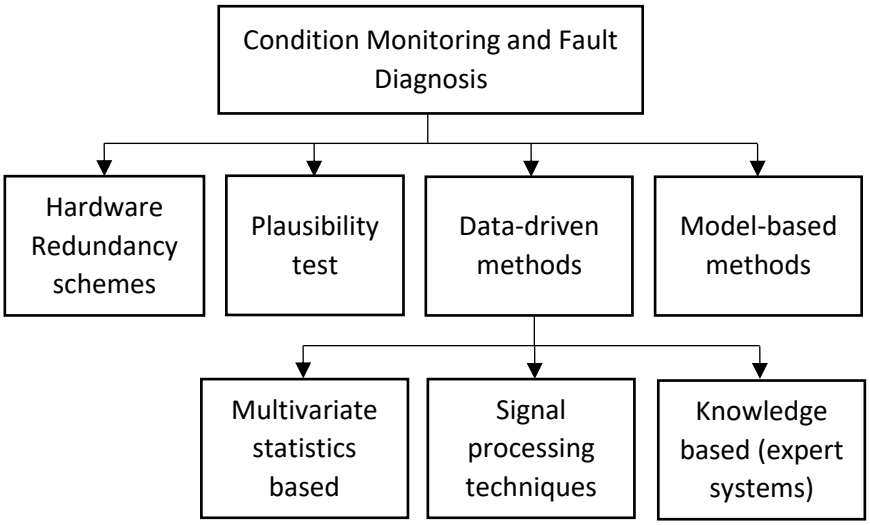

Figure 2.3: Classification of Condition Monitoring and Fault Diagnosis schemes.

Condition Monitoring and Fault Diagnosis schemes and methods can be categorized as shown in Figure 2.3. From these different CM-FD schemes that are well-established in the industry, the most popular methods of CM-FD [1], [6]–[8], [22], [23], [42] are briefly summarised as follows;

- **Model-based CM-FD** methods: in general contains a bank of models in which a nominal model (no faults) and different fault models (each model contains a complete system model with a specific fault induced) are run in parallel with the actual system to generate a residual vector, where a set of residuals or errors between each model output in the model bank and the actual system, is used for FD.
- **Multivariate statistics based CM-FD** methods: real-time data from the system inputs and outputs are compared using multivariate statistics with a bank of system input-output data that is already available. This bank of data contains data from nominal operations as well as specific fault operations.
- **Signal processing** methods: use traditional signal analysis tools, such as signal frequency spectrum, on the system output for FD and CM.
- **Knowledge-based CM-FD** methods: using expert knowledge about the system and its faults to diagnose faults using neural networks, fuzzy systems etc.

A brief overview of the different pros and cons, of these CM-FD schemes are mentioned in Table 1. Various developments are taking place in the field of FD and CM and numerous techniques are being proposed for eliminating many of the disadvantages present in current methods. However, many drawbacks still exist [5]–[7], [43] and continuous improvements in FD and CM methods are required to overcome these disadvantages. This is in reason to keep in pace with the development of more complex and large-scale systems in the industry.

Table 1: Pros and Cons of Fault Diagnosis schemes [5]–[7], [42], [44]

Fault Diagnosis scheme	Advantages	Disadvantages
Hardware redundancy scheme	High reliability	High cost
	Direct fault isolation	
Plausibility test	Faults can be categorized according to physical laws	Limited efficiency in complex systems
		Less adaptability
		Less novelty detection
Model-based	High effectiveness in dynamic processors	Efficiency limited to the details in plant model embedded
	Robust against noise and uncertainty, depending on the observer that is used to identify faults	Input signal not exciting all dynamics
		Less novelty detection in physical models
Multivariate statistics based	Ability to handle large amounts of high dimensional data	Availability of large amounts of data
	Requires lesser prior information about the process	Mainly applied to static processes
Signal processing	Efficiency in steady state situations	Limited efficiency in dynamic systems

		Not robust against noise or disturbances
Knowledge-based	Applicable in situations where high-fidelity mathematical models are not available.	Expert knowledge about faults is required.
	Robust against noise and uncertainties	Overfitting of data
		Training of complex model structures

An ideal CM-FD framework should be robust against noise and disturbances while maintaining sensitivity towards all types of system-wide faults. Furthermore, the framework should be sensitive to significant changes in the system to monitor its condition or progression towards faults. These could be system wide parameter changes, sensor faults and other additional system component faults. However, this should be achieved without any occurrences of false alarms or exhibiting false conditions about the system [5–10,12,26,27]. These considerations are a reflection of the qualities a CM-FD method should attain as discussed in the previous section.

Achieving the above-mentioned considerations are at times a compromise in the individual FD schemes. For instance, model-based Fault Diagnosis systems require prior information about the system and possible faults to build accurate models for good fault detectability and disturbance rejection [37], [46]. Whilst multivariate statistics based methods at times require large amounts of data depending on the complexity of the system. This data has to contain both healthy state and faulty state data in order to identify faults utilising multivariate statistics [6], [47]. However, [6], [48]–[51] have proposed new hybrid CM-FD schemes through the integration of data-driven methods for fault isolation and model-based methods for fault detection to attain a good compromise between the qualities mentioned before. Therefore, the hybrid methods for CM-FD are designed in such a way that they utilise the advantages of more than one methodology to overcome some of the individual disadvantages in each respective scheme. Thus, much of the research in the field is concentrated on these hybrid techniques to minimize the disadvantages of individual FD schemes [4], [52], [53].

Hybrid CM-FD techniques based on data-driven model parameter estimation approaches have been introduced in the past decade or so and is progressing to be a popular area of research in the field [15], [45], [54]–[60]. These range from subspace identification techniques, used in extracting state-space models [14], [61]–[63], to System Identification techniques which are used in the extraction of linear and nonlinear autoregressive time series models [8], [45], [52], [54], [55], [64]. These identified models

are utilized for the purpose of fault detection through either residual generation between the model and the actual system or as parameter comparisons [6]–[8], [10], [25], [45], [65]. This is similar to traditional model-based FDI methods however, the model in these methods are extracted through data-driven model identification techniques. In traditional model based FDI, the model is obtained through ordinary differential/difference equations (ODEs), which are derived from physical equations and first principles.

The following section of this chapter will briefly discuss some of the recent developments of the data-driven model identification approaches for CM-FD. This section also aims to introduce a new data-driven approach for CM-FD that has been recently proposed. This new approach is based on a method used in the field of control engineering for frequency domain analysis and design of control systems.

2.4 A control systems analysis approach to Condition Monitoring and Fault Diagnosis

A system perspective, system viewpoint or systems approach, is observing all the sub-procedures or sub-processes or sub-systems within as one whole entity, considering only the main inputs and outputs [66]–[68]. The figure below illustrates this briefly.

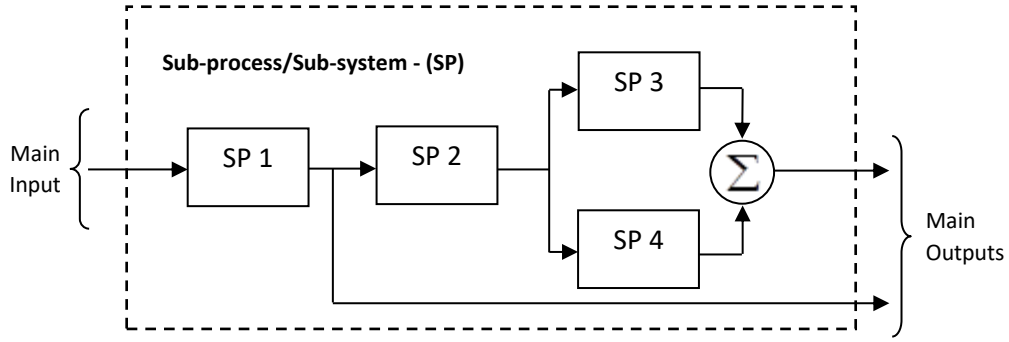

Figure 2.4: Example of a process and its sub processes in a system's perspective. The dotted box indicates that complete internal sub-processes are to be considered as just one system. The sub-processes or the sub-systems contained within the whole process are denoted as SP

Lang *et al.* in [66] presented a systems approach to PEC (Pulse Eddy Current) based NDE&T for structural defect detection, where a data-driven parameter estimation of a continuous-time transfer function model was first extracted and its parameters were used as fault specific features. Usually, PEC based NDE&T methods utilize only the output response of the PEC probe for diagnosis [66]. The proposed method in [66] uses both the excitation input and the system response for feature extraction by identifying a model and using the model parameters as fault specific features. Similarly, Munoz *et al.* in [69] proposed an ultrasound-based NDE&T technique coupled with ARX models to diagnose

structural faults in wind turbines. This was conducted utilizing residuals generated between an ARX model and the actual system outputs. The ARX model used was identified when the system was in a nominal state or normal state. Structural faults were identified when the mean of the residuals generated deviates from zero. In the same manner, Fassois *et al.* in [14] have used the ARX model based residual generations to identify faults in structures subjected to vibrations.

In the case of nonlinear systems, Fault Diagnosis studies have been conducted using the NARX model. Dimogianopoulos *et al.* in [56] have utilised NARX models for the Fault Diagnosis of aircraft systems. The authors carried out the diagnosis of faults by using the degree of correlation in the residuals between a previously identified system - nominal state NARX predictor model and the actual system outputs. Furthermore, the authors presented another method in the same paper where the residuals were used to identify a NAR (Nonlinear Auto-Regressive) model. The parameters of the NAR model are then compared with baseline NAR parameters for the diagnosis of faults. A similar Fault Diagnosis method for sensor and actuator faults in automotive engines based on residuals generated between a NARMAX model of the nominal system and the actual system was presented by Krishnaswami *et al.* in [70]. However, in this method, the residuals were processed using a certain form of nonlinear parity equations for the diagnosis of faults.

Black-box time-series models, such as ARX and NARX models, do not require much prior information about the physical characteristics of the system under consideration, as these are obtained from the system input-output time-series data itself [12]. This is because time-series models are based on the correlations between the signals involved with the system. Hence, the progress of the dynamics or states of the system in time is related to the past changes of these correlations backwards in time [24], [71], [72]. However, it is a well-known fact that a discrete-time representation of a continuous-time system does not have a unique solution [19], [24], [72]. Especially in the case of nonlinear systems, there may exist more than one solution to the identification of the model [24]. But given that, the model identification is done appropriately, and the model can correctly capture the dynamics of the system. The corresponding frequency response characteristics remain unchanged for all local solutions [19].

Frequency domain characteristics of an input-output system have: a direct relationship to its dynamics. This relationship has been used in the field of control systems engineering to conduct Frequency Response Analysis of dynamic systems. Frequency Response Analysis, is a well-established methodology of analysing and interpreting system dynamics for the purpose of designing controllers and compensators to achieve desired system responses and system stability [72]–[75]. Hence, by means of Frequency Response Analysis of an identified model of a system, the dynamics of the actual system can be observed in the frequency domain. Consequently, faults and other off-specification conditions that induce dynamic changes in a system can be detected by observing the frequency response of the system. Thus, the frequency domain characteristics of the system can be used as fault inspecting features. These features are directly linked to the system dynamics and will be fault specific since faults or off-specification conditions may dynamically affect the system significantly at certain frequencies relative to other faults.

Because of this, a dynamic interrelationship between the inspecting features and the faults could be comprehended which will be beneficial in fault isolation. Therefore, the system frequency response is a better approach and fault features obtained from it are better fault indicators than the direct use of black-box models for CM-FD [19], [24]. As a result, a comprehensive CM-FD framework for dynamic systems based on System Identification and Frequency Response Analysis has clear potential. Such a CM-FD framework essentially captures the current status of the system dynamics in the form of a time-series model through System Identification. These dynamics are observed by projecting the identified model to the frequency domain using Frequency Response Analysis. Therefore, any changes to these dynamics are observed via the Frequency Response Analysis of the model. If faults and different off-specification conditions of the system induce unique dynamic changes in the given system, then these faults and conditions could be detected and isolated successfully. Figure 2.5 illustrates the basic layout of such a framework. It should be noted that this type of CM-FD method is only used for multiplicative fault types, i.e. faults that affect the internal components of a system.

The Frequency Response Analysis of the identified model is conducted depending on the complexity of the time-series model obtained. In the case of linear auto-regressive models, the well-established Frequency Response Functions (FRFs) are used for the Frequency Response Analysis. The extensions of the linear FRFs to the nonlinear case, the Nonlinear Output Frequency Response Functions (NOFRFs), first proposed in [29], is used for the Frequency Response Analysis of non-linear auto-regressive models.

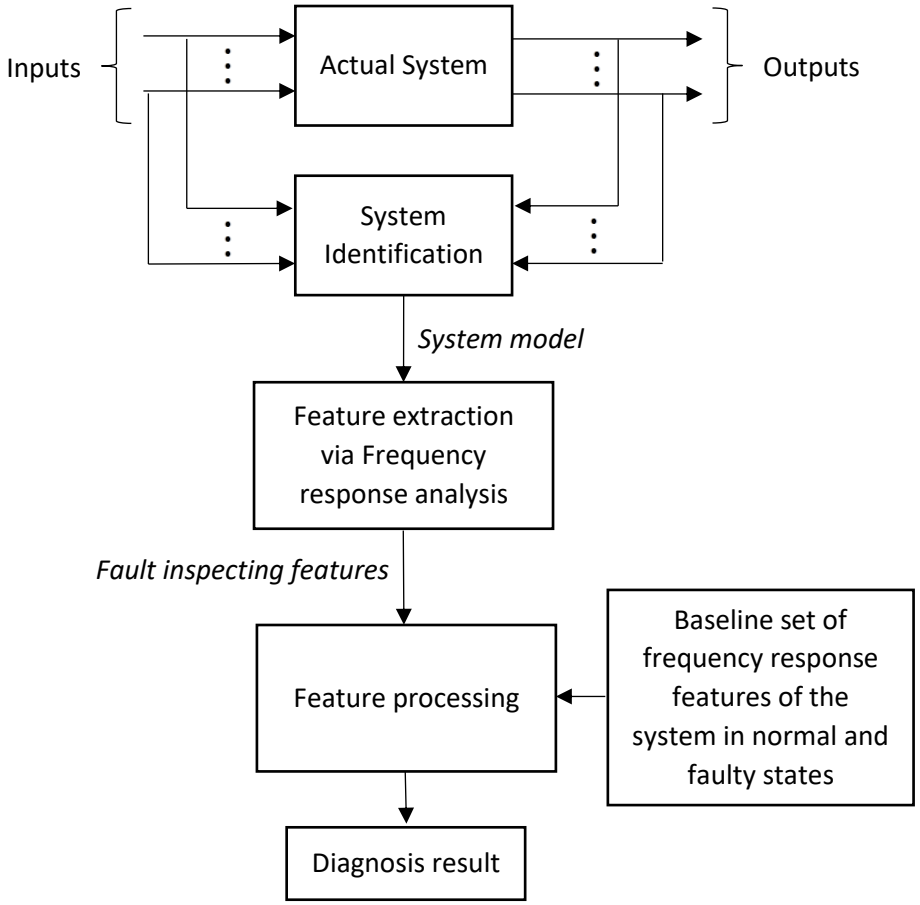

Figure 2.5: Basic layout of a CM-FD framework based on System Identification and frequency response analysis. Through System Identification the current status of the system dynamics is captured in the form of a time-series black-box model (ARX/NARX). The black-box model is then projected to the frequency domain via the frequency response analysis of the model (FRF/NOFRF). The features extracted from frequency response analysis is then compared with a set of prior obtained baseline features for processing and diagnosing faults.

2.5 Summary

This chapter aims to briefly introduce the terminologies and concepts that are widely used in the field of Condition Monitoring and Fault Diagnosis. Established approaches to CM-FD is overviewed in brief with regard to the various advantages and disadvantages the respective methods possess. The current progress in CM-FD using System Identification is covered in detail to illustrate the current state of the art in this type of FDI method and its advantages. Furthermore, the chapter introduces the recently proposed control systems analysis approach to CM-FD through System Identification and Frequency Response Analysis. The feasibility of such a CM-FD methodology was discussed in a qualitative manner. This was with regard to the underlying essence in a control systems analysis approach and the dynamic changes faults and off-spec conditions induce. The chapter overviewed the current progress of CM-FD through System Identification and Frequency Response Analysis while highlighting studies that have experimentally validated this concept for practical applications. The current study focuses on this approach in the context of the concerns highlighted in Chapter 1.

Chapter 3

Introduction to System Identification

3.1 Introduction

System Identification, is concerned with obtaining mathematical models of dynamic systems from the input-output data obtained from the system. Essentially the mathematical models attained through the System Identification process should be able to map the input data to the output data of the system [24], [72]. In addition, it is crucial that the model should be able to provide a description of the underlying system behaviour, in order to conduct an analysis of the system dynamics, for the purpose of design, control [76], [77] and Fault Diagnosis [8].

This chapter aims to provide an outline of the process of linear and non-linear System Identification in the context of discrete-time black-box modelling. As mentioned in previous chapters, in line with the research conducted in the current study, for the purpose of Condition Monitoring and Fault Diagnosis, the system is considered as a black box. This is, because in the modelling process, when the system is regarded as a black-box, knowledge of the physical properties of the system are not considered. Since the underlying system dynamics will be captured within the black-box model during the identification process. The knowledge of the physical nature of the system or its faults is not completely required as this will be obtained from the input-output data generated by the system. Also, the use of black-box models will facilitate the analysis of system characteristics which cannot be easily represented using physical equations [8], [12]. Various types of black-box model structures under different model classes such as; linear, non-linear, time-varying, time-invariant, discrete-time, continuous-time, parametric, non-parametric, etc. are available [78].

In line with the research undertaken and the work presented, this chapter reviews a number of linear and non-linear, discrete-time parametric, black-box model structures. Because of the use of parametric models and since the parameters are estimated from data parameter estimation and model structure detection are both significant. Essentially for accurate Condition Monitoring and Fault Diagnosis. The System Identification process needs to capture the true dynamics of the system from the input-output data. This has a direct relation to the model structure detection stage and thus attaining of a parsimonious representation of the system [24], [68], [72]. Therefore, the model structure detection process is of vital importance and is the most challenging stage of the identification process. Model structure detection involves in selecting the significant set of model terms, by searching from a pool of terms, which can best describe the input-output relationship of the system in a parsimonious manner. There are a number of commonly used model

structure detection search methods. These methods use certain criteria for the selection of terms. The criteria utilized - in these search methods usually come under two main modelling objectives, namely, Prediction Error Minimisation (PEM) and Simulation Error Minimisation (SEM) [24], [72], [79], [80]. These common search methods and the criteria used for model structure detection are also discussed.

3.2 The dynamic nature of linear and non-linear systems

Given that a system is time-invariant, i.e. the dynamic properties of the system remains unchanged over time, and that it satisfies the superposition principle, can be defined as linear time-invariant (LTI) systems [72]. Moreover, given the LTI system is casual, where the output at a given time is dependent only on the input up to that point in time. Then for time t, the system can be well described as a convolution between the impulse response $h(t)$ of the system and the input signal $u(t)$ as;

$$y(t) = \int_{\tau=0}^{\infty} h(\tau)u(t-\tau)\, d\tau \tag{3.1}$$

where $y(t)$ is the system output and τ is a time delay index. The impulse response defines the time domain characteristics of the system and it is the response of the system when excited by a unit impulse. Traditional systems theory based on LTI systems is a well-established area of research. However, it should be noted that usually, the LTI property of a system is an approximation which is often justified.

Non-linear systems are broadly defined as systems that do not hold the superposition principle and the behaviour of such a system is much more complex. In the case of LTI systems, the output frequency components of the output response are the same as the input. However, in non-linear systems, the output response is much richer in its frequency components than the respective input signal. This is because nonlinear systems have the ability to transfer energy between frequency components and also to frequency components that are not present in the input signal [29]. Non-linear systems can be described in the time domain, by extending the concept of convolutional integrals for LTI systems, equation (3.1), by a series of multi-dimensional convolution integrals, known as - the Volterra series. A class of nonlinear systems that are stable at zero equilibrium can be explained by the Volterra series in the neighbourhood of the equilibrium as shown in equation (3.2) below.

$$\begin{cases} y(t) = \sum_{n=1}^{N} y_n(t) \\ y_n(t) = \int_{-\infty}^{+\infty} \cdots \int_{-\infty}^{+\infty} h_n(\tau_1, \cdots, \tau_n) \prod_{i=1}^{n} u(t-\tau_i) d\tau_i \end{cases} \tag{3.2}$$

where $h_n(\tau_1, \cdots, \tau_n)$ is known as the n^{th} order Volterra kernel representing the time domain characteristics of the n^{th} order system nonlinearity, $y(t)$ is the system output,

$u(t)$ is the system input, $y_n(t)$ is called the n^{th} order nonlinear output or the output of the n^{th} order nonlinearity of the system where $n=1,\cdots,N$ and N is the highest order of nonlinearity [81].

3.3 The procedure of System Identification

As mentioned before System Identification involves in the development of mathematical models for dynamic systems to attain two main objectives;

- Accurate mapping of the input(s) to the output(s) of the system under consideration with the ability to predict new and unseen data.

- Capturing the underlying dynamics of the system within the model.

The latter objective is of vital importance in the context of CM-FD as system-wide faults and changes in the condition of the system affect the system dynamics (see Section 2.4 of Chapter 2). Therefore, the identification procedure needs to be able to capture the dynamics of the given system accurately in order to precisely assess the system operational conditions.

The methodical approach to System Identification involves the solution of four key problems [24], [72]. These key problems are: at times solved together, or iteratively depending on the type of identification algorithm and the strategy used [24], [72], [74], [82]–[87]. These four steps are summarised below and will be discussed in detail in the following sections.

1) **Structure detection**
   Depending on the type of system and the data acquired, determination of an appropriate structure that parsimoniously maps the input-output variables.

2) **Parameter estimation**
   For a given model structure the estimation of the parameters that weight each model term.

3) **Model selection**
   Selecting the best model that attains a good bias-variance compromise from a set of competing models.

4) **Model validation**
   Validation of the selected model in accordance with performance criteria and validation tests to attain confidence in the model depending on the intended purpose of modelling.

3.4 Model structure representation

The System Identification literature offers a variety of different black-box modelling structures such as; Volterra series, neural networks, fuzzy models and a host of linear and nonlinear auto-regressive time-series model structures [24], [72], [88], [89] are to name a few. The scope of this overview will focus on the different discrete-time black-box model structures based on linear and nonlinear auto-regressive with exogenous input type.

Considering the types of model structures reviewed in this section the System Identification task is to find a certain functional mapping from the past inputs, $\mathbf{u}(t-1)=\left[u(1),u(2),\cdots,u(t-1)\right]$ and past outputs, $\mathbf{y}(t-1)=\left[y(1),y(2),\cdots,y(t-1)\right]$ to a future output;

$$y(t)= f\left(\mathbf{u}(t-1)\,,\,\mathbf{y}(t-1)\right)+e(t) \tag{3.3}$$

where $y(t)$ and $u(t)$ are the output and input respectively and $e(t)$ is the error between the predicted output $f\left(\mathbf{u}(t-1)\,,\,\mathbf{y}(t-1)\right)$ and the actual output $y(t)$ at the time sample t.

3.4.1 Linear black-box models

A commonly accepted standard in System Identification of a generic linear black-box model structure [72] is shown in equation (3.4) below.

$$y(t)=\frac{B(z)}{F(z)A(z)}u(t)+\frac{C(z)}{D(z)A(z)}e(t) \tag{3.4}$$

where $u(t)\in\mathbb{R}$, $y(t)\in\mathbb{R}$ and $e(t)$ are the discretised input, output and noise signal respectively at the time step t. z^{-1} denotes the backward shift operator where $z^{-1}y(t)=y(t-1)$. The noise $e(t)$ is assumed to be independent, zero-mean and white.

$$\begin{aligned}
A(z) &= 1+a_1z^{-1}+\ldots+a_{n_a}z^{-n_a}\\
B(z) &= b_1z^{-1}+\ldots+b_{n_b}z^{-n_b}\\
C(z) &= 1+c_1z^{-1}+\ldots+c_{n_c}z^{-n_c}\\
D(z) &= 1+d_1z^{-1}+\ldots+d_{n_d}z^{-n_d}\\
F(z) &= 1+f_1z^{-1}+\ldots+f_{n_f}z^{-n_f}
\end{aligned} \tag{3.5}$$

where $\left\{a_1,\cdots,a_{n_a},b_1,\cdots,b_{n_b},c_1,\cdots,c_{n_c},d_1,\cdots,d_{n_d},f_1,\cdots,f_{n_f}\right\}\in\mathbb{R}$ is the set of model parameters that appropriately weights the relevant lagged input, output or error terms. n_a, n_b, n_c, n_d and n_f are non-negative integers which relate to the orders of the relevant polynomials and are usually known as the model orders or the model dynamic orders. In addition, equation (3.4) can be further simplified as;

$$G(z) = \frac{B(z)}{F(z)A(z)} \tag{3.6}$$

$$H(z) = \frac{C(z)}{D(z)A(z)} \tag{3.7}$$

where $G(z)$ is the input transfer function that describes the dynamics of the system which maps the input $u(t)$ to the output $y(t)$. Usually, the observed output may contain additive noise (due to sampling errors etc.) and other external disturbances which are not related to the system being excited by the input $u(t)$, i.e. uncorrelated disturbances [72]. It is assumed that all such extraneous behaviour to be described by the rational transfer function $H(z)$.

Some of the most common linear black-box models such as the Auto-Regressive model with eXogenous input (ARX) and the Auto-Regressive Moving Average model with eXogenous input (ARMAX) can be derived from the generic representation in equation (3.4) as shown below.

ARX model: By equating $C(z) = D(z) = F(z) = 1$ in equation (3.4);

$$y(t) = \frac{B(z)}{A(z)}u(t) + \frac{1}{A(z)}e(t) \tag{3.8}$$

is the transfer function description of the ARX model. By substituting appropriately from equation (3.5) into equation (3.8) and re-arranging, the time-series representation form of the ARX model shown in equation (3.8) can be obtained as;

$$y(t) = -a_1 y(t-1) - \ldots - a_{n_a} y(t-n_a) + b_1 u(t-1) + \ldots + b_{n_b} u(t-n_b) + e(t) \tag{3.9}$$

ARMAX model: By equating $D(z) = F(z) = 1$ in equation (3.4) the transfer function representation of the ARMAX model can be obtained as shown in equation (3.10) below.

$$y(t) = \frac{B(z)}{A(z)}u(t) + \frac{C(z)}{A(z)}e(t) \tag{3.10}$$

By substituting the relevant polynomials from equation (3.5) in equation (3.10) the time-series description of the ARMAX model can be attained as;

$$\begin{aligned} y(t) = & -a_1 y(t-1) - \ldots - a_{n_a} y(t-n_a) + b_1 u(t-1) + \ldots + b_{n_b} u(t-n_b) \\ & + e(t) + c_1 e(t-1) + \ldots + c_{n_c} e(t-n_c) \end{aligned} \tag{3.11}$$

3.4.2 Non-linear black-box models

When a system exhibits nonlinear characteristics (see Section 3.2), the model structure to be used to represent such a system must also be nonlinear in order to accurately model the system dynamics. The nonlinear extension to the linear ARX model given by equation (3.9), the Nonlinear Auto-Regressive with eXogenous input (NARX) model [90] has been widely used in research in model identification, analysis and control of a variety of complex nonlinear systems [91]–[99]. The NARX model can be represented by the difference equation;

$$y(t) = f(\,x(t)\,) + e(t) \tag{3.12}$$

where,

$$x(t) = (\,y(t-1),\cdots,y(t-n_y),u(t-1),\cdots,u(t-n_u)\,) \tag{3.13}$$

n_y and n_u denotes the maximum lags in the output and input respectively. The nonlinear dynamics are described by the nonlinear mapping function $f(.)$. The most common form of representing the NARX model structure is the polynomial NARX model [24] as shown in equation (3.14) below.

$$\begin{cases} y(t) = f(\,x(t)\,) + e(t) \\ f(\,x(t)\,) = \sum_{n=1}^{N_p} \varphi_n(\,x(t)\,) \\ \varphi_n(\,x(t)\,) = \sum_{p=0}^{n}\left(\sum_{k_1=1}^{n_y}\sum_{k_2=1}^{n_y}\cdots\sum_{k_n=1}^{n_u}\left(C_{p,q}\left(k_1,\cdots,k_{p+q}\right)\prod_{i=1}^{p} y(t-k_i)\prod_{i=p+1}^{p+q} u(t-k_i)\right)\right) \end{cases} \tag{3.14}$$

where n is the polynomial order in which $n=1,\cdots,N_p$ and N_p is the highest degree of polynomial nonlinearity or the maximum polynomial order. $q=n-p$. $\varphi_n(\,x(t)\,)$ is the n^{th} order part of the polynomial NARX model. $C_{p,q}(\cdots)$ refers to the model parameters of the n^{th} degree polynomial terms. For $n=1$, $\varphi_1(\,x(t)\,)$ will contain all the linear combinations of the input and output lagged terms while $\varphi_n(\,x(t)\,)$ for $n\geq 2$ will contain the nonlinear terms resulting from the n^{th} order nonlinear polynomial combinations of different input and output lagged terms.

The extension of the linear model structure ARMAX to the nonlinear instance, the Nonlinear Auto-Regressive Moving Average with eXogenous (NARMAX) model is also widely used in modelling nonlinear systems [24]. The NARMAX model can be represented by equation (3.12) where instead;

$$x(t) = (\,y(t-1),\cdots,y(t-n_y),u(t-1),\cdots,u(t-n_u),e(t-1),\ldots,e(t-n_c)\,) \tag{3.15}$$

in which n_c denotes the maximum lag in the error term $e(t)$. The polynomial NARX polynomial model given in equation (3.14) is composed of linear and nonlinear polynomial combinations of lagged output and input terms. Likewise, the polynomial NARMAX model will be a composition of linear and nonlinear polynomial combinations of the lagged output, input and error terms.

A compact parsimonious description of a wide range of nonlinear systems can be modelled by the NARMAX representation. This possesses a great advantage in the context of CM-FD. This is because NARMAX models can be used to describe complex systems and its faults of nonlinear in nature easily without any prior knowledge of the physics involved due to the black-box character of NARMAX models.

3.5 Parameter estimation

Parameter estimation is the process of estimating a local unbiased solution for a parameterized model structure from a set of input and output data acquired from a system.

Depending on the system under consideration, the model structure used and the main objective of using model identification, a variety of approaches can be taken for parameter estimation. Some of the commonly used methods are the least-squares based methods, recursive estimation, maximum likelihood, Bayesian estimation and evolutionary algorithms. These different methods have been successfully used to obtain unbiased estimates in both linear and nonlinear systems and more details about these methods can be found in [24], [72], [100]–[104]. The scope of the research undertaken falls under the least-squares (LS) based methods and recursive estimation methods based on recursive least squares (RLS). Hence this section of the thesis aims to review these two types of parameter estimation methods.

The black-box time-series models reviewed earlier in this chapter defined in equations (3.9), (3.11), (3.14) and (3.15) can be represented in a linear vector equation form as;

$$y(t) = \mathbf{x}(t)\boldsymbol{\theta} + e(t) \tag{3.16}$$

where $\mathbf{x}(t)$ is the vector of lagged variables, also known as the regression vector and $\boldsymbol{\theta}$ is the parameter vector. Depending on the type of model structure both $\mathbf{x}(t)$ and $\boldsymbol{\theta}$ will take different forms. Denote;

$$\boldsymbol{\varphi}_y(t) = \left[y(t-1), \cdots, y(t-n_y) \right] \tag{3.17}$$

$$\boldsymbol{\varphi}_u(t) = \left[u(t-1), \cdots, u(t-n_u) \right] \tag{3.18}$$

and

$$\boldsymbol{\varphi}_c(t) = \left[e(t-1), \cdots, e(t-n_c) \right] \tag{3.19}$$

In equations (3.17)-(3.19) above, n_y, n_u and n_c signifies the maximum lags in the output, input and the error respectively. Thus the ARX, ARMAX, NARX and NARMAX model structures, represented in equations (3.9), (3.11), (3.14) and (3.15) respectively can also be represented in the vector form as given by equation (3.16) as shown below.

- **ARX model structure:**

$$\mathbf{x}(t) = \left[-\boldsymbol{\varphi}_y(t)\,,\,\boldsymbol{\varphi}_u(t)\right],\ \boldsymbol{\theta} = \begin{bmatrix}\boldsymbol{\theta}_y \\ \boldsymbol{\theta}_u\end{bmatrix} \tag{3.20}$$

where $\boldsymbol{\theta}_y$ and $\boldsymbol{\theta}_u$ are the corresponding parameters that weight the output and input lag terms in $\boldsymbol{\varphi}_y(t)$ and $\boldsymbol{\varphi}_u(t)$ contained in $\mathbf{x}(t)$ respectively.

- **ARMAX model structure:**

$$\mathbf{x}(t) = \left[-\boldsymbol{\varphi}_y(t)\,,\,\boldsymbol{\varphi}_u(t)\,,\,\boldsymbol{\varphi}_c(t)\right],\ \boldsymbol{\theta} = \begin{bmatrix}\boldsymbol{\theta}_y \\ \boldsymbol{\theta}_u \\ \boldsymbol{\theta}_c\end{bmatrix} \tag{3.21}$$

where $\boldsymbol{\theta}_c$ corresponds to the parameters that weight the lagged error terms in $\boldsymbol{\varphi}_c(t)$ contained in $\mathbf{x}(t)$.

- **NARX model structure:**

$$\begin{cases} \mathbf{x}_1(t) = \left[-\boldsymbol{\varphi}_y(t)\,,\,\boldsymbol{\varphi}_u(t)\right] \\ \mathbf{x}(t) = \left[\mathbf{x}_1(t)\,,\,\mathbf{x}_2(t)\,,\cdots,\,\mathbf{x}_N(t)\right],\ \boldsymbol{\theta} = \begin{bmatrix}\boldsymbol{\theta}_1 \\ \boldsymbol{\theta}_2 \\ \vdots \\ \boldsymbol{\theta}_N\end{bmatrix} \end{cases} \tag{3.22}$$

where $\mathbf{x}_n(t)$ for $n = 1,\cdots,N_p$ contains the lagged input-output terms relating to n^{th} degree polynomial NARX model. For $n \geq 2$, the vector $\mathbf{x}_n(t)$ is comprised of the nonlinear lagged terms resulting from the n^{th} order nonlinear combinations between all the terms within the vector $\left[\boldsymbol{\varphi}_y(t)\,,\,\boldsymbol{\varphi}_u(t)\right]$. $\boldsymbol{\theta}_n$ corresponds to the parameters that weight the respective lagged terms contained in $\mathbf{x}_n(t)$.

- **NARMAX model structure:**

$$\begin{cases} \mathbf{x}_1(t) = \left[-\boldsymbol{\varphi}_y(t) , \boldsymbol{\varphi}_u(t) , \boldsymbol{\varphi}_c(t) \right] \\ \mathbf{x}(t) = \left[\mathbf{x}_1(t) , \mathbf{x}_2(t) , \cdots , \mathbf{x}_N(t) \right] , \ \boldsymbol{\theta} = \begin{bmatrix} \boldsymbol{\theta}_1 \\ \boldsymbol{\theta}_2 \\ \vdots \\ \boldsymbol{\theta}_N \end{bmatrix} \end{cases} \tag{3.23}$$

Similar to the NARX case above however, in the NARMAX instance for $n \geq 2$ where $n = 1, \cdots, N_p$, the vector $\mathbf{x}_n(t)$ is comprised of the nonlinear lagged terms resulting from the n^{th} order nonlinear combinations between all the terms within the vector $\left[\boldsymbol{\varphi}_y(t) , \boldsymbol{\varphi}_u(t) , \boldsymbol{\varphi}_c(t) \right]$. $\boldsymbol{\theta}_n$ corresponds to the parameters that weight the respective lagged terms contained in $\mathbf{x}_n(t)$.

The least-squares (LS) method and its variants are the most popular approaches for parameter estimation of model structures whose prediction error term, $e(t)$, does not depend on previous errors are known as models which are linear-in-the parameters. The ARX and the polynomial NARX models both fall under this class, see equations (3.9) and (3.13) respectively. This, however, is not the case with the ARMAX and the NARMAX models, as seen from equations (3.11) and (3.15). Thus, both ARMAX and NARMAX models fall under the category of nonlinear-in-the parameters and require the use of recursive parameter estimation methods.

3.5.1 Least squares

Linear-in-the parameters models can be represented in the matrix format. Therefore, a linear regression model can be formulated given past observations of inputs and outputs, for L number of observations at discrete-time sample t let;

$$\boldsymbol{\Phi} = \begin{bmatrix} \mathbf{x}(1) \\ \vdots \\ \mathbf{x}(L) \end{bmatrix} \tag{3.24}$$

and

$$\mathbf{Y} = \begin{bmatrix} y(1) \\ \vdots \\ y(L) \end{bmatrix} \tag{3.25}$$

where $\boldsymbol{\Phi}$ is the regression matrix containing all the lagged input and output terms. $\mathbf{Y}$ is the vector containing L samples of the observed output of the system. Therefore, the linear regression model is described as;

$$\mathbf{Y} = \mathbf{\Phi}\,\boldsymbol{\theta} + \mathbf{e} \tag{3.26}$$

where $\boldsymbol{\theta}$ contains the parameters of the model that corresponds to the respective lagged terms within the regression matrix $\mathbf{\Phi}$. For ARX type of models $\mathbf{x}(t)$, in equation (3.24) and $\boldsymbol{\theta}$ in equation (3.25) are defined in equation (3.20) accordingly. Similarly for the NARX case the corresponding $\mathbf{x}(t)$ and $\boldsymbol{\theta}$ to form the regression model are defined in equation (3.22) respectively. The estimation of the unknown true parameter vector $\boldsymbol{\theta}$ can be evaluated using the LS method as;

$$\boldsymbol{\theta} = \left[\mathbf{\Phi}^T\,\mathbf{\Phi}\right]^{-1}\mathbf{\Phi}^T\,\mathbf{Y} \tag{3.27}$$

where $\boldsymbol{\theta}$ contains the estimated parameters of the would-be actual parameters in $\boldsymbol{\theta}$. Given, $e(t) = y(t) - \hat{y}(t)$, where;

$$\hat{y}(t) = \mathbf{x}(t)\,\boldsymbol{\theta} \tag{3.28}$$

is the model estimated output, also known as the model generated output or the model predicted output, resulting from the estimated parameters. $\boldsymbol{\theta}$ will be an unbiased local solution to $\boldsymbol{\theta}$ if the resulting $e(t)$ is a zero-mean white-noise sequence.

3.5.2 Recursive least squares

The RLS algorithm evaluates the parameters of a given model recursively at each time step t by minimizing a weighted LS cost function given by;

$$J_{RLS} = \sum_{t=1}^{L} \lambda^{L-t}\left(\, y(t) - \mathbf{x}(t)\,\boldsymbol{\theta}(t-1)\,\right)^2 \tag{3.29}$$

where $\lambda \in \mathbb{R}^+$, known as the *forgetting factor*, is the weight that is used which exponentially gives a lesser weighting to older error samples. The equations involved with the RLS algorithm [100] are given by;

$$e(t) = y(t) - \mathbf{x}(t)\,\boldsymbol{\theta}(t-1) \tag{3.30}$$

$$\mathbf{k}(t) = \mathbf{P}(t-1)\,\mathbf{x}(t)\left(\,\lambda + \mathbf{x}(t)\,\mathbf{P}(t-1)\,\mathbf{x}^T(t)\,\right)^{-1} \tag{3.31}$$

$$\mathbf{P}(t) = \lambda^{-1}\left(\,\mathbf{I} - \mathbf{k}(t)\,\mathbf{x}(t)\,\right)\mathbf{P}(t-1) \tag{3.32}$$

$$\boldsymbol{\theta}(t) = \boldsymbol{\theta}(t-1) + \mathbf{k}(t)\,e(t) \tag{3.33}$$

3.6 Model structure detection

The selecting of a subset of regressors or model terms from a superset of candidate regressors and the estimation of the corresponding parameters that describe the system behaviour is the task of model structure detection. Depending on the manner in which the quality of the model is validated, the model's application and many other factors deem what the best subset of regressors are. This step is of vital importance in the identification of both linear and nonlinear models, in order to attain a parsimonious model that fits the data well while capturing the underlying dynamics of the system present within the data.

Compared to linear models the task of structure detection in nonlinear models is significantly difficult. In the case of polynomial NARX and NARMAX models (see Section 3.4.2) it is often common to select the relevant model terms from a predefined superset of candidate terms [88], [105], [106]. In the case of identifying models for the description of linear systems, usually, this superset is small. However, this is not the case with nonlinear systems. The search space for a model that can describe a nonlinear system rapidly becomes extremely large with the increasing complexity of the system. This can be illustrated as follows: considering a superset of all polynomial NARMAX model terms resulting from a maximum polynomial order $N_p = 3$ and dynamic orders $n_y = n_u = n_c = 3$, the search space is evaluated as [24];

$$S = \frac{\left(n + N_p\right)!}{n!N_p!} \tag{3.34}$$

where $n = n_y + n_u + n_c = 9$. n is the total number of linear lagged terms that would give the nonlinear model terms resulting from all the possible nonlinear polynomial combinations. Thus, the superset of model terms that comprise all the linear and nonlinear terms for the above scenario is $S = 220$ terms. Consequently increasing the maximum polynomial order to $N_p = 4$ would result in $S = 715$ and $N_p = 5$ would result in $S = 2002$. As such, an increase in the maximum polynomial order would rapidly increase the search space. Therefore, model structure detection methods are necessary in order to find a parsimonious description. Furthermore, in the context of real-time CM-FD, an efficient algorithm for model structure detection is vital even for linear systems as brute force approaches are time-consuming.

The model structure detection problem has to main categories which are linear and nonlinear regression. Linear regression is used for the class of models that are linear-in-the-parameters where the residual error terms are not a function of the model terms. In the case of nonlinear-in-the-parameters nonlinear regression is employed.

3.6.1 Linear regression

A variety of linear regression approaches are available and some of the commonly used methods are as follows:

Exhaustive search

This method involves the comparison of competing models resulting from all possible combinations of terms in the superset of candidate model terms. This is a brute force approach and can only be used when the search space is very small because of the computational cost required. However, in a general sense when considering CM-FD, due to the requirement of a relatively fast assessment of system conditions the use of this approach is discouraged.

Forward selection

Adding of model terms from the superset of candidate model terms; one at a time, according to a certain criterion, is known as forward selection. The model is first initialised as an empty set of terms. From the superset of candidate model terms, each competing term is assessed to see how it increases the quality of the model according to a certain measure. Further terms are added, in this manner repeatedly until a specific stopping criterion is satisfied.

Backward elimination

In backward elimination, the model is first initialised as a superset of candidate model terms. Each term is eliminated one at a time based on certain criteria. The elimination of the term should increase the model quality according to a certain measure. This iterative process is terminated if a certain stopping criterion is satisfied. Usually, this approach is used as a pruning method for models that result from, for example, forward selection.

Stepwise regression

An iterative combination of forward selection and backward elimination is involved in stepwise regression. This method can result in better models than using backward elimination, or forward selection separately [107], because some model terms may become redundant at future iterations in the forward selection process [106]. Therefore, each time after adding a certain term through forward selection, based on a certain criterion backward elimination is performed on the current set of terms included in the model. The process is carried out until a stopping criterion is met.

3.6.2 Criteria for model structure selection and model structure detection algorithms

As discussed throughout Section 3.6, model structure detection involves in the selection of appropriate regressors or model terms based on a certain criterion to improve the quality of the model. In this section; two criteria that are commonly used for term selection are introduced.

Orthogonal Least Squares and the ERR criterion

A frequently used method for linear regression is the Orthogonal Least Squares (OLS) method. The OLS method is used in combination with the Error Reduction Ratio (ERR) criterion [108] for the selection of model terms. In order to assess each term independently and sequentially, an orthogonal decomposition of the regression matrix is carried out [109]. The ERR is a measure with the capability of describing the contributions made by each model term to the observed output variance [24]. Thus based on the contribution to maximise the ERR, model terms are selected accordingly [108].

Once the regression matrix $\mathbf{\Phi}$ is orthogonalised to $\mathbf{W} = \left[\mathbf{w}_1, \cdots, \mathbf{w}_{N_s} \right]$, where $\mathbf{w}_i$ is i^{th} auxiliary orthogonal regressor corresponding to the i^{th} regressor in $\mathbf{\Phi}$ where $i = 1, \cdots, N_s$ and N_s is the total number of regressors, the ERR relating to the respective model term or the regressor is given by;

$$ERR_i = \frac{g_i^2 \mathbf{w}_i^T \mathbf{w}_i}{\mathbf{Y}^T \mathbf{Y}} \tag{3.35}$$

where g_i is the auxiliary parameter relating to $\mathbf{w}_i$.

The Forward Regression OLS algorithm (FRO) [109], [110] is a model structure detection method based on the OLS and the ERR criterion to efficiently choose regressors in a forward selection approach. Model terms (regressors) are added at each step using the ERR criterion. The FRO algorithm has been studied extensively in real-world applications and is often used as a benchmark because of the wide body of literature developed for the identification of NARX and NARMAX models [24]. System Identification algorithms such as the FRO method formed around the OLS-ERR strategy fall under the PEM approach.

In practice when the data is not well conditioned, it is difficult to assess the actual significance of a model term using the ERR criterion [106]. This is because the ERR is dependent on the order in which the terms are selected thus the first few terms selected will often be able to explain the observed output variance. Hence, after the first few terms are selected the ERR associated with further model terms drops rapidly even though those model terms might be of actual importance to explain the system dynamics [106], [111]. Therefore, downsampling data is advantageous for structure detection as shown in [28].

Simulation error minimisation

An alternative approach to PEM such as the OLS-ERR based methods is the SEM approach. Piroddi and Spinelli in [106] and Billings and Mao in [86] have used a SEM strategy for System Identification. A model term selection criterion based on this approach was proposed in [106] and is known as the Simulation error Reduction Ratio (SRR). The SRR selects model terms (regressors) based on the ability to predict future data and is given by equation (3.36) below.

$$SRR_j = \frac{MSSE(\mathrm{M}_i) - MSSE(\mathrm{M}_{i+1})}{\frac{1}{L}\left(\mathbf{Y}^T\mathbf{Y}\right)} \tag{3.36}$$

in which the model obtained at the i^{th} iteration is M_i and M_{i+1} is the model attained at the subsequent iteration with the inclusion of the j^{th} candidate model term. $MSSE$ is the mean squared simulation error between the observed output and the simulation output. The simulation output of a model is also known as the model predicted output. Thus, SRR_j is defined as the decrease in the $MSSE$ attained by the inclusion of the j^{th} candidate model term which is normalised against the output variance. It is reported that the models with a better long rage prediction accuracy can be attained by using criteria based on the model predicted output for model structure detection [86], [106]. However, such criteria come with higher computational cost due to the repeated simulations that are needed to be done for the assessment of models.

3.6.3 Non-linear regression

Considering the class of model structures which are nonlinear-in-the-parameters such as ARMAX and NARMAX models, nonlinear regression methods are to be used for the model structure detection problem of these models. The regression matrix of these types of models contains lagged residual error terms, $e(t-i)$ where $i = 1,\cdots,n_c$. Furthermore, these lagged residual error terms are dependent on the model structure since $\hat{e}(t-i) = y(t-1) - \hat{y}(t-1)$ where $\hat{y}(t) = \mathbf{x}(t)\,\boldsymbol{\theta}$ (see Section 3.5). Therefore, linear regression based model structure detection methods and criteria mentioned earlier cannot be applied directly to nonlinear regression. In [108], modification to the ERR based linear regression procedures is introduced as a solution to the nonlinear regression problem. This method is summarised as follows;

1. Assuming the residual errors to be zero as if identifying a NARX/ARX model, detect the model structure and estimate all model parameters which do not include any of the residual error terms using OLS-ERR based procedures.

2. Evaluate the residual error, $\hat{e}(t)$, between the observed system output $y(t)$ and the estimated output of the model $\hat{y}(t)$ obtained in step 1.

3. Using the same OLS-ERR based procedures detect the structure of the noise model (the sub model containing the residual error terms), the MA part of NARMAX/ARMAX models and estimate the parameters associated with the residual error terms.

4. Repeat steps 2 and 3 iteratively until a certain convergence test is satisfied.

When identifying noise models, the process model (the sub model containing all terms not associated with the residual error terms) is to be first identified.

3.7 Model selection

The process of model selection is distinctively different from structure detection. Model structure detection is the procedure of selecting the appropriate lagged terms to be included in the model. Model structure detection algorithms often can provide more than one competing model from which to choose. An example of this instance is, by varying the ERR threshold in the FRO algorithm, the search path of the algorithm changes thus providing different competing models. Model selection is the methodology of choosing an appropriate model, from a set of candidate models that is able to predict unseen data fairly well while attaining a good bias-variance compromise.

3.7.1 Bias-variance trade-off in models

Bias and variance in model predictions occur due to different sources of error in the modelling process. Simply, bias relates to how the well model fits a certain data set. While variance relates to, the flexibility of the model to describe different aspects of a system (for example, one model to describe different operating points) [72].

In order for a model to be more flexible or less bias, it needs to be more complex. In parametric models, this relates to a higher number of terms [112]. Increasing the number of terms reduces the error between the model prediction and the observed value. However, this leads to the model fitting the data too well, including the noise (overfitting) in the data resulting, in a higher variance. Conversely, decreasing the model number of model terms leads to a decreased fit and hence a higher bias but a lower variance.

Given that a new dataset was obtained when the system was in the same operating conditions as the dataset for identification was acquired. The performance of the model over this unseen data will be poor in both overly complex and overly simple models. This is because an overly simple model will not be able to capture the underlying true dynamics of the system and an overly complex model is fitted to random noise sequences [24], [72]. Thus, the choice of an appropriate model structure is, therefore, a compromise. This trade-off depends on the required purpose of the model [72].

AIC (Akaike's Information Criteria), FPE (Final Prediction Error) and BIC (Bayesian Information Criteria) are commonly used model selection criteria. These information

criteria give a score to models in relation to the error between the models predicted output and the observed output and the model complexity. The scoring is such that a certain penalty is applied when the model complexity is relatively higher. The models that yield the lowest score is to be chosen. In comparison to AIC and FPE, BIC applies a higher penalty for a higher model complexity [71]. Therefore, the models that result in minimising the BIC score will have a lesser complexity in comparison to models that are obtained when minimising the AIC and FPE scores.

3.8 Model validation

A true description of a system can never be attained from an identified model and at best can only be considered as a sufficient representation of certain aspects that are of interest [72]. Model validation tests are therefore needed to be carried out on identified models. These tests assess whether the model performance is valid and to put certain confidence on the model for its intended purpose.

Model validation tests in System Identification of parametric models are based on the residuals produced between the model generated output and the actual output of the system [24], [72]. These tests are carried out, utilizing a separate dataset to the dataset used for estimating the parameters. To validate models, commonly used methods comprised of various correlation tests performed on the residuals. Furthermore, different performance indicators are used to examine the goodness-of-fit [68], [72].

The residuals represent the fragments of validation dataset that cannot be produced or explained by the model. Hence, correlation tests on the residuals are carried out in order to know whether;

- The residuals are white noise sequences. This test is called the autocorrelation test and is performed in order to realise that the model can explain the actual output appropriately [72].

- The residuals are not correlated with the input. This test is performed in order to validate that the model can explain the necessary part of the dynamics from the input to the output [72]. It is known as the cross-correlation test. It should be noted that if there is feedback present in the system then, correlations are expected in the negative lags between the input and the residuals. If so, the test is done concentrating on the positive lags.

In order to quantify the goodness-of-fit performance indicators such as the MSE (Mean Square of Error), RMSE (Root Mean Square Error) are commonly used.

3.9 Summary

In this chapter, the time-domain characteristics of linear and nonlinear systems in relation to convolutional integral functions were discussed. Therefore, a detailed overview of System Identification and related procedures were provided. Model structure representations of both linear and nonlinear time-series were outlined. Different term selection methods in linear regression and a commonly used method for nonlinear regression in the OLS-ERR framework was discussed. Commonly used model structure selection criteria under two different approaches to System Identification in the forward selection framework were outlined. System Identification, is the first step that is used as a tool for capturing the system dynamics in the CM-FD method based on the control systems analysis approach. In the next chapter, the Frequency Response Analysis methods are reviewed, in relation to linear and nonlinear systems.

Chapter 4

Frequency Response Analysis of Dynamic Systems

4.1 Introduction

In the field of control systems engineering, FRFs are used for in-depth dynamic analysis, design and control of various systems [72], [75]. Linear frequency domain methods are popularly used in the field of control and are comprehensive tools for both implementations of control strategies, as well as analysis and interpretation of system dynamics [35]. Across many disciplines of science, especially in engineering, the analysis of systems in the frequency domain is thus considered of fundamental importance [72], [75]. The GFRF and NOFRF methodologies extend the use of Frequency Response Analysis from linear to non-linear systems.

The frequency response of analysis of an identified ARX model for linear systems can be done by transforming the time-domain difference equation of the model into the discrete domain (z - domain) to obtain the discrete FRF. In the case of nonlinear systems, the output frequency characterisation is significantly more complex than in the linear systems. As such, the Volterra series based methods such as the GFRFs or the NOFRFs can be used to project the identified NARX model into the frequency domain. The GFRFs are the direct extension of the FRF to the nonlinear instance. In comparison, the NOFRFs show the energy transfers from the input to different orders of nonlinearities in the frequency domain and it is considered a more natural extension of the linear FRF to the nonlinear instance [29].

This chapter aims to introduce the basic concepts of Frequency Response Analysis and the output frequency characterisation of linear and nonlinear systems. In the context of Condition Monitoring and Fault Diagnosis of nonlinear systems, the concept of NOFRFs is of interest. This is because the output frequency characterisation of nonlinear systems using NOFRFs is similar to the linear FRF. Furthermore, the NOFRFs has clear advantages over the GFRFs when concerning computational effort and ease of interpretation. Thus, with regard to nonlinear systems Frequency Response Analysis, this chapter focuses more on the NOFRFs.

4.2 Analysis of linear systems in the frequency domain

In control systems analysis and design, frequency domain analysis of linear systems is carried out using the well-established methodology of linear FRFs. A complete description of the steady-state dynamics of a linear system is provided by the linear FRF and so, is unique regardless of the time-domain model used to represent the system [72]. The quantitative measure of the output spectra of a system in response to an exciting input is known as frequency response or Frequency Response Function of that system. The FRF of a system is a tool used to observe the system dynamics over a range of frequencies. It's a comparison of, output magnitude and phase, with regard to the input as a function of frequency in the format of a bode plot [75]. Essentially the ratio of the output spectrum to the input spectrum. In LTI systems the output frequency response, for all frequencies ω can be explicitly characterised, given the knowledge of the FRF, for any input signal as;

$$Y(j\omega) = G(j\omega)U(j\omega) \tag{4.1}$$

where $Y(j\omega)$ and $U(j\omega)$ are the frequency spectra of the output and the input respectively and $G(j\omega)$ is the FRF.

The FRF can be interpreted as a nonparametric model of a linear system in the frequency domain and can be readily evaluated from an identified ARX model. The estimated ARX model after System Identification of an actual linear system is given by;

$$\hat{y}(t) = -\hat{a}_1\hat{y}(t-1) - \ldots - \hat{a}_{n_a}\hat{y}(t-n_a) + \hat{b}_1u(t-1) + \ldots + \hat{b}_{n_b}u(t-n_b) \tag{4.2}$$

where $\hat{y}(t)$ is the estimated output from the model and $u(t)$ is the actual input to the system. $\hat{a}_1,\cdots,\hat{a}_{n_a}$ and $\hat{b}_1,\cdots,\hat{b}_{n_b}$ are the estimated parameters corresponding to the output and input lagged terms. Re-arranging equation (4.2) and taking the z - transform (representing in terms of the forward shift operator) of both sides of the difference equation will result in the corresponding estimated z - domain (discrete domain) transfer function;

$$\hat{G}(z) = \frac{\hat{y}(z)}{u(z)} = \frac{b_1z^{-1} + \ldots + b_{n_b}z^{-n_b}}{1 + a_1z^{-1} + \ldots + a_{n_a}z^{-n_a}} \tag{4.3}$$

Over a given set of angular frequency points ω, by equating $z = e^{j\omega T_s}$ [113] in (4.3) the corresponding estimated discrete linear FRF can thus be evaluated as;

$$\hat{G}(j\omega T_s) = \frac{\hat{b}_1e^{-j\omega T_s} + \ldots + \hat{b}_{n_b}e^{-n_bj\omega T_s}}{1 + \hat{a}_1e^{-j\omega T_s} + \ldots + \hat{a}_{n_a}e^{-n_aj\omega T_s}} \qquad 0 \le \omega T_s \le \pi \tag{4.4}$$

where T_s is the sampling period. It should be noted that due to the periodic and symmetric characteristics of the discrete FRF the effective frequencies of interest is given by $0 \le \omega \le f_s/2$ where $f_s = 2\pi/T_s$ is the sampling frequency in radians per second. If the ARX model identified can describe the dynamics of the system well, then the estimated discrete FRF $\hat{G}(j\omega T_s)$ evaluated using (4.4) will be a good estimate to the actual continuous time FRF $G(j\omega)$ of the system. Hence features from $\hat{G}(j\omega T_s)$ can be used effectively for CM-FD of a system that can be adequately described by an ARX model.

4.3 Analysis of non-linear systems in the frequency domain

It is well-established that the possible output frequency components of linear systems are the same as the frequency components contained within the input signal [72], [75]. However, this is not the same in the nonlinear instance, in which the output frequency response of nonlinear systems is much more complex. A simple example of this would be, if the input to a nonlinear system is only composed of a single frequency component ω_1. Then the corresponding output may contain the input frequency component ω_1, its super-harmonics such as $2\omega_1$, $3\omega_1$ and sub-harmonics such as $\omega_1/2$, $\omega_1/3$ and so on. However, if the input contains many frequency components, for example ω_1, ω_2, ω_3. Then the possible frequency components of the output will be composed of the original input frequencies ω_1, ω_2, ω_3, the super-harmonics and sub-harmonics of those frequencies and also frequency components, that arise from the intermodulation between the input frequencies such as $\omega_1 - \omega_2$, $\omega_1 - \omega_2 + \omega_3$, $\omega_1 + \omega_3$ so on with many others. Therefore, nonlinear systems hold a distinct property in comparison to its linear counterparts. Explicitly, the output spectra of nonlinear systems are much richer and reveal more frequency components than the associated input spectra. Hence, it is well known that in the nonlinear instance there is a transference of energy from the input frequency modes, to other modes of frequencies, which is known as the nonlinear phenomena [29], [114]–[117]. Figure 4.1 illustrates this phenomenon in a more general sense.

Concerning CM-FD of nonlinear systems, it is therefore important to consider the behaviour of nonlinear systems as certain faults exhibit nonlinear characteristics [13]. Thus linear analysis methods would not be sufficient to characterise these faults and nonlinear systems analysis methods are needed to be used [16], [118], [119]. In the context of a control systems analysis approach to CM-FD, this section aims to review the Frequency Response Analysis methods used for nonlinear systems, the GFRFs and the NOFRFs. These are extensions of the linear system Frequency Response Analysis method, the linear FRFs, to the nonlinear instance.

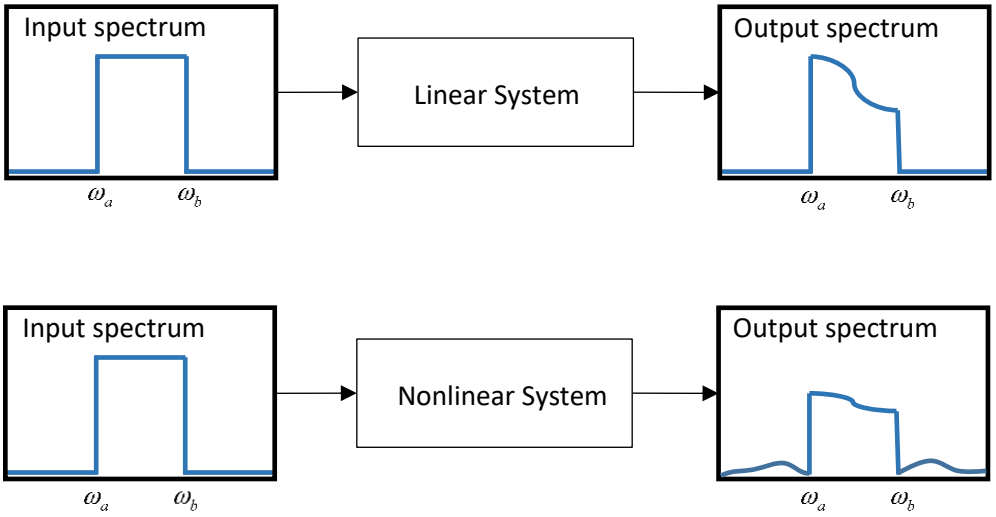

Figure 4.1: Comparison between the output frequency responses of linear and nonlinear systems. $[\omega_a, \omega_b]$ is the frequency range of the input spectrum. The output spectrum of a linear systems is explicitly within this range. While the output spectrum of nonlinear systems will contain frequency components that are present in the input and other frequency components outside the input frequency range.

4.3.1 Output frequency response of non-linear systems

In Section 4.2 the output frequency response characteristics of linear systems are defined by equation (4.1). However, as mentioned above, because of the complex nature of the output frequency response of nonlinear systems, equation (4.1) is not valid in the nonlinear instance. The time domain description of a class of nonlinear systems that are stable at zero equilibrium can be described by the Volterra series as shown in equation (3.2) and is discussed in Section 3.2. Based on this description of nonlinear systems Lang and Billings in [117] derived an expression to characterise the output frequency response $Y(j\omega)$ of a nonlinear system as;

$$\begin{cases} Y(j\omega) = \sum_{n=1}^{N} Y_n(j\omega) \ \ for \ \forall\omega \\ Y_n(j\omega) = \dfrac{1/\sqrt{n}}{(2\pi)^{(n-1)}} \displaystyle\int_{\omega=\omega_1+\cdots+\omega_n} H_n(j\omega_1,\ldots,j\omega_n) \prod_{i=1}^{n} U(j\omega_i)\, d\sigma_{n\omega} \end{cases} \tag{4.5}$$

where N is the highest order of nonlinearity to be considered. $Y_n(j\omega)$ is the frequency characteristics of the n^{th} order nonlinear output (output frequency response of the n^{th} order nonlinearity) and $U(j\omega)$ is the frequency spectra of the input. $H_n(j\omega_1,\ldots,j\omega_n)$ is defined as the n^{th} order GFRF which provides a description of the dynamic characteristics

of the n^{th} order nonlinearity in the frequency domain. Thus, the GFRFs are the direct extension of the linear FRF to the nonlinear case and similarly, the GFRF is unique regardless of the time-domain model used to represent the corresponding nonlinear system. The natural extension of equation (4.1) which characterises the output frequency response of linear systems to the nonlinear instance is given by the expression in equation (4.5) above.

The generation of the output frequencies of a nonlinear system, as shown by equation (4.5) is the sum over the output frequencies contributed by each order of nonlinearity, $Y_n(j\omega)$. Thus by considering the output frequency range f_{Y_n} of each nonlinear order $Y_n(j\omega)$, the frequency range, f_Y of the output response of a nonlinear system is much greater [116], [117] such that;

$$f_Y = \bigcup_{n=1}^{N} f_{Y_n} \tag{4.6}$$

In [116] the authors presented a general algorithm which can be used to evaluate the possible output frequency ranges of a nonlinear system, that can be explained using the Volterra series, using the frequency range of the input excitation signal. This algorithm can be used with any bandlimited frequency range $[a\ ,\ b]$ in which the input spectrum can be described as;

$$U(j\omega) = \begin{cases} U(j\omega) & when\ |\omega| \in (a,b) \\ 0 & otherwise \end{cases} \tag{4.7}$$

where $b > a \geq 0$. The detail description of the algorithm is as follows;

$$\begin{cases} f_Y = \bigcup_{n=1}^{N} f_{Y_n} \\ f_{Y_n} = \begin{cases} \bigcup_{k=0}^{i^*-1} I_k \ , when\ \dfrac{nb}{(a+b)} - \left\lfloor \dfrac{na}{(a+b)} \right\rfloor < 1 \\ \bigcup_{k=0}^{i^*} I_k \ , when\ \dfrac{nb}{(a+b)} - \left\lfloor \dfrac{na}{(a+b)} \right\rfloor \geq 1 \end{cases} \\ where \lfloor . \rfloor\ means\ to\ take\ the\ ineteger\ part \\ i^* = \left\lfloor \dfrac{na}{(a+b)} \right\rfloor + 1 \\ I_k = \left[na - k(a+b)\ ,\ nb - k(a+b) \right]\ for\ k = 0, \cdots, i^* - 1 \\ I_{i^*} = \left[0\ ,\ nb - i^*(a+b) \right] \end{cases} \tag{4.8}$$

where f_Y and f_{Y_n} are the possible non-negative frequency ranges of the output frequency spectrum $Y(j\omega)$ and the output frequency spectrum of the n^{th} order system nonlinear output $Y_n(j\omega)$, respectively. This algorithm can also be applied to the case of single tone sinusoidal inputs where $a = b$. It should be noted, although this algorithm can be used for the evaluation of the possible output frequency ranges of nonlinear systems as well as the output frequency ranges of each individual nonlinear order. It does not provide any information on the exact output frequencies. Lang and Billings in [29] introduced the concept of NOFRFs which can provide this information.

4.3.2 Generalised Frequency Response Functions

The behaviour of nonlinear systems, as discussed earlier, is vastly more complex than linear systems. This can be seen from the time domain description of nonlinear systems using the Volterra series, as shown in equation (3.2) as compared to the linear counterpart shown in equation (3.1), where the time domain dynamics of each order of nonlinearity is described by separate multidimensional Volterra kernels. The Fourier transform of the time-domain impulse response of a linear system, $h(t)$ in equation (3.1) is defined as the linear FRF [72]. Similarly, George in [120] introduced the concept of GFRFs defined as the Fourier transform of the Volterra kernels, $h_n(\tau_1,\cdots,\tau_n)$ terms in equation (3.2) and the GFRF of a n^{th} order nonlinearity is thus given by;

$$H_n(j\omega_1,\ldots,j\omega_n) = \int_{-\infty}^{+\infty}\cdots\int_{-\infty}^{+\infty} h_n(\tau_1,\cdots,\tau_n)\times e^{-(\omega_1\tau_1+\ldots.+\omega_n\tau_n)j}\,d\tau_1\cdots d\tau_n \tag{4.9}$$

Hence the concept of GFRFs is the direct extension of the linear FRF to the nonlinear case. As seen from equation (4.9) GFRFs are multidimensional frequency functions and it describes the complex dynamics of each order of nonlinearity.

In linear systems, the FRF can be used explicitly to characterise the output frequency response of a linear system as shown in equation (4.1) and discussed in Section 4.2. This, however, is not the same in the case of nonlinear systems because of the association of high dimensional frequency functions of each order of system nonlinearities [117], [121]. To explain this complex relationship between the GFRFs and the system output frequency response, Lang and Billings in [117] derived the expression shown in equation (4.5) in Section 4.3.2. As discussed earlier this expression characterises the output frequency response of nonlinear systems in terms of the GFRFs. It is shown by this expression how the n^{th} order nonlinear dynamics (n^{th} order GFRF) operate on the input spectrum to produce the output frequency response of the corresponding nonlinearity, $Y_n(j\omega)$, and thus, the sum of all the output spectra of all nonlinearities add up to the actual output frequency response, $Y(j\omega)$, of the system.

As discussed earlier nonlinear systems exhibit a distinct property in which there is a transference of energy from the input frequencies to other frequencies that are not

present in the input. This is because of how the n^{th} order nonlinear dynamics operate on the input spectrum to result in the final output frequency response, as mentioned above. Thus, this phenomena cannot be completely explained by GFRFs [29]. Lang and Billings introduced the concept of NOFRFs in [29] which can comprehensively describe the energy transference from the input to different orders of system nonlinearities and thus, the generation of new frequency components. The NOFRFs can be considered as another extension of the linear FRF to the nonlinear instance and so complements the GFRFs. The NOFRFs and its properties will be discussed in detail in the following section along with its viability for CM-FD over the GFRFs.

4.3.3 Non-linear Output Frequency Response Functions

Lang and Billings in [29] introduced the concept of NOFRFs in order to explain the energy transfer phenomena of nonlinear systems. The authors, in [29], also introduced another concept, which is the natural extension of the input spectrum $U(j\omega)$ to the n^{th} order nonlinear case and is given by;

$$U_n(j\omega) = \frac{1/\sqrt{n}}{(2\pi)^{(n-1)}} \int_{\omega=\omega_1+\cdots+\omega_n} \prod_{i=1}^{n} U(j\omega_i)\, d\sigma_{n\omega} \tag{4.10}$$

where $U_n(j\omega)$ is the n^{th} order nonlinear composition of the input $U(j\omega)$ and can be considered as the output frequency response of a n^{th} order static nonlinear system [29] such as;

$$y(t) = k u^n(t) \tag{4.11}$$

in which $k = 1$ and the output frequency response is given by;

$$Y(j\omega) = k U_n(j\omega) \tag{4.12}$$

where $U_n(j\omega)$ is related to the Fourier transform, $FT\{.\}$, of $u^n(t)$ such that;

$$U_n(j\omega) = \frac{1/\sqrt{n}}{(2\pi)^{(n-1)}} \times FT\{u^n(t)\} \tag{4.13}$$

The concept of $U_n(j\omega)$ is of importance in the explanation of the energy transfer phenomena of nonlinear systems and in the definition of the NOFRFs, as shown in [29], which will be discussed below.

The second expression in equation (4.5), the output frequency response of the n^{th} order nonlinearity $Y_n(j\omega)$ is restated here as;

$$Y_n(j\omega) = \frac{1/\sqrt{n}}{(2\pi)^{(n-1)}} \int_{\omega=\omega_1+\cdots+\omega_n} H_n(j\omega_1, \ldots, j\omega_n) \prod_{i=1}^{n} U(j\omega_i)\, d\sigma_{n\omega} \tag{4.14}$$

Equation (4.14) can be written in terms of equation (4.10) as;

$$Y_n(j\omega) = \frac{\displaystyle\int_{\omega=\omega_1+\cdots+\omega_n} H_n(j\omega_1,\ldots,j\omega_n)\prod_{i=1}^{n}U(j\omega_i)d\sigma_{n\omega}}{\displaystyle\int_{\omega=\omega_1+\cdots+\omega_n}\prod_{i=1}^{n}U(j\omega_i)d\sigma_{n\omega}} \times \left(\frac{1/\sqrt{n}}{(2\pi)^{(n-1)}} \int_{\omega=\omega_1+\cdots+\omega_n}\prod_{i=1}^{n}U(j\omega_i)d\sigma_{n\omega} \right) \tag{4.15}$$

Since the expression in the parenthesis in equation (4.15) above is $U_n(j\omega)$, $Y_n(j\omega)$ therefore can be re-written in the form;

$$Y_n(j\omega) = G_n(j\omega)U_n(j\omega) \tag{4.16}$$

where

$$G_n(j\omega) = \frac{\displaystyle\int_{\omega=\omega_1+\cdots+\omega_n} H_n(j\omega_1,\ldots,j\omega_n)\prod_{i=1}^{n}U(j\omega_i)\,d\sigma_{n\omega}}{\displaystyle\int_{\omega=\omega_1+\cdots+\omega_n}\prod_{i=1}^{n}U(j\omega_i)\,d\sigma_{n\omega}} \tag{4.17}$$

G_n in equation (4.17) above is defined as the n^{th} order NOFRF. $G_n(j\omega)$ is only valid in the frequency space ω in which;

$$\int_{\omega=\omega_1+\cdots+\omega_n}\prod_{i=1}^{n}U(j\omega_i)\,d\sigma_{n\omega} \neq 0 \tag{4.18}$$

Thus the output frequency response $Y(j\omega)$ of a nonlinear system, shown in equation (4.5) in Section 4.3.1, can be explicitly expressed using the NOFRFs $G_n(j\omega)$, $n=1,\cdots,N$ [29] by introducing equation (4.16) into equation (4.5) as;

$$Y(j\omega) = \sum_{n=1}^{N} Y_n(j\omega) = \sum_{n=1}^{N} G_n(j\omega)U_n(j\omega) \tag{4.19}$$

where N is the highest order of nonlinearity to be considered. Therefore, equation (4.19) can be defined as the NOFRFs based characterisation of the output frequency response of a nonlinear system [29]. It can be seen that this description of the output frequency response of nonlinear systems is similar to that of the linear systems description in equation (4.1). The authors of [29] outlined three important properties of the NOFRFs representation of $Y(j\omega)$ and these are summarised as follows;

1) The NOFRFs are able to describe $Y_n(j\omega)$ in an identical manner to how the linear FRF describes the output frequency response of linear systems, equation (4.1) in Section 4.2 and thus the complete characterisation of $Y(j\omega)$ in equation (4.19) is of a similar nature.

2) For a signal given by equation (4.7), in Section 4.3.1, the valid frequency range ω of the n^{th} order NOFRF $G_n(j\omega)$ given by equation (4.18) is equal to f_{Y_n}, in equation (4.8) of Section 4.3.1, which is the possible output frequency range contributed by the n^{th} order nonlinearity.

3) The NOFRFs are input dependent, as seen by equation (4.17). However, it is insensitive to a change of the input spectrum $U(j\omega)$ by a constant amplitude gain. This is shown by equation (4.20) below.

$$G_n(j\omega)\Big|_{U(j\omega)=\alpha\bar{U}(j\omega)} = \frac{\alpha^n \int_{\omega=\omega_1+\cdots+\omega_n} H_n(j\omega_1,\cdots,j\omega_n)\prod_{i=1}^{n}\bar{U}(j\omega_i)\,d\sigma_{n\omega}}{\alpha^n \int_{\omega=\omega_1+\cdots+\omega_n} \prod_{i=1}^{n}\bar{U}(j\omega_i)\,d\sigma_{n\omega}} = G_n(j\omega)\Big|_{U(j\omega)=\bar{U}(j\omega)} \tag{4.20}$$

Lang and Billings [29] evidently described the energy transfer phenomena and the generation of new frequency components using the concept of NOFRFs. In brief, this energy transfer mechanism is as follows;

- The nonlinear composition of $U_n(j\omega)$ from $U(j\omega)$ produces the possible frequency components f_{Y_n} of $Y_n(j\omega)$.

- The NOFRF $G_n(j\omega)$ functions like a dynamic filter over the frequency range of f_{Y_n} which operates on $U_n(j\omega)$ to produce the n^{th} order output frequency response $Y_n(j\omega)$ of the system. This is a clear reflection of the third property of the NOFRFs above along with equation (4.15).

- The combined effect of the output frequency responses of all the nonlinearities, $Y_n(j\omega)$ for $n=1,\cdots,N$ thus produces the final output frequency response $Y(j\omega)$.

- Hence $Y(j\omega)$ will contain more frequency components than the corresponding excitation output $U(j\omega)$. This is illustrated in Figure 4.2.

The NOFRFs $G_n(j\omega)$ for $n \geq 2$, as seen from equation (4.17), is clearly dependent on the frequency domain characteristics of the n^{th} order nonlinear dynamics (which is described by the GFRF $H_n(j\omega_1, \cdots, j\omega_n)$ and the input spectrum. This reliance of $G_n(j\omega)$ on the input spectrum is a clear reflection on the fact that the behaviour of nonlinear systems in the frequency domain, in general, depends on the system properties and the corresponding input as well [116], [117].

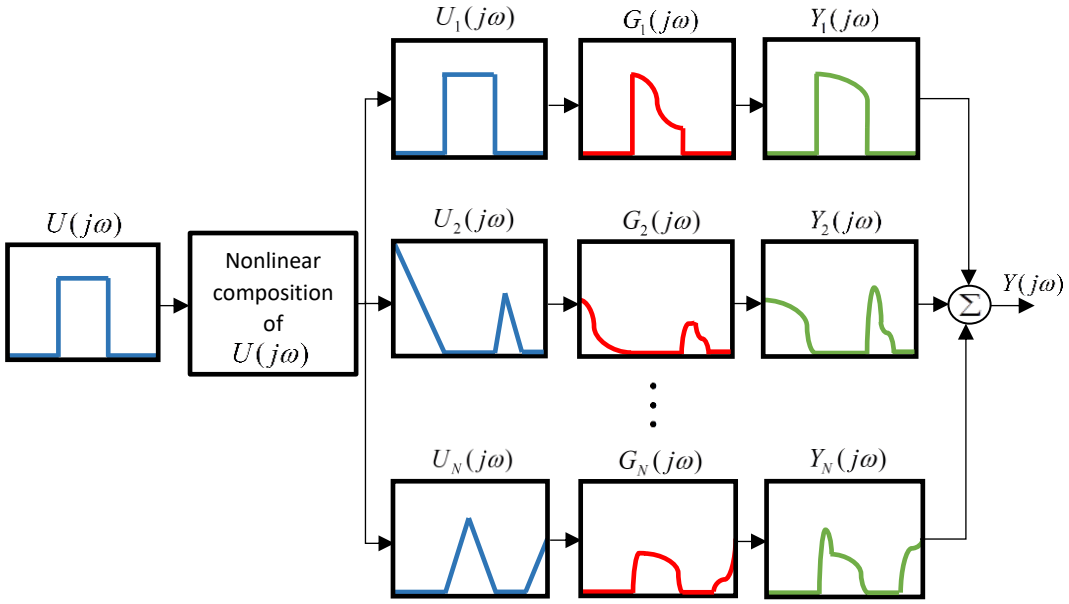

Figure 4.2: Pictorial representation of how the NOFRFs act on the input spectrum to produce the final output frequency response of a nonlinear system. $U_n(j\omega)$ is the nonlinear composition of the input spectrum $U(j\omega)$ is attenuated by the n^{th} order NOFRF $G_n(j\omega)$ to form the output frequency response of the n^{th} order nonlinearity $Y_n(j\omega)$ of the system and thus the final output frequency response .

It is evident from equation (4.17) that the effect $U(j\omega)$ has on the n^{th} order NOFRF $G_n(j\omega)$ is complex. However, the authors of [29] qualitatively explained the relationship between $U(j\omega)$ and $G_n(j\omega)$ by re-writing equation (4.17) as;

$$G_n(j\omega) = \int_{\omega=\omega_1+\cdots+\omega_n} H_n(j\omega_1, \ldots, j\omega_n) \times \left(\frac{\prod_{i=1}^{n} U(j\omega_i)\, d\sigma_{n\omega}}{\int_{\omega=\omega_1+\cdots+\omega_n} \prod_{i=1}^{n} U(j\omega_i)\, d\sigma_{n\omega}} \right) \qquad (4.21)$$

In equation (4.21) ;

- $\int_{\omega=\omega_1+\cdots+\omega_n} \prod_{i=1}^{n} U(j\omega_i)\, d\sigma_{n\omega}$ is the summation of $\prod_{i=1}^{n} U(j\omega_i)$ over the *n*-dimensional hyperplane $\omega = \omega_1 + \cdots + \omega_n$.

- Thus, $\left(\dfrac{\prod_{i=1}^{n} U(j\omega_i)\, d\sigma_{n\omega}}{\int_{\omega=\omega_1+\cdots+\omega_n} \prod_{i=1}^{n} U(j\omega_i)\, d\sigma_{n\omega}} \right)$ is the normalisation of $\prod_{i=1}^{n} U(j\omega_i)$ in the same $n-$ dimensional hyperplane.

- This normalisation of $\prod_{i=1}^{n} U(j\omega_i)$ acts as a weight to the GFRF $H_n(j\omega_1, \cdots, j\omega_n)$ at each point of $\{\omega_1, \cdots, \omega_n\}$.

- Thus the n^{th} order NOFRF $G_n(j\omega)$ can be described as the weighted sum of the n^{th} order GFRF $H_n(j\omega_1, \cdots, j\omega_n)$ across the *n*–dimensional hyperplane $\omega = \omega_1 + \cdots + \omega_n$.

- Therefore, the n^{th} order NOFRF $G_n(j\omega)$ mainly relies on the corresponding GFRF $H_n(j\omega_1, \cdots, j\omega_n)$. This also points out how $G_n(j\omega)$ is formed through the effect of the input spectrum $U(j\omega)$, revealing the manner in which $H_n(j\omega_1, \cdots, j\omega_n)$ is combined across the $n-$ dimensional hyperplane to form the final output frequency response.

The qualitative description above of the NOFRFs emphasises that the NOFRFs are sensitive to the dynamics of a nonlinear system because of its key reliance on the GFRFs. This is fundamental in using the concept of NOFRFs for the analysis of nonlinear systems and thus CM-FD. Furthermore, the NOFRFs is one-dimensional in nature therefore, NOFRFs can be easily interpreted and visual analysis of higher order nonlinearities is possible [29], [114], [122]. The concept of NOFRFs, unlike the GFRFs, are input dependent however, in the case of sinusoidal or harmonic inputs there is an exception. Peng *et al.* in [114], [122] described in detail that the NOFRFs in the instance of a harmonic input is explicitly independent of the input. Thus the valid frequency components of the n^{th} order NOFRF under a harmonic input (shown in equation (4.18) and can be evaluated using the algorithm in equation (4.8)) is equal to the n^{th} order GFRF at the corresponding frequencies.

These are the clear advantages of NOFRFs over the multi-dimensional GFRFs. GFRF based Fault Diagnosis schemes have been proposed before in [18]. However, due to the multidimensional nature of the GFRFs, as seen from equation (4.9), it is difficult to interpret [121]. Therefore, it comes with a significant computational cost to process and to extract information due to the amount of memory involved [16].

In reason to the ease of use of the NOFRFs, it was proposed as a viable tool for CM-FD of nonlinear systems by Peng *et al.* in [13]. The same authors in [119] showed how cracks could be detected using NOFRFs. In [19] a feasibility study was conducted in structural damage assessment of aluminium plates by identification of a NARX model and then using the NOFRFs for the analysis. Furthermore, the concept of NOFRFs has been used in many real-world applications of CM-FD [16], [118], [123]–[125].

Evaluation of NOFRFs using a least squares approach

Equation (4.19), the NOFRFs based description of the output frequency response $Y(j\omega)$ of a nonlinear system, can be represented as;

$$\begin{aligned} Y(j\omega) &= \sum_{n=1}^{N} Y_n(j\omega) = \sum_{n=1}^{N} G_n(j\omega)U_n(j\omega) \\ &= \sum_{n=1}^{N} \left(G_n^R(\omega) + jG_n^I(\omega)\right)\left(U_n^R(\omega) + jU_n^I(\omega)\right) \\ &= \sum_{n=1}^{N} \left(G_n^R(\omega)U_n^R(\omega) - G_n^I(\omega)U_n^I(\omega)\right) + j\left(G_n^R(\omega)U_n^I(\omega) + G_n^I(\omega)U_n^R(\omega)\right) \end{aligned} \tag{4.22}$$

where $G_n^R(\omega)$ and $G_n^I(\omega)$ are the respective real and imaginary parts of $G_n(j\omega)$ while $U_n^R(\omega)$ and $U_n^I(\omega)$ are the real and imaginary parts of $U_n(j\omega)$ respectively at the corresponding frequency point ω. Therefore, equation (4.22) can be represented in a linear regression format as;

$$\begin{bmatrix} \mathrm{Re}Y(j\omega) \\ \mathrm{Im}Y(j\omega) \end{bmatrix} = \begin{bmatrix} U_1^R(\omega), & \cdots, U_N^R(\omega), & -U_1^I(\omega), & \cdots, -U_N^I(\omega) \\ U_1^I(\omega), & \cdots, U_N^I(\omega), & U_1^R(\omega), & \cdots, U_N^R(\omega) \end{bmatrix} \begin{bmatrix} \mathbf{G}^R(\omega) \\ \mathbf{G}^I(\omega) \end{bmatrix} \tag{4.23}$$

where $\mathbf{G}^R(\omega) = \left[G_1^R(\omega), \cdots, G_N^R(\omega)\right]^T$ and $\mathbf{G}^I(\omega) = \left[G_1^I(\omega), \cdots, G_N^I(\omega)\right]^T$.

As mentioned earlier the NOFRFs are insensitive to a change of the input spectrum $U(j\omega)$ by a constant amplitude gain. Using this property of the NOFRFs Lang and Billings in [29] presented a LS based approach for the evaluation of NOFRFs to any arbitrary nonlinearity. The procedure of evaluating NOFRFs using this method is summarised as follows;

1) Excite the nonlinear system by a set of test inputs where,

$$\alpha_m u(t),\ m = 1, \cdots, M \tag{4.24}$$

to obtain the corresponding outputs $y^{(m)}(t)$, $m = 1, \cdots, M$, $M \geq N$ in which α_m, $m = 1, \cdots, M$ are appropriately chosen constants.

2) Evaluate;

- the Fourier transform of the original input $u(t)$, $U_1(j\omega)$,
- the Fourier transform of $u^n(t)$, for $n=1,\cdots,N$, and calculate the corresponding $U_n(j\omega)$ using equation (4.13)
- the Fourier transform of $y^{(m)}(t)$, $Y^{(m)}(j\omega)$ for $m=1,\cdots,M$.

3) Extend equation (4.23) into the matrix form as;

$$\begin{bmatrix} \mathrm{Re}\,\mathbf{Y}(\omega) \\ \mathrm{Im}\,\mathbf{Y}(\omega) \end{bmatrix} = \mathbf{AU}(\omega) \times \mathbf{G}(\omega) \tag{4.25}$$

where

$$\begin{cases} \mathbf{G}(\omega) = \begin{bmatrix} \mathbf{G}^R(\omega) \\ \mathbf{G}^I(\omega) \end{bmatrix} \\ \mathbf{G}^R(\omega) = \left[G_1^R(\omega),\cdots,G_N^R(\omega)\right]^T \\ \mathbf{G}^I(\omega) = \left[G_1^I(\omega),\cdots,G_N^I(\omega)\right]^T \end{cases} \tag{4.26}$$

$$\mathbf{Y}(j\omega) = \left[Y^{(1)}(j\omega),\cdots,Y^{(M)}(j\omega)\right]^T \tag{4.27}$$

and

$$\mathbf{AU}(\omega) = \begin{bmatrix} \alpha_1 U_1^R(\omega), & \cdots, & \alpha_1^N U_N^R(\omega), & -\alpha_1 U_1^I(\omega), & \cdots -\alpha_1^N U_N^I(\omega) \\ \vdots & & \vdots & \vdots & \vdots \\ \alpha_M U_1^R(\omega), & \cdots, & \alpha_M^N U_N^R(\omega), & -\alpha_M U_1^I(\omega), & \cdots -\alpha_M^N U_N^I(\omega) \\ \alpha_1 U_1^I(\omega), & \cdots, & \alpha_1^N U_N^I(\omega), & \alpha_1 U_1^R(\omega), & \cdots \alpha_1^N U_N^R(\omega) \\ \vdots & & \vdots & \vdots & \vdots \\ \alpha_M U_1^I(\omega), & \cdots, & \alpha_M^N U_N^I(\omega), & \alpha_M U_M^R(\omega), & \cdots \alpha_M^N U_N^R(\omega) \end{bmatrix} \tag{4.28}$$

to evaluate the estimate of $\mathbf{G}(\omega)$ using a least squares approach as;

$$\mathbf{G}(\omega) = \left[\mathbf{AU}(\omega)^T \times \mathbf{AU}(\omega)\right]^{-1} \mathbf{AU}(\omega)^T \begin{bmatrix} \mathrm{Re}\,\mathbf{Y}(\omega) \\ \mathrm{Im}\,\mathbf{Y}(\omega) \end{bmatrix} \tag{4.29}$$

It should be noted that the evaluated estimates of the NOFRFs, $\hat{G}_n(j\omega)$, $n=1,\cdots,N$, can only be used over the frequencies where the NOFRF $G_n(j\omega)$, $n=1,\cdots,N$, is valid. This range of frequencies is equal to f_{Y_n} given by equation (4.8). The LS approach to the evaluation of NOFRFs is a compact simple method that can be used with input-output data either directly exciting a nonlinear system or an identified NARX model.

4.4 Summary

In this chapter, the output frequency response characteristics of linear and nonlinear systems were overviewed and Frequency Response Analysis methods of linear systems, the FRF, and nonlinear systems, GFRFs and NOFRFs, were outlined. Output frequency response characterisation of nonlinear systems, the description of the nonlinear phenomena and analysis of a nonlinear system dynamics in the frequency domain using the concept of NOFRFs were reviewed. Hence the potential of using NOFRFs over GFRFs for CM-FD of nonlinear systems was discussed. This is because the NOFRFs, even though are input dependent, its main reliance on the GFRF as a weighted sum of the input signal and its ability to represent nonlinear systems as a one-dimensional frequency function. This makes the analysis of nonlinear systems easier to interpret and thus much easier to extract fault specific features for CM-FD. This has been demonstrated by several different studies as discussed. In the following chapter, the numerical issues in the least squares method of evaluating NOFRFs will be discussed and method to address this issue will be presented.

Chapter 5

An Effective Least Squares Method of Evaluating Nonlinear Output Frequency Response Functions of Nonlinear Systems

5.1 Introduction

It is well known that nonlinear systems can often produce more output frequency components than that contained in the input. The output frequencies of nonlinear systems, in general, may contain sub-harmonics, super-harmonics and inter-modulation between the frequency components of the input. Hence, there is a transference of energy from the input frequencies to other frequencies [24]. The Generalised Frequency Response Functions (GFRFs) [120] have been used to study these behaviours of nonlinear systems. The GFRFs which are the Fourier Transforms of the multi-dimensional Volterra series is inherently multi-dimensional thus require very high computational demands to evaluate. Furthermore, due to the multi-dimensional character higher order GFRFs cannot be visualised and are therefore difficult to interpret.

The concept of Nonlinear Output Frequency Response Functions (NOFRFs) is one-dimensional frequency functions introduced by Lang *et al.* in [29] as an alternative method of analysis of nonlinear systems in the frequency domain. Due to the one-dimensional character, the NOFRFs can be much easily visualised and interpreted.

Peng *et al.* in [13] have used the NOFRFs as a viable analysis tool for the fault detection of nonlinear systems in the frequency domain. The NOFRFs have also found applications in SHM to identify cracks in beams and damage in aluminium plates [19], [119]. For electrical systems, Chen and Zhai *et al*. in [123] have applied the NOFRFs in the detection of damaged power cable insulations. In [125] the authors proposed a novel method of Fault Diagnosis by using features obtained from the NOFRFs and the Dempster-Shafer theory of evidence to process the features for the isolation of faults. Recently the NOFRF concept has also been studied in Fault Diagnosis of hydro generators as well as hydro-turbine governing systems in [16] and [118] respectively. In these applications, an accurate evaluation of the NOFRFs is essential as the damage is uniquely identified using the system frequency features obtained from the NOFRFs.

Currently, the NOFRFs can be evaluated using two methods. One is the LS based method presented in [29] and the other is the Associated Linear Equations (ALEs) approach for the NOFRFs introduced by Bayma *et al.* in [15]. In [30] the authors compared the performance of both these methods in evaluating the NOFRFs. It was shown that even though both methods can be used for damage detection, they both have limitations. A system model of differential equations and the evaluation of its corresponding ALEs are required for the ALEs based approach. While the LS approach does not require a model, the system must be excited by test inputs with appropriately chosen amplitudes for the evaluation of the NOFRFs. In addition, the LS approach may experience numerical errors due to the ill-conditioning of the information matrix and consequently cannot produce accurate NOFRFs sometimes.

The chapter is concerned with the development of a new method for the improvement of the LS based NOFRFs evaluation directly using the system input-output data. The new method is known as the M-LS method. In the M-LS method, the information matrix for the LS operation at each frequency is constructed according to the contribution made by each order of system nonlinearity to the system output response at this frequency. This addresses the possible numerical issues associated with matrix inversion. The effectiveness of the new method is then demonstrated using simulation studies on two different nonlinear systems subject to a general band limited and a harmonic input, respectively. The new M-LS method can significantly increase the accuracy of the NOFRFs evaluation directly using system testing data and facilitate the use of the NOFRFs and associated approaches in many practical applications such as engineering system Fault Diagnosis and SHM.

As a result of addressing the numerical issued in evaluating NOFRFs with the M-LS method, novel significant observations were made on the convergence of the Volterra series where sever nonlinear behaviour occur. This convergence of the Volterra series around the regions of severe nonlinear behaviour was deemed impractical and even impossible. However, it has been theoretically argued in [31] that convergence does exist given the use of an extremely high order of nonlinearity. With regard to GFRFs being multi-dimensional, the use of extremely high orders of nonlinearity is impractical due to the extensive computational efforts. However, since the NOFRFs are one-dimensional and because of the numerical accuracy attained using the M-LS method. In this chapter, the convergence analysis of the Volterra series using NOFRFs is revisited. Therefore, the theoretical possibility of a convergent Volterra series is validated practically for the first time.

5.2 The Modified Least Squares method for the evaluation of Nonlinear Output Frequency Response Functions

The valid frequency range of the n^{th} order NOFRF, $G_n(j\omega)$, $n = 1,\cdots,N$ is defined by equation (4.18) and is known as the possible output frequency ranges of the n^{th} order nonlinearity, denoted as f_{Y_n} (see Section 4.3.3). This frequency range is the region in the frequency space in which the NOFRFs $G_n(j\omega)$ operate on the respective nonlinear composition of the input spectrum $U(j\omega)$ which is $U_n(j\omega)$. f_{Y_n} can be evaluated using the algorithm shown in equation (4.8). Thus from the two expressions, equations (4.8) and (4.18), it is evident that the n^{th} order nonlinear composition of the input spectrum, $U_n(j\omega)$, is of the form;

$$U_n(j\omega) = \begin{cases} U_n(j\omega) & when\ |\omega| \in f_{Y_n} \\ 0 & otherwise \end{cases} \tag{5.1}$$

$U_n(j\omega)$ is evaluated using the Fourier transform as shown in equation (4.13). In practice, however, when using a FFT (Fast Fourier Transform) algorithm to obtain the frequency spectrum, $U_n(j\omega)$ is often not zero but relatively small when $|\omega| \notin f_{Y_n}$. This can make the information matrix $\mathbf{AU}(\omega)$ in the original LS method, equations (4.25)-(4.29), become sparse and ill-posed over certain frequency points, inducing significant numerical errors.

The M-LS method, introduced in this chapter, is formulated to address this issue by appropriately constructing the matrix $\mathbf{AU}(\omega)$ at each frequency point ω. This is achieved by the use of the algorithm for the evaluation of f_{Y_n}, given by equation (4.8), to determine the most relevant terms and only include these terms in the information matrix to produce a dense information matrix $\overline{\mathbf{AU}}(\omega)$. Denote;

$$\mathbf{au}_{1,n_k}(\omega) = \begin{bmatrix} \alpha_1^{n_k} U_{n_k}^R(\omega) \\ \vdots \\ \alpha_M^{n_k} U_{n_k}^R(\omega) \\ \alpha_1^{n_k} U_{n_k}^I(\omega) \\ \vdots \\ \alpha_M^{n_k} U_{n_k}^I(\omega) \end{bmatrix}, \quad \mathbf{au}_{2,n_k}(\omega) = \begin{bmatrix} -\alpha_1^{n_k} U_{n_k}^I(\omega) \\ \vdots \\ -\alpha_M^{n_k} U_{n_k}^I(\omega) \\ \alpha_1^{n_k} U_{n_k}^R(\omega) \\ \vdots \\ \alpha_M^{n_k} U_{n_k}^R(\omega) \end{bmatrix} \tag{5.2}$$

Thus the matrix $\mathbf{AU}(\omega)$ in equation (4.28) of the original LS method for evaluating NOFRFs can be re-written in terms of the vectors $\mathbf{au}_{1,n_k}$ and $\mathbf{au}_{2,n_k}$ where $n_k = 1,\cdots,N$ such that;

$$\mathbf{AU}(\omega) = \left[\mathbf{au}_{1,1}(\omega)\,,\cdots,\mathbf{au}_{1,N}(\omega)\,,\mathbf{au}_{2,1}(\omega)\,,\cdots,\mathbf{au}_{2,N}(\omega)\right] \tag{5.3}$$

However instead, given;

$$n_k \in \{1\,,\cdots,N\}\,,\ k = 1\,,\cdots,K \tag{5.4}$$

are the orders of the system nonlinearities which literally contribute to the system output frequency response at the frequency ω. This can be determined using equation (4.8) when ω is given. Based on $\mathbf{au}_{1,n_k}(\omega)$ and $\mathbf{au}_{2,n_k}(\omega)$ for $k = 1,\cdots,K$ introduced in equations (5.2) and (5.4), $\overline{\mathbf{AU}}(\omega)$ can be constructed as follows;

$$\overline{\mathbf{AU}}(\omega) = \left[\mathbf{au}_{1,n_1}(\omega)\,,\cdots,\mathbf{au}_{1,n_k}(\omega)\,,\mathbf{au}_{2,n_1}(\omega)\,,\cdots,\mathbf{au}_{2,n_k}(\omega)\right] \tag{5.5}$$

By replacing $\mathbf{AU}(\omega)$ in equation (4.28) within equation (5.5), much more reliable estimates of the NOFRFs, $G_{n_k}(j\omega)$, $k = 1,\cdots,K$ can be evaluated. This is best described by an example as shown below.

Example 5.1 - Construction of the information matrix $\overline{\mathbf{AU}}(\omega)$ according to the respective possible output frequency components of the n^{th} order nonlinearity

The M-LS method for a nonlinear system, considering nonlinearities up to the 3rd order, i.e. $N = 3$, and is subjected to a band-limited input over the frequency range of $[30,55]$ can be implemented as follows.

From equation (4.8) with $a = 30$ and $b = 55$, it is known that;

$$f_{Y_1} = [30\,,\,55] \tag{5.6}$$

$$f_{Y_2} = [0\,,\,25]\bigcup[60\,,\,110] \tag{5.7}$$

$$f_{Y_3} = [5\,,\,80]\bigcup[90\,,\,165] \tag{5.8}$$

Hence for different ω over the range of $\omega = 0,\cdots,165$, the matrix $\overline{\mathbf{AU}}(\omega)$ can be constructed as follows:

- For $\omega = 0,\cdots,4;\ K = 1,\ n_1 = 2$ and

$$\overline{\mathbf{AU}}(\omega) = \left[\mathbf{au}_{1,2}(\omega),\quad \mathbf{au}_{2,2}(\omega)\right] = \begin{bmatrix} \alpha_1^2 U_2^R(\omega), & -\alpha_1^2 U_2^I(\omega) \\ \vdots & \vdots \\ \alpha_M^2 U_2^R(\omega), & -\alpha_M^2 U_2^I(\omega) \\ \alpha_1^2 U_2^I(\omega), & \alpha_1^2 U_2^R(\omega) \\ \vdots & \vdots \\ \alpha_M^2 U_2^I(\omega), & \alpha_M^2 U_2^R(\omega) \end{bmatrix} \tag{5.9}$$

which will produce $\hat{\mathbf{G}}(\omega) = \begin{bmatrix} \hat{\mathbf{G}}^R(\omega) \\ \hat{\mathbf{G}}^I(\omega) \end{bmatrix} = \begin{bmatrix} \left[\hat{G}_2^R(\omega)\right]^T \\ \left[\hat{G}_2^I(\omega)\right]^T \end{bmatrix}$.

- For $\omega = 5,\cdots,25;\ K = 2,\ n_1 = 2,\ n_2 = 3$ and

$$\overline{\mathbf{AU}}(\omega) = \left[\mathbf{au}_{1,2}(\omega),\quad \mathbf{au}_{1,2}(\omega),\quad \mathbf{au}_{2,3}(\omega),\quad \mathbf{au}_{2,3}(\omega)\right] = \begin{bmatrix} \alpha_1^2 U_2^R(\omega), & \alpha_1^3 U_3^R(\omega), & -\alpha_1^2 U_2^I(\omega), & -\alpha_1^3 U_3^I(\omega) \\ \vdots & \vdots & \vdots & \vdots \\ \alpha_M^2 U_2^R(\omega), & \alpha_M^3 U_3^R(\omega), & -\alpha_M^2 U_2^I(\omega), & -\alpha_M^3 U_3^I(\omega) \\ \alpha_1^2 U_2^I(\omega), & \alpha_1^3 U_3^I(\omega), & \alpha_1^2 U_2^R(\omega), & \alpha_1^3 U_3^R(\omega) \\ \vdots & \vdots & \vdots & \vdots \\ \alpha_M^2 U_2^I(\omega), & \alpha_M^3 U_3^I(\omega), & \alpha_M^2 U_2^R(\omega), & \alpha_M^3 U_3^R(\omega) \end{bmatrix} \tag{5.10}$$

which will produce $\hat{\mathbf{G}}(\omega) = \begin{bmatrix} \hat{\mathbf{G}}^R(\omega) \\ \hat{\mathbf{G}}^I(\omega) \end{bmatrix} = \begin{bmatrix} \left[\hat{G}_2^R(\omega)\ ,\ \hat{G}_3^R(\omega)\right]^T \\ \left[\hat{G}_2^I(\omega)\ ,\ \hat{G}_3^I(\omega)\right]^T \end{bmatrix}$.

- For $\omega = 26,\cdots,29;\ K = 1,\ n_1 = 3$ and

$$\overline{\mathbf{AU}}(\omega) = \left[\mathbf{au}_{1,3}(\omega),\quad \mathbf{au}_{2,3}(\omega)\right] = \begin{bmatrix} \alpha_1^3 U_3^R(\omega), & -\alpha_1^3 U_3^I(\omega) \\ \vdots & \vdots \\ \alpha_M^3 U_3^R(\omega), & -\alpha_M^3 U_3^I(\omega) \\ \alpha_1^3 U_3^I(\omega), & \alpha_1^3 U_3^R(\omega) \\ \vdots & \vdots \\ \alpha_M^3 U_3^I(\omega), & \alpha_M^3 U_3^R(\omega) \end{bmatrix} \tag{5.11}$$

which will produce $\hat{\mathbf{G}}(\omega) = \begin{bmatrix} \hat{\mathbf{G}}^R(\omega) \\ \hat{\mathbf{G}}^I(\omega) \end{bmatrix} = \begin{bmatrix} \left[\hat{G}_3^R(\omega)\right]^T \\ \left[\hat{G}_3^I(\omega)\right]^T \end{bmatrix}$.

- For $\omega = 30,\cdots,55$; $K = 2,\ n_1 = 1,\ n_2 = 3$ and

$$\overline{\mathbf{AU}}(\omega) = \left[\mathbf{au}_{1,1}(\omega),\ \ \mathbf{au}_{1,1}(\omega),\ \ \mathbf{au}_{2,3}(\omega),\ \ \mathbf{au}_{2,3}(\omega)\right]$$
$$= \begin{bmatrix} \alpha_1 U_1^R(\omega), & \alpha_1^3 U_3^R(\omega), & -\alpha_1 U_1^I(\omega), & -\alpha_1^3 U_3^I(\omega) \\ \vdots & \vdots & \vdots & \vdots \\ \alpha_M U_1^R(\omega), & \alpha_M^3 U_3^R(\omega), & -\alpha_M U_1^I(\omega), & -\alpha_M^3 U_3^I(\omega) \\ \alpha_1 U_1^I(\omega), & \alpha_1^3 U_3^I(\omega), & \alpha_1 U_1^R(\omega), & \alpha_1^3 U_3^R(\omega) \\ \vdots & \vdots & \vdots & \vdots \\ \alpha_M U_1^I(\omega), & \alpha_M^3 U_3^I(\omega), & \alpha_M U_1^R(\omega), & \alpha_M^3 U_3^R(\omega) \end{bmatrix} \qquad (5.12)$$

which will produce $\hat{\mathbf{G}}(\omega) = \begin{bmatrix} \hat{\mathbf{G}}^R(\omega) \\ \hat{\mathbf{G}}^I(\omega) \end{bmatrix} = \begin{bmatrix} \left[\hat{G}_1^R(\omega)\ ,\ \hat{G}_3^R(\omega)\right]^T \\ \left[\hat{G}_1^I(\omega)\ ,\ \hat{G}_3^I(\omega)\right]^T \end{bmatrix}$.

As shown above, the information matrix $\overline{\mathbf{AU}}(\omega)$ is constructed appropriately for the complete frequency space of the output frequency response, until $\omega = 165$, of the nonlinear system considered.

Once the estimate of the NOFRFs has been obtained, the estimate for the output frequency spectrum of the system n^{th} order nonlinearity, $\hat{Y}_n(j\omega)$, and consequently the estimate for the system output frequency spectrum $\hat{Y}(j\omega)$ can be generated using equation (4.19). The results can then be used to compare with the actual system output spectrum $Y(j\omega)$ obtained. In the next section, a comparison is made between the new M-LS method and the original LS method for evaluation of NOFRFs under three different input types in order to illustrate the significance of the M-LS method.

5.3 Comparison of the Least Squares and Modified Least Squares based methods of Nonlinear Output Frequency Response Functions evaluation

The accuracy of the evaluated NOFRFs is important to accurately decompose the output spectrum into the respective output spectra of each individual nonlinearity. To demonstrate the significant accuracy attained in evaluating NOFRFs using the M-LS method three different case studies are given in this section.

5.3.1 Comparison for the case of a general input

To demonstrate the accuracy of NOFRFs under a general input that is described by equation (4.7) a nonlinear oscillator with a 5th order nonlinear stiffness as shown in equation (5.13) is used.

$$M\,\ddot{y}(t) + C\,\dot{y}(t) + K_1\,y(t) + K_3\,y^3(t) + K_5\,y^5(t) = u(t) \tag{5.13}$$

where $M = 0.013$, $C = 0.0607$, $K_1 = 40$, $K_3 = -2.1\times10^5$ and $K_5 = 4.21\times10^9$. The NOFRFs of the above nonlinear system under the inputs;

$$u_i(t) = A_i \frac{3}{2\pi} \times \frac{\sin(2\pi\, f_1 t) - \sin(2\pi\, f_2 t)}{t}\ ,\ i = 1,\cdots,M \tag{5.14}$$

is evaluated using both the LS and new M-LS method with, $f_1 = 70$, $f_2 = 50$, $t = -10.55,\cdots,10.56$ and $A_i = 9.8\alpha_i$ where $i = 1,\cdots,M$.

Figure 5.1 illustrates the input and output spectra, $U(j\omega)$ and $Y(j\omega)$, produced by evaluating the response of the nonlinear system in equation (5.13) subjected to the input is shown in equation (5.14) using the Runge-Kutta 4 (RK-4) algorithm. From Figure 5.1 it can be clearly seen the new frequency components generated in the output spectrum. Figure 5.2 shows a comparison of the actual output spectrum and the output spectra evaluated using equation (4.19) and the NOFRFs obtained from the original LS method and the new M-LS method, respectively. The NOFRFs obtained from both methods were all evaluated up to the 5th order, i.e. $N = 5$, with the five excitation amplitudes, i.e. $M = 5$, where $[\alpha_1,\cdots,\alpha_5] = [1, 0.85, 0.7, 0.55, 0.4]$.

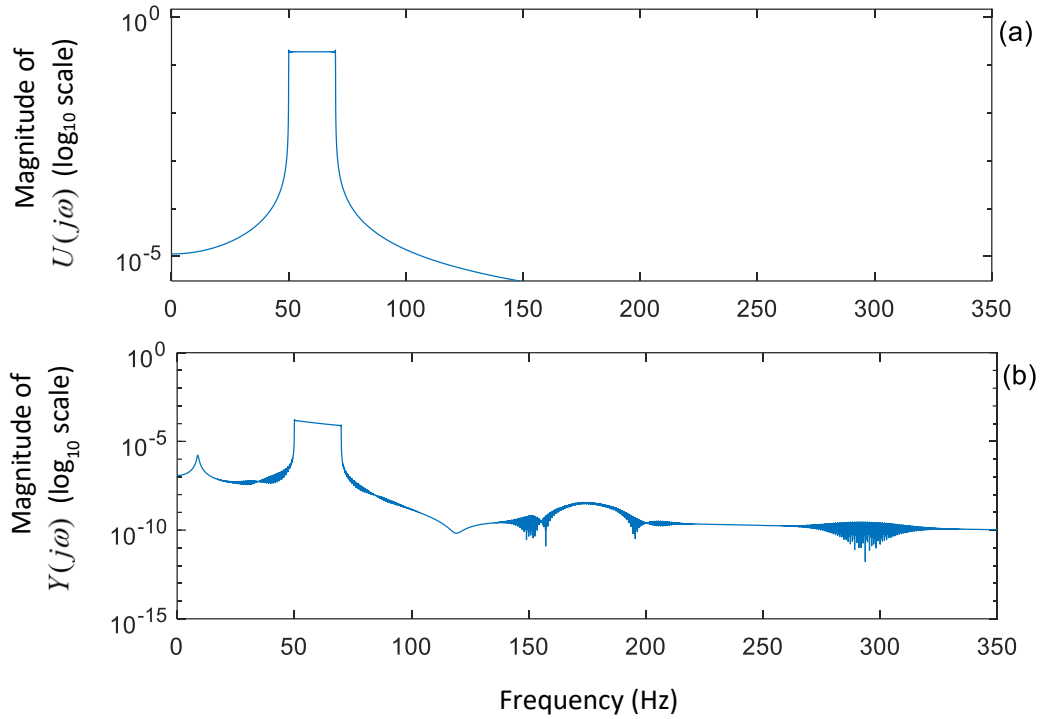

Figure 5.1: (a) and (b) shows the input and output spectra respectively of the system represented by equation (5.13) when excited by the input in equation (5.14)

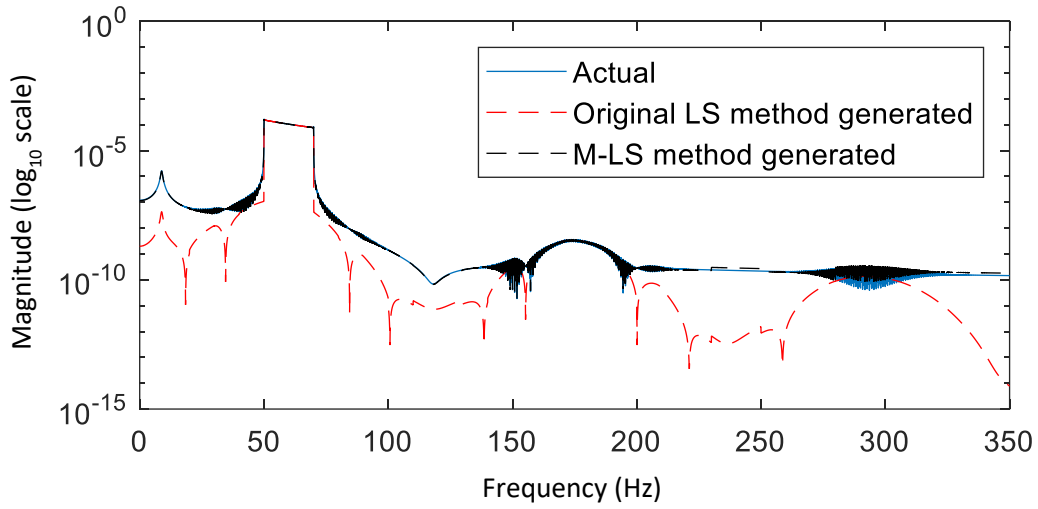

Figure 5.2: Comparison of the actual output spectra with the spectra evaluated using the NOFRFs obtained from original LS and M-LS methods, respectively. As seen from the figure the NOFRFs evaluated using the M-LS method has good accuracy in re-producing the actual output frequency response. The actual output spectrum (Blue), the output spectrum produced by NOFRFs evaluated from the original LS method (Red dashed), the output spectrum produced by NOFRFs evaluated from the M-LS method (Black dashed).

It is clearly observable from Figure 5.2 that the NOFRFs evaluated from the M-LS method is much more accurate as the estimate of the output spectrum generated is almost the same to the actual. This means that the decomposition of the output spectrum $Y(j\omega)$ to the respective output nonlinearities by the NOFRFs is done appropriately. Thus, the NOFRFs $G_n(j\omega)$ estimated using the M-LS method is more accurate.

Figure 5.3 shows the respective contributions of each order of nonlinearity in the frequency space for a nonlinear system subject to an input excitation given by equation (5.14). This is determined by equation (4.8). The accuracy of the M-LS method is due to the $\mathbf{AU}(\omega)$ (from here on the matrix $\overline{\mathbf{AU}}(\omega)$ will be referred to as $\mathbf{AU}(\omega)$) matrices at each frequency point ω only contains the appropriate $\alpha_m^n U_n^R(\omega)$ and $\alpha_m^n U_n^I(\omega)$ terms according to the relevant contributions made by each order of nonlinearity at that particular frequency point as revealed in Figure 5.3.

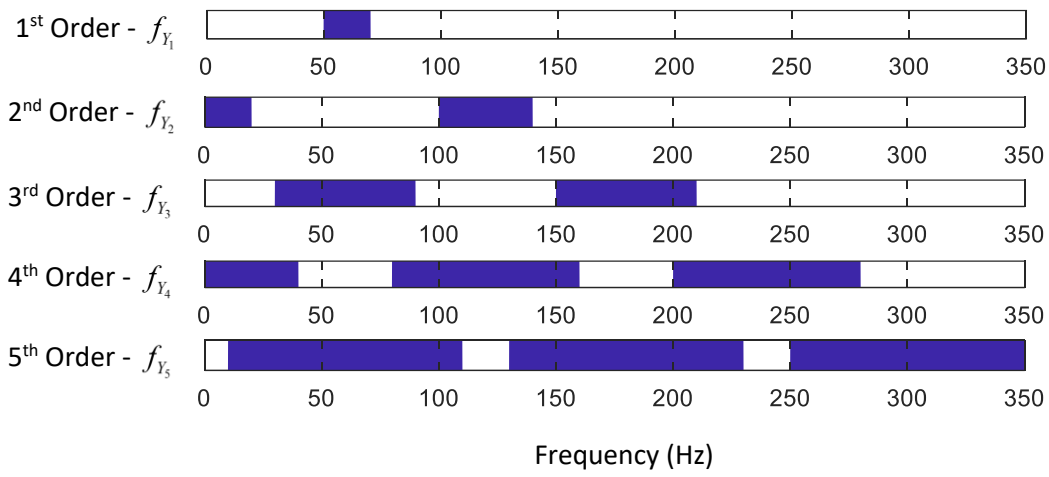

Figure 5.3: The space of output frequencies contributed by each order of the nonlinearities when a nonlinear system is subject to input excitation given by equation (5.14). As seen from the figure each order of nonlinearity will produce frequency components in the respective frequency regions f_{Y_n}, $n=1,\cdots,N$. The NOFRFs $G_n(j\omega)$ are only valid to these respective frequency regions. The respective NOFRFs operate on $U_n(j\omega)$ which exists at the respective frequency regions f_{Y_n} to produce the output frequency response of the nth order nonlinearity $Y_n(j\omega)$. Thus in the M-LS method the $\mathbf{AU}(\omega)$ matrices are constructed appropriately according to the respective contributions made by each individual nonlinearity at the frequency point ω.

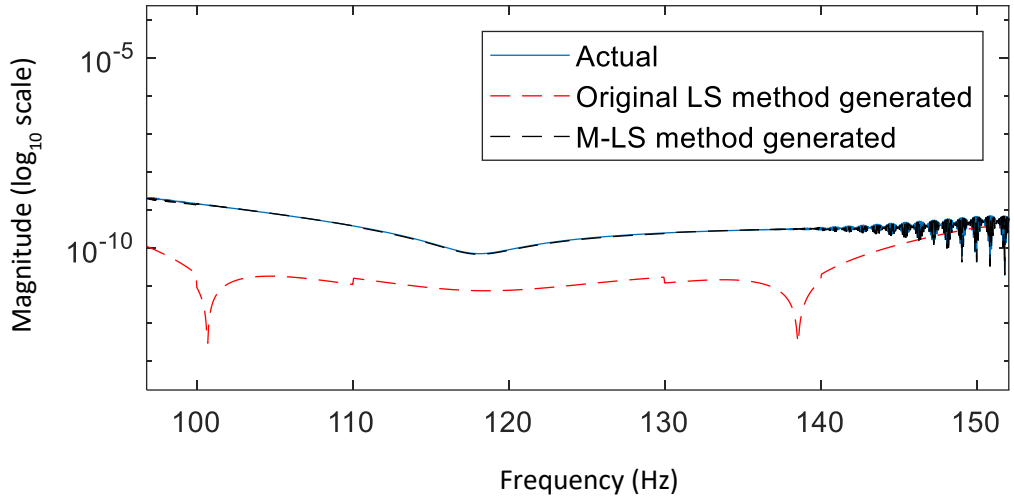

Figure 5.4: The frequency region between 100 Hz and 150 Hz of Figure 5.1

For example over the frequency range of 100 Hz to 150Hz, as shown in Figure 5.4, it can be observed from Figure 5.3 that the nonlinear orders which contribute to the system output are different at different frequencies and, consequently, an information matrix $\mathbf{AU}(\omega)$ associated with each different points of frequencies should be used to evaluate the NOFRFs using the M-LS method in the corresponding case. More specifically,

- For $\omega = 100,\cdots,110$; Only the 2nd, 4th and 5th orders of nonlinearities contribute to the output, therefore;

$$\mathbf{AU}(\omega) = \begin{bmatrix} \alpha_1^2 U_2^R(\omega), & \alpha_1^4 U_4^R(\omega), & \alpha_1^5 U_5^R(\omega), & -\alpha_1^2 U_1^I(\omega), & -\alpha_1^3 U_3^I(\omega) & -\alpha_1^3 U_3^I(\omega) \\ \vdots & \vdots & \vdots & \vdots & \vdots & \vdots \\ \alpha_M^2 U_2^R(\omega), & \alpha_M^4 U_4^R(\omega), & \alpha_M^5 U_5^R(\omega), & -\alpha_M^2 U_1^I(\omega), & -\alpha_1^3 U_3^I(\omega) & -\alpha_1^3 U_3^I(\omega) \\ \alpha_1^2 U_2^I(\omega), & \alpha_1^4 U_4^I(\omega), & \alpha_1^5 U_5^I(\omega), & \alpha_1 U_1^R(\omega), & \alpha_1^3 U_3^R(\omega) & \alpha_1^3 U_3^R(\omega) \\ \vdots & \vdots & \vdots & \vdots & \vdots & \vdots \\ \alpha_M^2 U_2^I(\omega), & \alpha_M^4 U_4^I(\omega), & \alpha_M^5 U_5^I(\omega), & \alpha_1 U_1^R(\omega), & \alpha_1^3 U_3^R(\omega) & \alpha_1^3 U_3^R(\omega) \end{bmatrix} \quad (5.15)$$

- For $\omega = 111,\cdots,129$; Only the 2nd and 4th orders of nonlinearities contribute to the output, therefore;

$$\mathbf{AU}(\omega) = \begin{bmatrix} \alpha_1^2 U_2^R(\omega), & \alpha_1^4 U_4^R(\omega), & -\alpha_1^2 U_2^I(\omega), & -\alpha_1^4 U_4^I(\omega) \\ \vdots & \vdots & \vdots & \vdots \\ \alpha_M^2 U_1^R(\omega), & \alpha_M^4 U_4^R(\omega), & -\alpha_M^2 U_2^I(\omega), & -\alpha_M^4 U_4^I(\omega) \\ \alpha_1^2 U_2^I(\omega), & \alpha_1^4 U_4^I(\omega), & \alpha_1^2 U_2^R(\omega), & \alpha_1^4 U_4^R(\omega) \\ \vdots & \vdots & \vdots & \vdots \\ \alpha_M^2 U_2^I(\omega), & \alpha_M^4 U_4^I(\omega), & \alpha_M^2 U_2^R(\omega), & \alpha_M^4 U_4^R(\omega) \end{bmatrix} \quad (5.16)$$

- For $\omega = 130,\cdots,140$; Only the 2nd, 4th and 5th orders of nonlinearities contribute to the output, therefore the respective structure of the matrix $\mathbf{AU}(\omega)$ will be the same as shown in equation (5.15).

- For $\omega = 141,\cdots,150$; Only the 4th and 5th orders of nonlinearities contribute to the output, therefore;

$$\mathbf{AU}(\omega) = \begin{bmatrix} \alpha_1^4 U_4^R(\omega), & \alpha_1^5 U_5^R(\omega), & -\alpha_1^4 U_4^I(\omega), & -\alpha_1^5 U_5^I(\omega) \\ \vdots & \vdots & \vdots & \vdots \\ \alpha_M^4 U_4^R(\omega), & \alpha_M^5 U_5^R(\omega), & -\alpha_M^4 U_4^I(\omega), & -\alpha_M^5 U_5^I(\omega) \\ \alpha_1^4 U_4^I(\omega), & \alpha_1^5 U_5^I(\omega), & \alpha_1^4 U_4^R(\omega), & \alpha_1^5 U_5^R(\omega) \\ \vdots & \vdots & \vdots & \vdots \\ \alpha_M^4 U_4^I(\omega), & \alpha_M^5 U_5^I(\omega), & \alpha_M^4 U_4^R(\omega), & \alpha_M^5 U_5^R(\omega) \end{bmatrix} \tag{5.17}$$

Thus, the $\mathbf{AU}(\omega)$ matrices are formulated differently over different frequencies where the NOFRFs are valid to ensure a more accurate evaluation of the NOFRFs at the respective frequencies. This prevents the ill-conditioning effect of the information matrix that may arise in the original LS method. Also, it should be emphasised that this prevents any unwanted energy leakages from different orders of NOFRFs to the regions in which other respective NOFRFs are not supposed to exist.

5.3.2 Comparison for the case of a harmonic input

The nonlinear system used in this case is a duffing oscillator with a 3rd order nonlinear stiffness as shown in equation (5.18) below.

$$M\,\ddot{y}(t) + C\,\dot{y}(t) + K_1\,y(t) + K_3\,y^3(t) = u(t) \tag{5.18}$$

where $C = 3.84\pi$, $K_1 = (12\pi)^2$ and $K_3 = 0.1(12\pi)^6$. The parameterized system shown in equation (5.18) is excited by a harmonic input $u(t) = A\sin(\omega t)$, where $A = 0.4$.

$$Trans(\omega) = \frac{|Y(j\omega)|}{|U(j\omega)|} \tag{5.19}$$

In order to comprehensively illustrate the comparison, the transmissibility of the system shown in equation (5.18) is used. Transmissibility at a particular excitation frequency, $Trans(\omega)$, is taken as the ratio of the output spectral magnitude, $|Y(j\omega)|$, to the input spectral magnitude, $|U(j\omega)|$ at that respective frequency as shown in equation (5.19) above.

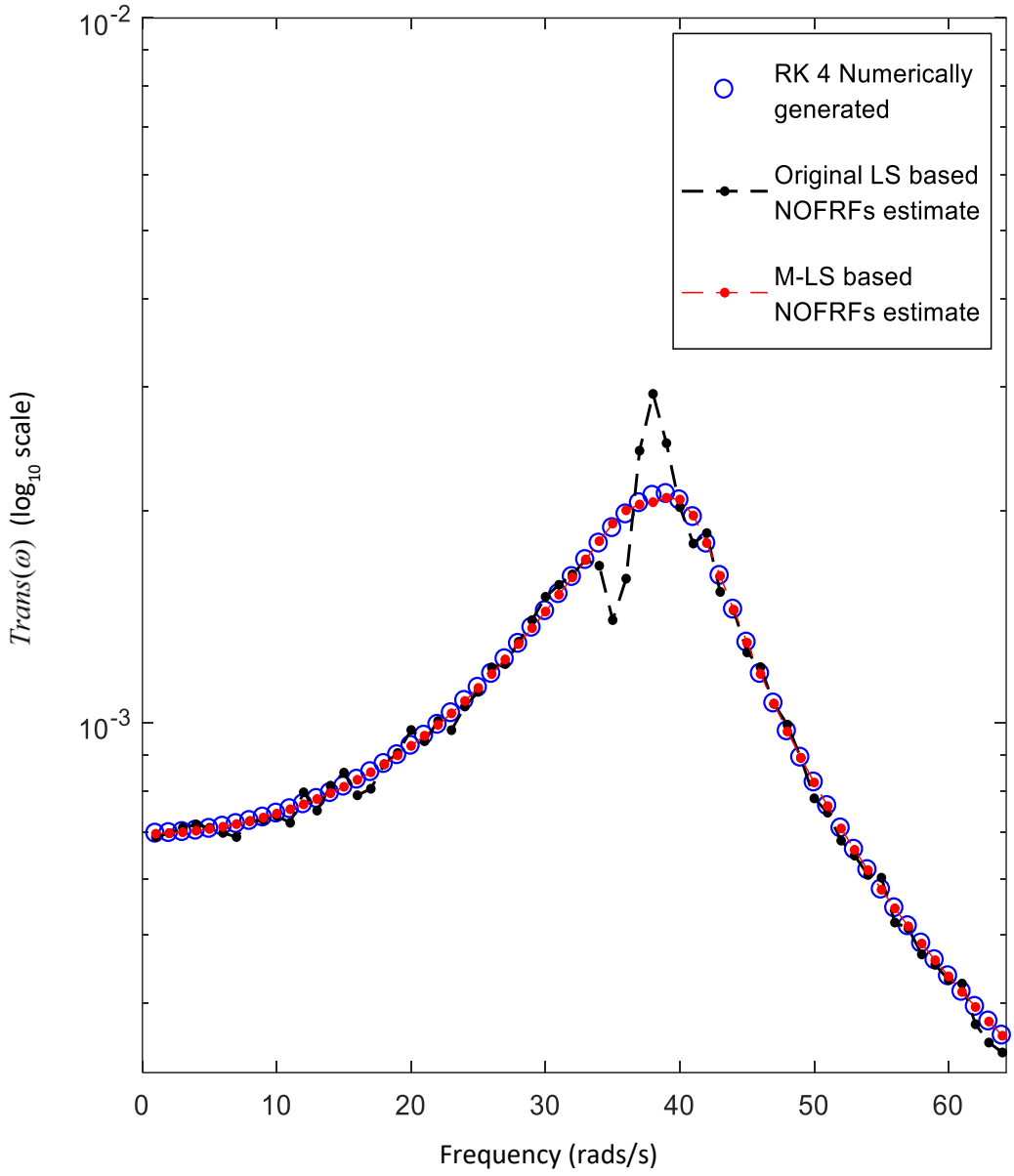

Figure 5.5: Transmissibility curve of the system shown by equation (5.18) excited with a harmonic input amplitude $A = 0.4$ and NOFRFs generated transmissibility curves. The actual transmissibility curve of the system (Blue circle), Transmissibility curve generated by NOFRFs evaluated: original LS method (Black dash dot), M-LS method (Red dash dot). The NOFRFs from both methods are evaluated using the amplitudes in equation (5.20) but the transmissibility curves were evaluated using these NOFRFs at $A = 0.4$. Thus it is evident that the NOFRFs evaluated from the M-LS method has captured the frequency domain dynamics of the actual system to a harmonic input significantly well.

Figure 5.5 shows the transmissibility curves generated from simulating the ODE shown in equation (5.18) using the RK-4 algorithm. The results obtained are from the NOFRFs evaluated using the LS and M-LS based methods, respectively. The NOFRFs from both methods were generated up to the 7th order, i.e. $N = 7$ of nonlinearity using 7 input amplitudes, i.e. $M = 7$, which are;

$$A = \left[0.2\ ,\ 0.18333\ ,\ 0.16667\ ,\ 0.15\ ,\ 0.13333\ ,\ 0.11667\ ,\ 0.1\right] \qquad (5.20)$$

As seen from Figure 5.5 the M-LS evaluation of NOFRFs and the resultant transmissibility curve generated from these NOFRFs are more accurate compared to the transmissibility curve generated using the original LS based method.

It is worth emphasising that the NOFRFs from both methods were generated using the test inputs with amplitudes mentioned in equation (5.20), which are in the range of $0.1-0.2$. However, the transmissibility curves shown in Figure 5.5 were evaluated using the same NOFRFs but for an input of amplitude $A = 0.4$, which is outside the range of amplitudes where the NOFRFs were determined. This implies that the NOFRFs thus determined, represent inherent system dynamics and can, therefore, be potentially used in many practical applications.

5.4 Convergence analysis of Volterra series representation of Duffing's oscillator

Nonlinear systems, in theory, are needed to be expressed using an infinite Volterra series, however, an accurate approximation to the response of the system can be made using a truncated series [81], [126]. Therefore, the convergence of the Volterra series is vital to adequately represent the responses of nonlinear systems.

The Volterra series representation of nonlinear systems and methods based on this, such as GFRFs and NOFRFs, have been used extensively for the study of nonlinear systems, as discussed throughout this thesis. However, analysis based on the Volterra series can only be directly applied to weakly nonlinear systems [31], [127], [128]. This is because weakly nonlinear systems can be adequately represented by a Volterra series with a finite number of nonlinearities, i.e. a convergent Volterra series. Nonlinear systems that exhibit severe nonlinear phenomena such as sub-harmonics, chaos and jump [129], [130] are known as severely nonlinear systems. Consequently, it is known that the Volterra series cannot be directly applied to regions in which a nonlinear system exhibits such behaviour [31] because of a divergent Volterra series. The regions in which a nonlinear system would reveal this type of behaviour depends on the frequency of excitation, the amplitude of excitation and the parameters of the system. Hence the convergence of Volterra series depends on these factors [31], [131]. Therefore, in order to apply the Volterra series for appropriate analysis of nonlinear systems, convergence criteria are necessary. Such criteria to predict the upper limit, the limit in which a system would begin to exhibit severe nonlinearities, have been put forward in [31], [131]–[135].

Convergence analysis and criteria for nonlinear systems that can be represented using the Duffing's oscillator in the frequency domain has been conducted in [31], [134], [135]. The Duffing's oscillator, despite its simple form, has been used as a benchmark example in many studies. This is because it is possible to find nearly every reported nonlinear phenomenon in Duffing's equation [136]. In [135] the authors based the convergence analysis and the criterion on the NOFRFs. In this section, the convergence analysis is revisited using the M-LS method to NOFRFs and novel significant observations are made on the convergence of the Volterra series representation of the Duffing's oscillator.

Initially, the nonlinear system is analysed in the frequency domain using a Response Spectrum Map (RSM) diagram in order to visually analyse the regions in which severe nonlinear behaviour would occur. RSM diagrams were first introduced by Billings and Boaghe in [137] as a frequency domain alternative to the well-known Bifurcation diagrams and it was shown to be more accurate than the Bifurcation diagram. Once the regions of severe nonlinear behaviour are known these regions are then analysed using the NOFRFs evaluated using the M-LS method.

The observations made gives new insight into the Volterra series representation of severe nonlinear systems and the analysis of such systems when exhibiting severe nonlinear behaviour.

5.4.1 NOFRF based local approximation of severe non-linear oscillator exhibiting the jump phenomena

Analysis of a nonlinear stiffness oscillator exhibiting the well-known jump phenomena is conducted using a Duffing's oscillator given by equation (5.21) which was adapted from [138].

$$\ddot{y}(t) + C\,\dot{y}(t) + K_1\,y(t) + K_3\,y^3(t) = A\cos(\omega_F t) \tag{5.21}$$

where $C = 0.96\pi$, $K_1 = (12\pi)^2$ and $K_3 = 0.1(12\pi)^6$. $f_F = {\omega_F}/{2\pi}$ is the excitation frequency ω_F in Hertz (Hz).

The nonlinear system shown in equation (5.21) is first analysed using RSP diagrams as illustrated in Figure 5.7. The RSP diagram is used to see how the Power Spectral Density (PSD) of the output response of the system varies against a change in one aspect of the system. The RSP diagram shown in Figure 5.7-top illustrates how the energy in each frequency component of the output varies against a change in the excitation frequency, f_F. The excitation amplitude A for this RSP diagram is kept at a constant where $A = 1$. For a constant excitation frequency f_A, ${\omega_F}/{2\pi} = f_A = 38\,Hz$ (approximate resonant frequency of the system), the change in the PSD against a varying excitation amplitude A is shown in Figure 5.7-bottom.

It is evident from Figure 5.7 that for this particular system, in the output frequency response, the energy transferred from the excitation input to super harmonics reduces as f_F increases. Thus, the super harmonics higher than the 3rd order diminishes away after a certain f_F. However, the energy transferred to the 3rd order superharmonic, even though is seen to reduce as f_F increases, it is relatively much lesser than other higher order super harmonics. Hence the significance of the 3rd order super harmonic is retained throughout the f_F range shown. From Figure 5.7-bottom it is seen that for this system, given in equation (5.21), for a particular excitation frequency, $f_A = 38\,Hz$, an increase in the excitation amplitude A seem to increase the energy transferred from the excitation input to the higher order harmonics. It is evident from Figure 5.7-bottom that as A increases the overall energy in the output frequency components of the given system increases.

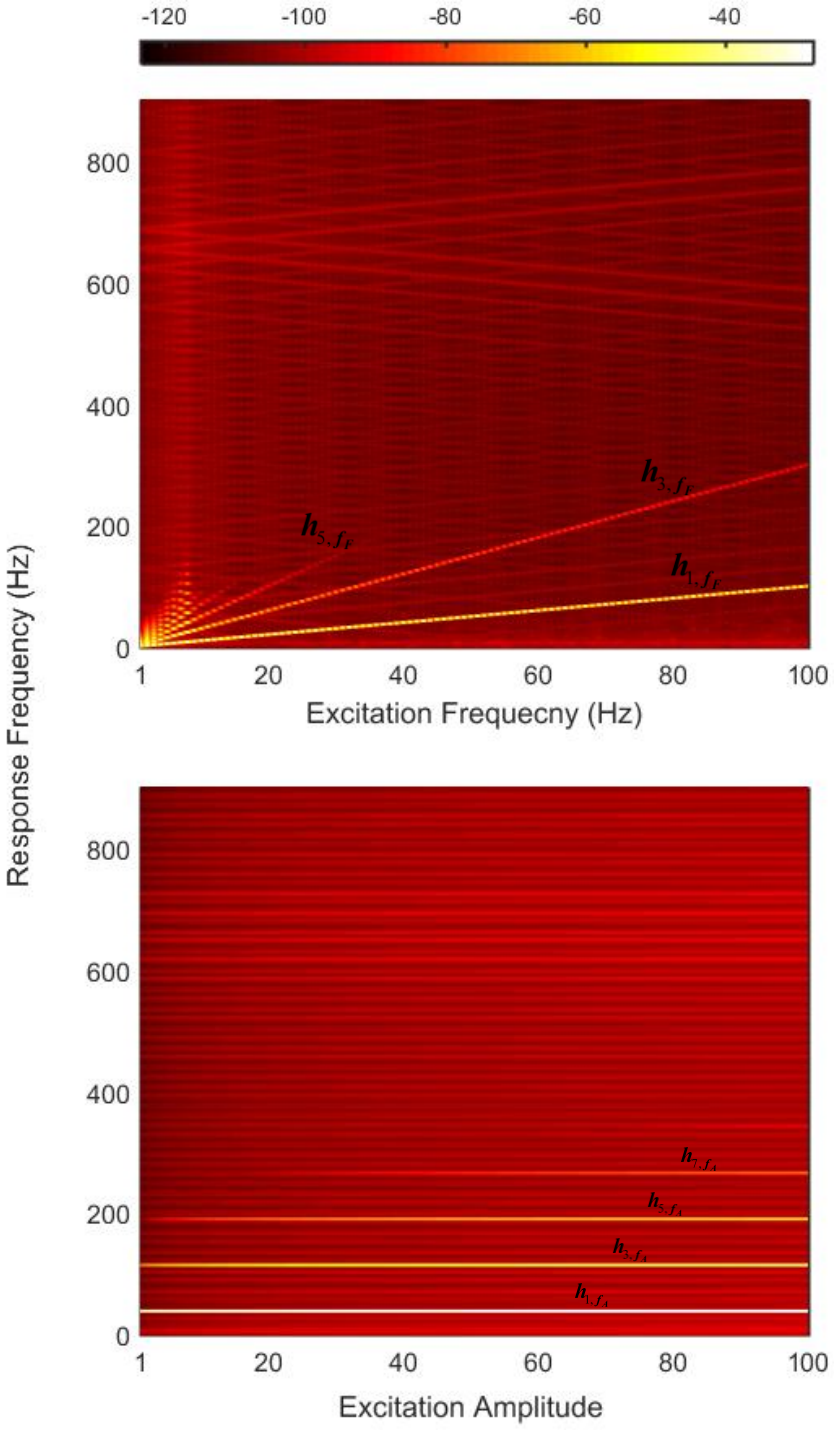

Figure 5.6: RSM diagrams of the nonlinear system shown in equation (5.21) for varying excitation frequency f_F (top) and varying excitation amplitude A at an excitation frequency $f_A = 38$ Hz (bottom). The colour-map illustrates the log magnitude of the PSD. h_{1,f_F}, h_{3,f_F} and h_{5,f_F} shows the progression of the 1st, 3rd and 5th order harmonics with a changing f_F. h_{1,f_A}, h_{3,f_A}, h_{5,f_A} and h_{7,f_A} shows the progression of the 1st, 3rd, 5th and 7th order harmonics with a changing A.

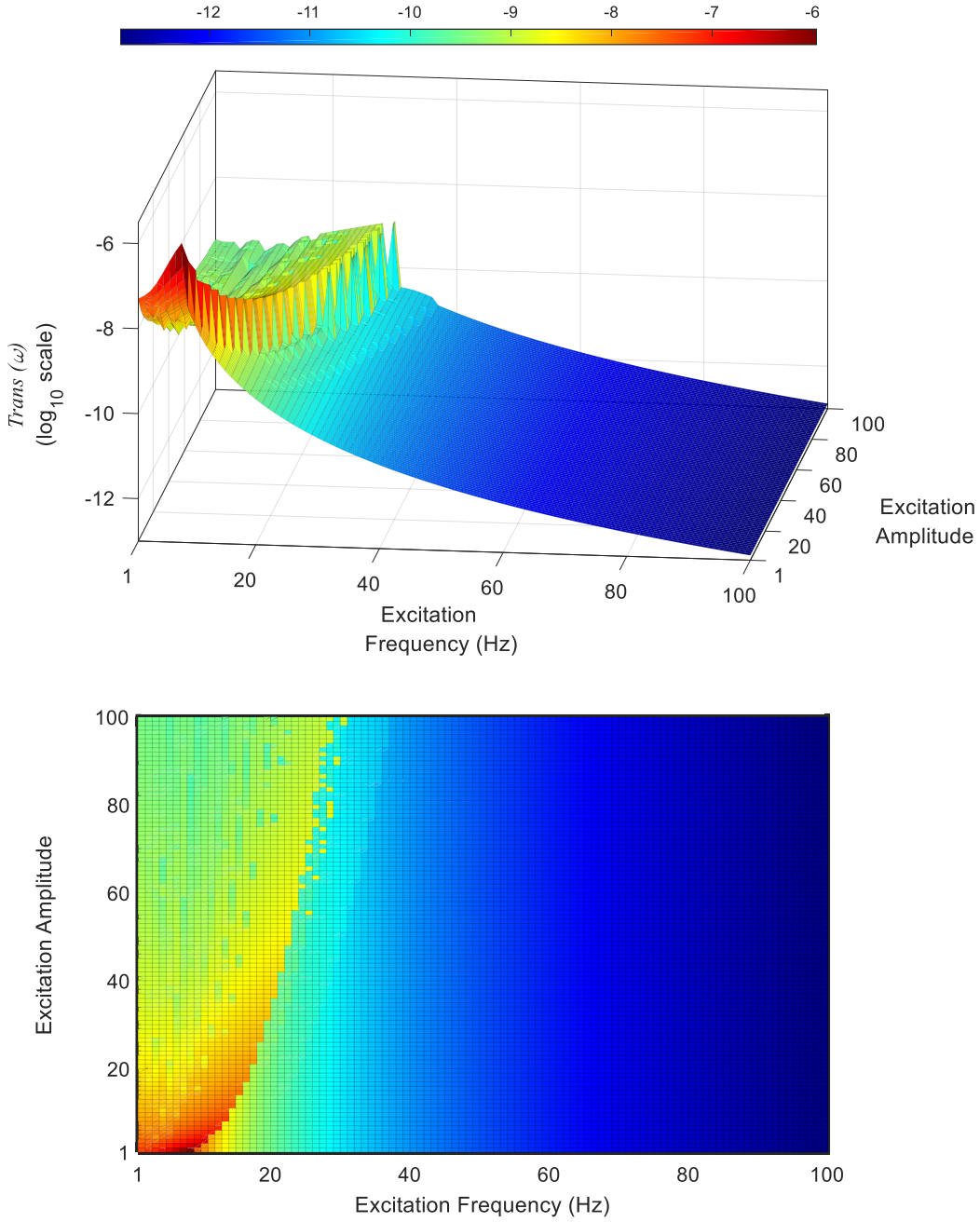

Figure 5.7: Transmissibility map of the system shown in equation (5.21). The regions in which the jump phenomena occur can be clearly seen from the transmissibility map (in the top). Furthermore, the change of the jump location seems to vary with the excitation amplitude while the intensity of the jump is higher at relatively lower excitation frequencies. For this particular system, for the excitation frequency and excitation amplitude ranges shown, a small change in the excitation frequency requires a relatively larger change in the excitation amplitude to create the jump.

Figure 5.7 shows the transmissibility map of the same system where transmissibility $Trans(\omega)$, is the same as defined in equation (5.19) (see Section 5.3.2). The transmissibility map illustrates how the system transmissibility over a range of excitation frequencies f_F changes against a varying excitation amplitude A. It is seen from Figure 5.7-top that the system given in equation (5.21) exhibits the jump phenomena in which there is an abrupt drop in the transmissibility. Figure 5.7 reveals that for this particular nonlinear oscillator the location of the jump region and the intensity of the jump changes with the excitation amplitude and frequency. Furthermore, it is shown from Figure 5.7-bottom that for a small change in the excitation frequency a relatively larger change in the excitation amplitude is required to achieve the jump.

The above qualitative analysis of Figure 5.7 is a reflection of the RSP diagrams of the system shown in Figure 5.6 in which, as mentioned earlier, lower excitation frequencies seem to result in higher energy levels in the output frequency components, especially in the sub-harmonics and higher order super harmonics. Furthermore, as the excitation frequency increases, for the same excitation amplitude, the energy in the sub-harmonics and higher order super harmonics seem to diminish. Therefore, as the excitation frequency is increased a relatively higher excitation amplitude is required in order to transfer more energy from the excitation input to higher order super and subharmonics (Figure 5.6-bottom) in order to achieve a jump as revealed by Figure 5.7-bottom. However, it should be emphasised that from Figure 5.7 it is evident, for the system given in equation (5.21), the jumps occur with a much higher intensity at relatively lower excitation frequencies. Therefore, it is appropriate to state that the excitation frequency plays an important role in combination with the excitation amplitude in which a nonlinear system exhibits severe nonlinear behaviour. Hence frequency domain analysis is required in order to further understand systems that exhibit severe nonlinear behaviour.

NOFRFs based local approximation of the given system

As discussed above both the excitation frequency and the amplitude defines the manner in which severe nonlinear behaviour occurs in the output response and a convergent Volterra series at regions where these behaviours occur is a restriction. However, it is known that theoretically a convergent Volterra series representation around the excitation amplitudes and frequencies where sever nonlinear behaviour occur exists [31]. Such a Volterra series, however, can only be achieved by using extremely high order GFRFs. Since higher order GFRFs are hyper-dimensional frequency functions, this incurs a high computational cost for the evaluation of such GFRFs and thus impractical. However, NOFRFs are one-dimensional frequency functions regardless of the order considered. Thus, with the numerical accuracy of the M-LS method in evaluating NOFRFs, it can be shown that a convergent NOFRFs based representation can be achieved at regions of severe nonlinear behaviour. It should be noted that as an inherent property, the NOFRFs are invariant of amplitude change, thus it is natural that the convergence of the NOFRFs at severe nonlinear regions would be only possible within certain amplitude ranges, hence it would be a local approximation. Therefore, it is shown below that the

NOFRFs can be used to represent severe nonlinear behaviour at different regions within certain amplitude ranges.

The system given in equation (5.21) is used to generate the transmissibility of the system using NOFRFs evaluated from the M-LS method (as similar to the case study in Section 5.3.2). The NOFRFs are used to locally approximate the transmissibility of the given system, Figure 5.7, at two different amplitude regions. For a comprehensive comparison, two types of transmissibility curves are employed. The fundamental transmissibility, $Trans(\omega)$ as shown in equation (5.19), where $\omega = \omega_F = 2\pi f_F$ and the transmissibility of the third order harmonic frequency of the output response, which is given by;

$$Trans_3(3\omega) = \frac{|Y(j3\omega)|}{|U(j\omega)|} \tag{5.22}$$

where $\omega = \omega_F = 2\pi f_F$. f_F is the excitation frequency in Hertz (Hz). $Y(j3\omega)$ is the output response $Y(j\omega)$ at the 3rd harmonic frequency and $U(j\omega)$ is the frequency spectrum of the input at ω.

The normalised mean square error (NMSE) was used as a measure of the closeness of fit between the NOFRFs generated and the actual transmissibility curves, which is given by;

$$NMSE_{Trans} = \frac{\sum\left(|Trans(\omega_F)| - |Trans_{NOFRF}(\omega_F)|\right)^2}{\frac{1}{F_L}\sum\left(|Trans(\omega_F)| - \left(|Trans_{NOFRF}(\omega_F)|\right)\right)^2}, \quad \omega_F = 2\pi f_F \tag{5.23}$$

where F_L is the number of harmonic excitation frequencies used for the generation of the transmissibility curves.

As mentioned earlier the NOFRFs are evaluated at two different amplitude ranges $\bar{A}_1 = \left[A_{H_1}, A_{L_1}\right]$ and $\bar{A}_2 = \left[A_{H_2}, A_{L_2}\right]$, where A_{H_1} and A_{H_2} are the highest amplitudes and A_{L_1} and A_{L_2} are the lowest amplitudes of the ranges $\bar{A}_1$ and $\bar{A}_2$ respectively. The difference $A_{H_1} - A_{L_1} = A_{H_2} - A_{L_2} = \nabla A_{H,L}$. The low amplitude region $\bar{A}_1 = [1.3, 1.2]$ and the high amplitude region $\bar{A}_2 = [99.3, 99.2]$ thus $\nabla A_{H,L} = 0.1$. The NOFRFs evaluated at the region $\bar{A}_1$ is used to generate transmissibility curves at A_{p_1}, where $A_{p_1} > A_{H_1}$. Similarly, the NOFRFs evaluated at $\bar{A}_2$ is used to generate transmissibility curves at A_{p_2}, where $A_{p_2} > A_{H_2}$. Thus the NOFRFs obtained at $\bar{A}_1$ and $\bar{A}_2$ are tested outside the respective regions in order verify that the NOFRFs have indeed captured the underlying dynamics. The quality of the NOFRFs generated transmissibility curves are assessed using the NMSE against the respective true transmissibility curves at A_{p_1} and A_{p_2}.

Local approximation of the severe nonlinear dynamics at $\bar{A}_1 = [1.3, 1.2]$

NOFRFs at $\bar{A}_1$ are evaluated using the set of amplitudes within $\bar{A}_1$, as shown in Table 2, and considering a maximum order of nonlinearity $N = 9$. Figure 5.8 illustrates that the NOFRFs evaluated using this set of amplitudes and can regenerate the transmissibility curves at these respective amplitudes well. Table 2 shows how well the NOFRFs generated transmissibility curves are in terms of the NMSE. It should be noted that throughout this

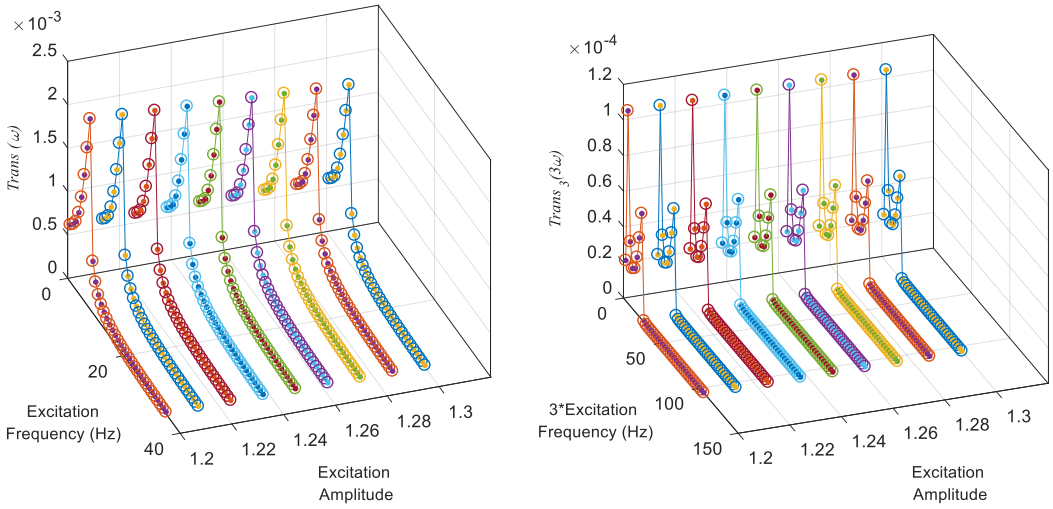

Figure 5.8: Actual and NOFRFs estimated transmissibility curves within the amplitude range shown in Table 2. The NOFRFs are evaluated using the amplitudes A shown. In comparison to the systems actual transmissibility (line with dot), the NOFRFs generated (circle) transmissibility curves are shown to be accurate. This means that the NOFRFs evaluated using the given amplitudes are able to regenerate the respective transmissibility curves well. The diagram on the left is transmissibility of the fundamental frequency, i.e. the excitation frequency. The diagram on the right illustrates the transmissibility of the 3rd order harmonic frequency.

Note: Throughout this section, e refers to the base of 10 and not the Euler's number, i.e. $e = 10$.

Table 2: NMSE between actual and NOFRFs generated transmissibility curves.

NOFRFs evaluation amplitudes (A)	$NMSE_{Trans}$	$NMSE_{Trans_3}$
1.300	$4.8656e^{-15}$	$2.4686e^{-10}$
1.2875	$4.0928e^{-14}$	$7.2178e^{-10}$
1.2750	$7.6648e^{-15}$	$1.2471e^{-10}$

1.2625	$2.7984e^{-14}$	$2.1336e^{-10}$
1.2500	$2.6736e^{-16}$	$5.5674e^{-10}$
1.2375	$3.1613e^{-14}$	$7.8171e^{-11}$
1.225	$4.2856e^{-15}$	$3.2823e^{-10}$
1.2125	$4.888e^{-14}$	$8.1695e^{-10}$
1.2000	$7.2746e^{-15}$	$4.8329e^{-10}$

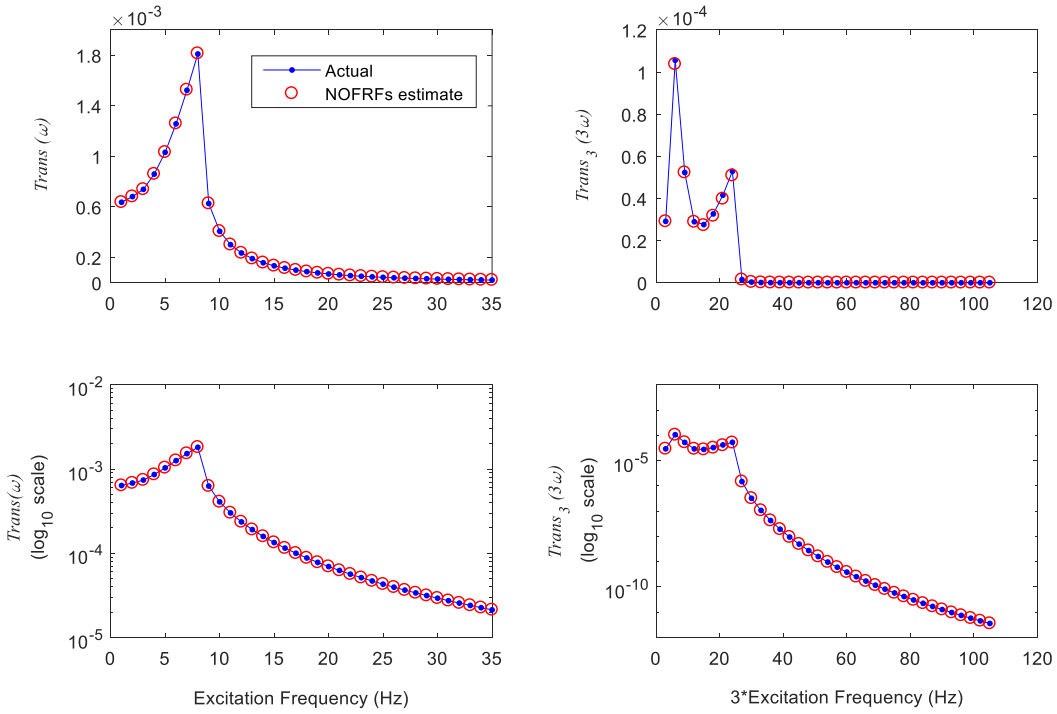

Figure 5.9: Comparison of the actual system transmissibility curves to the NOFRFs generated at the excitation amplitude $A_{P_1} = 1.5$. It is evident that the NOFRFs, of the given system, evaluated at $\bar{A}_1$ has captured the dynamics well as the NOFRFs generated transmissibility curves match well with the actual.

The NOFRFs evaluated should capture the dynamics of the system within the amplitude range well. To verify this, the evaluated NOFRFs are used to generate transmissibility curves outside $\bar{A}_1$. Thus the NOFRFs evaluated are used to generate

transmissibility curves at the amplitude $A_{p_1} = 1.5$ as shown in Figure 5.9. From Figure 5.9 it is evident that the NOFRFs have captured the dynamics, within $\bar{A}_1$ well. The NMSE between the actual and the NOFRFs generated transmissibility curves of the fundamental, $Trans(\omega)$, and the 3rd order harmonic, $Trans_3(3\omega)$, at A_{p_1} are $1.2416e^{-4}$ and $2.2501e^{-2}$ respectively. It should be noted that beyond $A_{p_1} = 1.5$ the NOFRFs generated transmissibility curves do not fit well with the actual. Therefore, the NOFRFs evaluated within $\bar{A}_1$ with $N = 9$ are invalid beyond this amplitude. However, by using an amplitude range $\bar{A}_1^*$ closer to the values beyond $A_{p_1} = 1.5$ for the evaluation of NOFRFs would result in accurate approximations for $A_{p_1} > 1.5$.

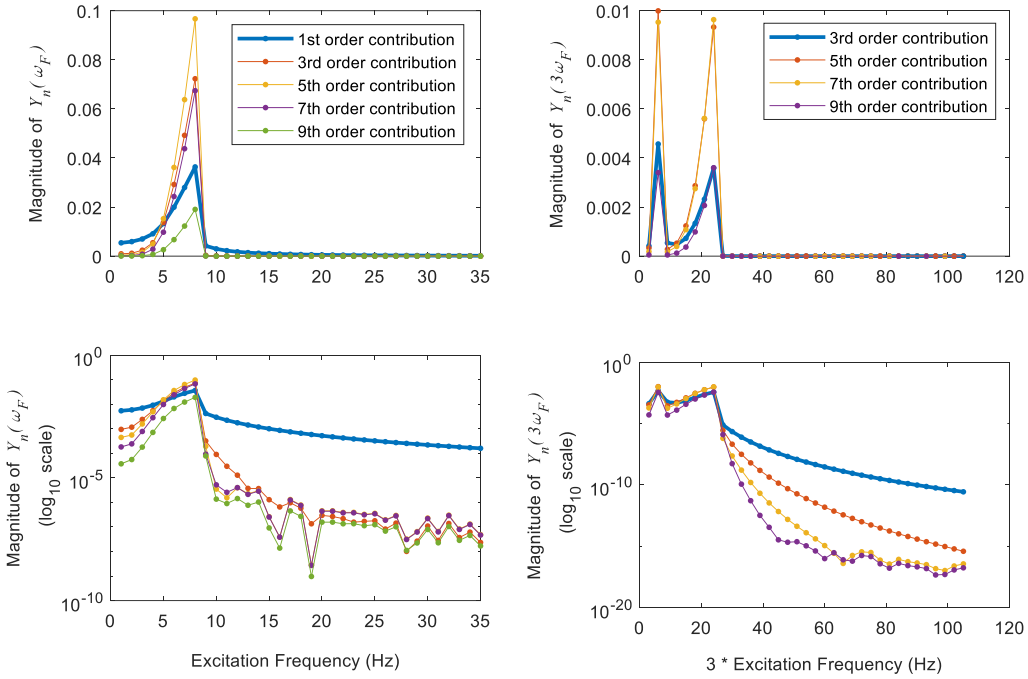

Figure 5.10: The output frequency responses of each order of nonlinearity at each excitation frequency point, f_F, (left) and 3rd order harmonic of f_F (Right). Produced using the evaluated NOFRFs with a harmonic input of excitation amplitude $A_{p_1} = 1.5$. It is evident that the NOFRFs based approximation is convergent because the contributions made by the highest order of nonlinearity is lower than the corresponding lowest order of nonlinearity.

Figure 5.10 shows the respective contributions made by the output frequency response of the n^{th} order of nonlinearity $Y_n(\omega)$, $n = 1, \cdots, N$ to the final output response $Y(j\omega)$. Figure 5.10-left illustrates the contributions by $Y_n(\omega)$ at each excitation frequency point f_F while Figure 5.10-right shows the contributions made at the corresponding 3rd order harmonic $3f_F$. It is seen from Figure 5.10-left, for $Trans(\omega)$, that

all the orders of nonlinearity, except $Y_9(j\omega)$, have higher contributions than $Y_1(j\omega)$ at the jump region where $f_F \approx [5,10]$. The NOFRFs are convergent at this region because the contributions made by $Y_9(j\omega)$ to the final output response is lesser than $Y_1(j\omega)$. Thus, the system can be represented by a finite set of nonlinearities. Similarly, for $Trans_3(3\omega)$, in Figure 5.10-right the highest order of nonlinearity $Y_9(j3\omega)$ contributes lesser than the lowest order $Y_3(j3\omega)$ for the output response at the 3rd order harmonic. Therefore, the evaluated NOFRFs are also convergent at the 3rd order harmonic in the output response of the system.

The initial choice of $N = 9$ was found to be the minimum requirement for the NOFRFs to be convergent when testing the evaluated NOFRFs within $\bar{A}_1$ itself. That is $|Y_9(j\omega)| < |Y_1(j\omega)|$ and $|Y_9(j3\omega)| < |Y_3(j3\omega)|$ for $\omega = \omega_F$ at amplitudes shown in Table 2. Furthermore, it was observed that the evaluated NOFRFs remain convergent for excitation amplitudes outside $\bar{A}_1$ until $A_{p_1} = 1.5$. As the evaluated NOFRFs were tested for $A_{p_1} > 1.5$ the NOFRFs were found to be divergent, i.e. $|Y_n(j\omega)| > |Y_1(j\omega)|$ for $n > 1$ and $|Y_n(j3\omega)| > |Y_3(j3\omega)|$ for $n > 3$. Thus, the fit between the actual and the NOFRFs generated transmissibility curves were poor for $A_{p_1} > 1.5$.

Local approximation of the severe nonlinear dynamics at $\bar{A}_2 = [99.3, 99.2]$

Similar to the above, a NOFRFs based local approximation was made at the high amplitude region $\bar{A}_2$. The NOFRFs were evaluated within $\bar{A}_2$ using the set of amplitudes shown in Table 3. The NOFRFs were evaluated considering a maximum order of nonlinearity $N = 13$ such that it was the minimum value of N for which the NOFRFs exhibited the convergent property at the amplitudes shown in Table 3. That is at these amplitudes, when observing the output frequency response of each order of nonlinearity, $Y_n(\omega)$, $n = 1, \cdots, N$, the highest order of nonlinearity, N, should contribute lesser than the lowest order at that frequency. Thus $|Y_N(j\omega)| < |Y_1(j\omega)|$ and $|Y_N(j3\omega)| < |Y_3(j3\omega)|$ at the amplitudes shown in Table 3 for $\omega = \omega_F$. Furthermore, it was verified that the transmissibility curves regenerated using the evaluated NOFRFs would fit well with the actual at $\bar{A}_2$.

In order to verify that the evaluated NOFRFs have actually captured the dynamics within $\bar{A}_2$, these NOFRFs were tested at the excitation amplitudes $A_{p_2} = 99.35$ and $A_{p_2} = 99.4$ which are outside $\bar{A}_2$. The NMSE between the actual and the NOFRFs generated transmissibility curves at these amplitudes are shown in Table 4.

Table 3: NMSE between actual and NOFRFs generated transmissibility curves.

NOFRFs evaluation amplitudes (A)	$NMSE_{Trans}$	$NMSE_{Trans_3}$
99.300	$1.6053e^{-5}$	$1.6104e^{-4}$
99.292	$1.4390e^{-5}$	$2.6120e^{-4}$
99.283	$3.2963e^{-5}$	$9.1425e^{-5}$
99.275	$1.7547e^{-5}$	$1.4727e^{-4}$
99.267	$2.6894e^{-6}$	$1.6563e^{-3}$
99.258	$6.4897e^{-5}$	$8.0240e^{-4}$
99.250	$7.3784e^{-6}$	$1.4369e^{-4}$
99.242	$1.9374e^{-5}$	$3.6998e^{-4}$
99.233	$4.5994e^{-5}$	$3.6176e^{-4}$
99.225	$1.3774e^{-5}$	$3.3659e^{-4}$
99.217	$6.2013e^{-6}$	$8.9426e^{-4}$
99.208	$4.3877e^{-5}$	$9.7498e^{-4}$
99.200	$2.3241e^{-5}$	$2.8465e^{-4}$

Table 4: NMSE between actual and NOFRFs generated transmissibility curves.

NOFRFs test amplitudes (A)	$NMSE_{Trans}$	$NMSE_{Trans_3}$
99.35	$3.6900e^{-4}$	$7.73134e^{-3}$
99.40	$1.6216e^{-3}$	$5.9161e^{-2}$

It is can be seen from the transmissibility map of the given system, Figure 5.7, in the amplitude region $\bar{A}_2 = \left[A_{H_2}, A_{L_2} \right] = [99.3, 99.2]$ jumps occur at a lesser intensity than the lower amplitude regions. However, when inspecting the RSM diagram of the given system at an excitation amplitude $A = 99.3$ (which is A_{H_2}), as shown in Figure 5.11-top. The output frequency characteristics for different excitation frequencies is much more complex than at lower excitation amplitudes, Figure 5.6-top. This is also evident from the transmissibility of the given system at $A = 99.3$ as shown in Figure 5.11-bottom. At this excitation amplitude, the transmissibility curve shows the occurrences of more than one jump. Hence it is appropriate to say that for the given system at higher excitation amplitudes, exhibits relatively more severe nonlinearities than at lower amplitudes. However, a local approximation of the system using the NOFRFs is achieved.

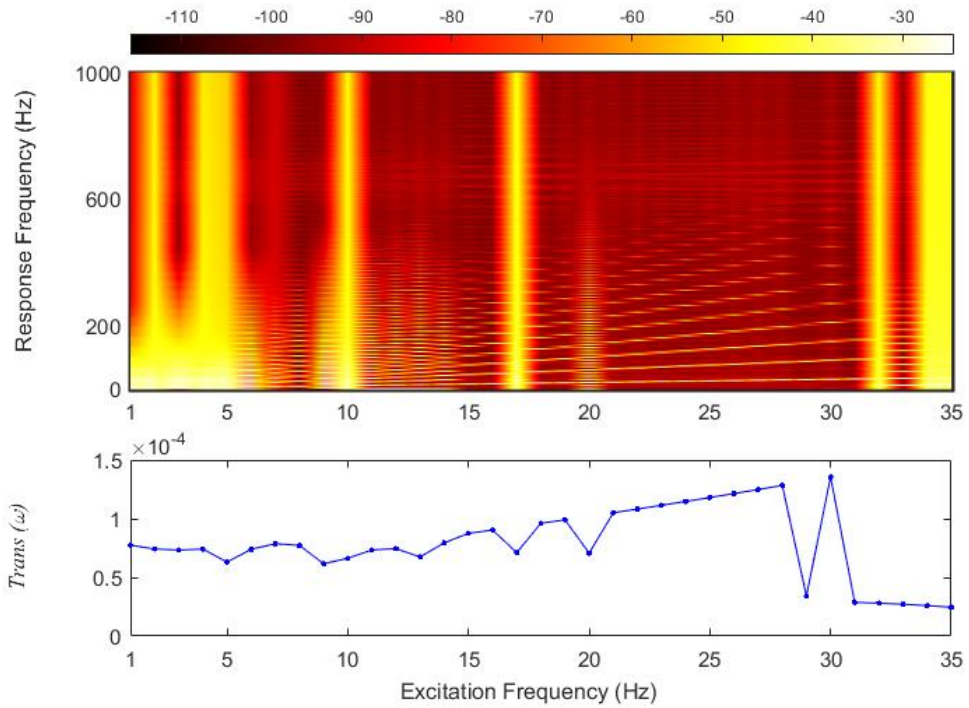

Figure 5.11: RSM (top) and transmissibility (bottom) diagrams of the given system for an excitation amplitude $A = 99.3$. It is seen from both these diagrams that the given system at the excitation amplitude $A = 99.3$ exhibits more severe nonlinear behaviour than at lower excitation amplitudes.

The NOFRFs evaluated at $\bar{A}_2$ when tested at $A_{p_2} = 99.35$ were able to generate the transmissibility curves $Trans(\omega)$ and $Trans_3(3\omega)$ which fit well with the actual at all frequency points for $\omega = \omega_F$. Furthermore, it was verified that the evaluated NOFRFs were indeed convergent by observing the output frequency response of each order of nonlinearity, $Y_n(\omega)$, $n = 1, \cdots, N$, where the highest order of nonlinearity did contribute

lesser than the lowest order. However, this wasn't the case for $A_{p_2} = 99.4$ thus the NOFRFs evaluated at $\bar{A}_2$ is only valid till $A_{p_2} = 99.35$.

Considering that the difference $\nabla A_{H,L}$, where $\nabla A_{H,L} = A_{H_2} - A_{L_2} = A_{H_1} - A_{L_1}$ as mentioned earlier, it is worth emphasising that choice of $N = 13$ for the same $\nabla A_{H,L}$ at higher evaluation amplitudes is a reflection of the characteristics of the given system. This is that at higher excitation amplitudes the output response exhibits more severe nonlinearities than at lower excitation amplitudes as mentioned earlier.

Figure 5.12 illustrates the comparison between the transmissibility curves generated by the evaluated NOFRFs when tested at $A_{p_2} = 99.4$. The fundamental transmissibility $Trans(\omega)$ curve generated by the NOFRFs fits well along all the frequency points and was

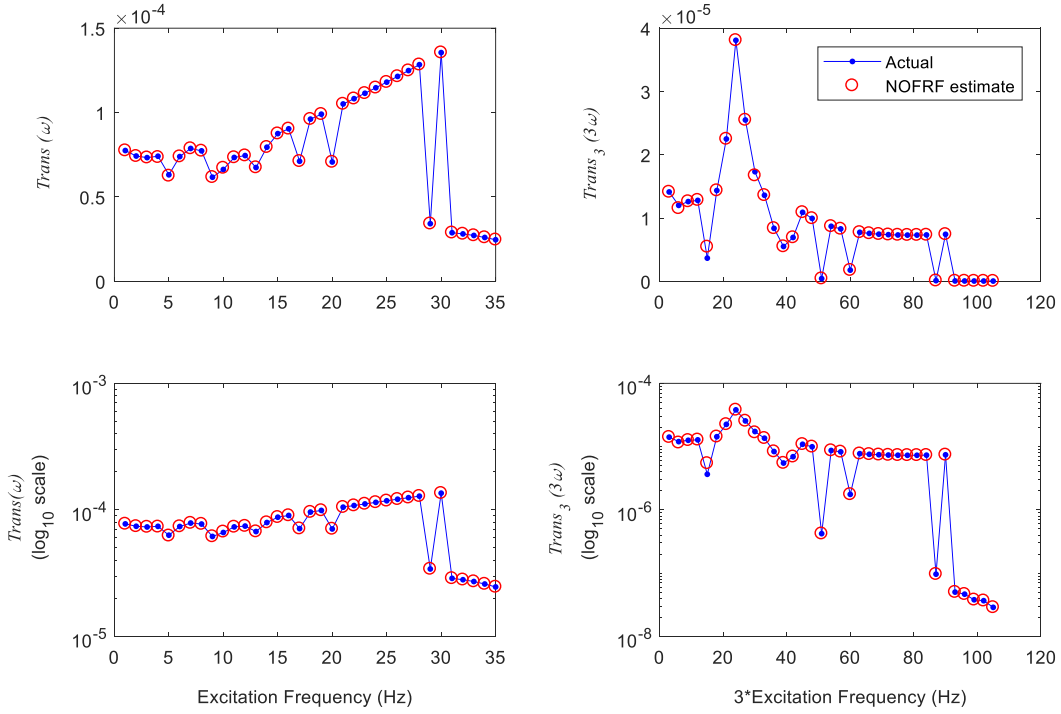

Figure 5.12: Comparison of the actual system transmissibility curves to the NOFRFs generated at the excitation amplitude $A_{p_2} = 99.4$. It is evident that the NOFRFs, of the given system, evaluated using the amplitudes shown in Table 3 has captures the dynamics fairly well as the NOFRFs generated transmissibility curves match well with the actual except for $Trans_3(3\omega)$ at the frequency points $3f_F = 6, 15$.

convergent considering $Y_n(\omega)$, $n = 1, \cdots, N$. However, $Trans_3(3\omega)$ generated by the NOFRFs at this amplitude generally fits well along all the frequency points except at $3f_F = 6, 15$. This is because at these frequency points the contributions made to the final output response at the 3rd harmonic, $Y(j3\omega)$, by the output frequency responses of all

the higher orders of nonlinearities $Y_n(j3\omega)$, $n=5,\cdots,N$ where $N=13,$ were higher than the contribution made by the lowest order which is $Y_3(j3\omega)$. This is shown in Figure 5.13, where the inner axes show a zoomed in section of the outer axes at the frequency point $3f_F=15$.

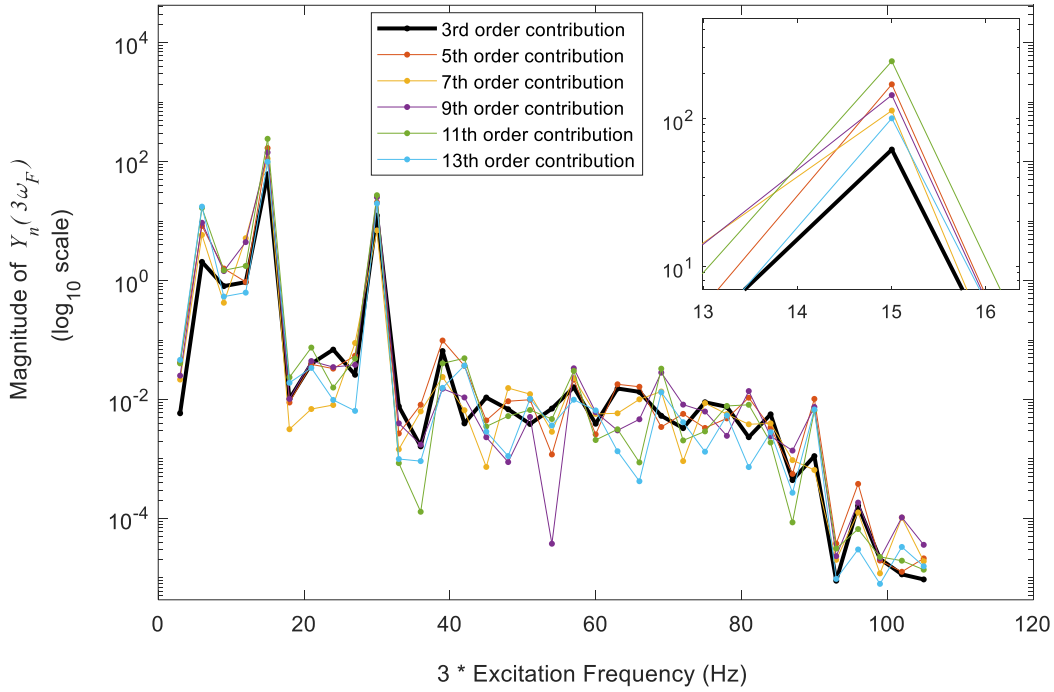

Figure 5.13: The output frequency responses of each order of nonlinearity at the 3rd order harmonics of each excitation frequency point, f_F. Is obtained when the evaluated NOFRFs were tested for a harmonic input with an excitation amplitude $A=99.4$. The inner axes illustrate the outer axes zoomed in at the frequency point $3f_F=15$.

Considering the evaluation of NOFRFs at an amplitude region $\bar{A}^*=\left[A_{H_*},A_{L_*}\right]$. Given the NOFRFs evaluated are able to generate transmissibility curves, outside $\bar{A}^*$, providing a good fit with the actual transmissibility curves along all the frequency points considered. Also, NOFRFs approximation exhibits convergence when considering the contributions of each order of nonlinearity to the output at amplitudes outside $\bar{A}^*$. Let the maximum excitation amplitude outside $\bar{A}^*$ in which the evaluated NOFRFs can achieve this until be A'_{p_*}, where $A'_{p_*}>A_{H_*}$. Therefore, the NOFRFs from the region $\bar{A}^*$ is valid until A'_{p_*}.

In the case of NOFRFs based local approximation of the given system at the region $\bar{A}_1=[1.3,1.2]$, $A'_{p_*}=1.5$ while for the case of $\bar{A}_2=[99.3,99.2]$, $A'_{p_*}=99.35$. Recall that $\nabla A_{H,L}=A_{H_2}-A_{L_2}=A_{H_1}-A_{L_1}$. Thus from the analysis of the above two cases, at excitation

amplitude region $\bar{A}^*$ where the nonlinear behaviour is relatively more severe, the maximum excitation amplitude in which the NOFRFs are valid until, A'_{p*}, is much closer to region $\bar{A}^*$. This is given that the choice of N used for the evaluation of NOFRFs is such that it is the minimum requirement for the evaluated NOFRFs to be convergent within $\bar{A}^*$. However, for the case $\bar{A}_2 = [99.3, 99.2]$, it was found that $A'_{p*} \to 99.4$ when the NOFRFs are re-evaluated at the same amplitude range but with a much higher value of N, $N \gg 13$.

From the above analysis, it is evident that the theoretical convergence of the Volterra series at regions of severe nonlinear behaviour is indeed possible when using the NOFRFs. This is because the NOFRFs are one-dimensional frequency functions based on the Volterra series thus enabling the use of higher-order nonlinearities with ease. It should be emphasised the use of NOFRFs for such a convergence was achieved because of the numerical accuracy in the M-LS method to the evaluation of NOFRFs. Furthermore, it should be mentioned that a convergence of a Volterra series based concept, such as the NOFRFs, at the regions of severe nonlinear behaviour has not been reported before to the best knowledge of the author of this thesis. The observations made above and the ability to use the NOFRF to analyse a system that exhibits severe nonlinear behaviour has many advantages in analysis, design and Fault Diagnosis of these types of systems. Furthermore, this could be an initial step into the analysis of severe nonlinear systems in the frequency domain.

5.5 Summary

This chapter presents an improvement to the original LS method [29] of evaluating NOFRFs. It is shown that this new method, the M-LS method, has better accuracy in the evaluation of NOFRFs. This higher accuracy is gained by appropriate construction of the information matrix used in the least-squares such that only the necessary terms are included at each frequency point. This increases the condition number of the information matrix but most importantly the decomposition to the respective orders of nonlinearities is attained appropriately. This allows the NOFRFs to be evaluated more accurately with just the system input-output data. The NOFRFs can be used to decompose the output of a nonlinear system to its respective output nonlinearities in the frequency domain and therefore facilitate practical nonlinear system analysis with applications including engineering system Fault Diagnosis and structural system health monitoring. Because of the accurate decomposition of the nonlinearities by the NOFRFs using the M-LS method and the NOFRFs being one-dimensional frequency functions based on the Volterra series. For the first time, the theoretical convergence of such a method is observed for sever nonlinear systems at regions which it was not possible or impractical. This is because of the high computational inefficiencies that are inherently present in the multi-dimensional nature of the Volterra series based methods such as the GFRFs.

The system under investigation was analysed qualitatively in detail using a transmissibility map and RSM diagrams drawing relationships between both. In this

analysis, it was pointed out that the excitation frequency and the amplitude play an important part in the exhibition of severe nonlinear behaviour. The exhibition of severe nonlinear behaviour was studied at two different amplitude regions. The severe nonlinearity that was investigated in this study was the jump phenomenon. The NOFRFs of the system evaluated under the two amplitude regions was confirmed to converge at the jump phenomenon given the adequate choice of maximum nonlinearity N. It was discussed in detail how the choice of N was made. The choice of N, should be high enough so that the contribution of the N^{th} order of nonlinearity to the output should be less than the contribution of the corresponding lowest order, at that the respective harmonic. This is an initial step and new insight into the analysis of severe nonlinear systems in a pure Frequency Response Analysis approach. This will facilitate the analysis, design and Fault Diagnosis of systems that exhibit severe nonlinear behaviour.

Chapter 6

Data-driven Condition Monitoring and Fault Diagnosis Using System Identification and Frequency Response Analysis

6.1 Introduction

As mentioned in Chapter 1 and Chapter 2 CM-FD provides the means for safe and reliable operation of engineering systems ensuring confidence in the state of the system to the user. Through CM-FD necessary information of the state of the system can be obtained for predictive maintenance and operation of the system safely. In Chapter 2 Section 2.4 a control systems perspective to CM-FD through System Identification of black-box time-series models and the analysis of these models based on Frequency Response Analysis was discussed. By using black-box modelling techniques avoids the need for detail physical models, which is often not feasible in practise [22]. Discrete-time black-box models of a continuous-time system are not a unique solution, therefore, the Frequency Response Analysis is used to obtain unique fault specific features for CM-FD (see Section 2.4). The principle behind this approach is that any changes in the physical properties of the system can be observed from the changes in the Frequency Response Analysis. Thus CM-FD is conducted by observing features extracted from the Frequency Response Analysis. In the case of linear systems, the identified ARX model will be analysed in the frequency domain using the well-known linear FRFs. Similarly, in the nonlinear instance, the identified NARX model will be analysed using the NOFRFs.

As mentioned in Chapter 4 Section 4.3 and because the significant improvement of the extraction of NOFRFs, introduced in Chapter 5, the NOFRFs are more feasible in relation to the GFRFs for the Frequency Response Analysis of nonlinear systems, especially in the context of CM-FD. Peng *et al.* in [19] proposed and demonstrated the performance of the basic methodology of combining NARMAX modelling and NOFRFs to conduct CM-FD of engineering systems. Bayma and Lang in [15], built on the idea proposed in [19], introduced a comprehensive framework for CM-FD using NARMAX modelling and NOFRFs. The authors of [15] proposed the use of a priori trained PCA (Principal Component Analysis) algorithm in order to extract representative features from a larger set of NOFRFs based frequency domain features. The features where then processed using a priori trained neural network based classifier to indicate the status of the system.

This chapter mainly focuses on the practical implementation of using System Identification and Frequency Response Analysis for CM-FD with the emphasis on System Identification. Some of the major practical concerns in using System Identification are; the adequate choice of sampling time, inputs which do not persistently excite the system and the assurance of evaluating a stable model from the System Identification methodology. Inadequate inputs which are not persistently exciting and not being able to excite important dynamics of a system are widely present in CM-FD. In the wider context of CM-FD, at times, nothing can be done about this. This is because CM-FD has to be carried out without disrupting normal operations of the system by feeding different inputs [25]. Such concerns regarding System Identification have not been considered in the literature in the context of FDI, either using SI on its own or even in combination with FRA. Thus, a more optimised methodology of System Identification for practical applications is presented.

The chapter discusses in detail the concepts and the importance of the appropriate selection of sampling time, selection of the maximum dynamic order and the formulation of a stable model under inadequate excitation inputs. The System Identification methodology is formulated considering these concepts by using some of the already known methods. However, in order to efficiently produce stable time-series models under inadequate inputs a new System Identification algorithm is presented. It should be emphasised that a complete System Identification methodology, for CM-FD, that addresses the above-mentioned concerns for practical applications has not been presented or discussed before in the literature.

6.2 Sampling time, System Identification and nonlinearity detection

Sampling time is a critical factor that needs to be considered for the quality of dynamical reconstruction of nonlinear systems from input-output data [28], [139]–[142]. It is well known that the performance of structure detection and parameter estimation algorithms are affected by the sampling time of the data under investigation [28]. Worden *et al.* in [143] pointed out that the effects of sampling time while does not affect the validity of the model but however, produces models that are overly complex. Although overly complex model at times is adequate for prediction purposes [143], including more terms than required will usually lead to models that exhibit spurious dynamical effects that are not actually present in the real system and at worst be numerically unstable [26], [27]. If the sampling time or the delay time between samples, T_s is too long the data will be undersampled and this will cause a loss of dynamic behaviour that is present within the data. Conversely, if the sampling time is too short then the data will be oversampled and be highly correlated, i.e. $y(t) \approx y(t-1)$, which will result in numerical issues.

Billings and Aguirre in [28] demonstrated that smaller sampling times favoured accurate parameter estimation while higher sampling times improved structure detection capabilities. However, the authors also pointed out that as $T_s \to 0$, $y(t-1) \to y(t)$ will cause numerical problems leading to a deterioration in the accuracy of parameter

estimation. It should also be emphasised that in the case where the sampling time is too small and $y(t) \approx y(t-1) \approx y(t-2)$, the parameter estimation process will give a higher weighting to output lagged terms such as $y(t-1)$ and $y(t-2)$. Consequently, this will result in a deteriorate in the dynamical effect of a black-box model thus deterring the attempt to reconstruct the dynamical mapping of the input $u(t)$ of the system to the output $y(t)$. As such this would affect the detection of the model structure, especially the detection and parameter estimation of nonlinear model terms. Therefore, a compromise in the selection of sampling time is necessary. Thus, in order to obtain satisfactory results, it may be necessary to downsample the observed data appropriately before conducting System Identification. The appropriate sampling time can be chosen using several available methods [144] and a commonly used method is based on the correlation function [145]. In order to accommodate nonlinear correlations the method of selecting an appropriate sampling time has been proposed in [28] based on nonlinear autocorrelation functions. The performance of this method and its consistency has been demonstrated and a rigorous analysis of the method and the justification of its use is available in [28], [139], [140]. The specifics of this method are as follows;

- Considering the correlation functions;

$$\begin{cases} \Phi_{yy}(\tau_c) = \mathrm{E}\left[\left(y(t) - \overline{y(t)} \right) \left(y(t-\tau_c) - \overline{y(t)} \right) \right] & , \ \tau_c = 0,1,\cdots, \\ \Phi_{y^{2'}y^{2'}}(\tau_c) = \mathrm{E}\left[\left(y^2(t) - \overline{y^2(t)} \right) \left(y^2(t-\tau_c) - \overline{y^2(t)} \right) \right] & , \ \tau_c = 0,1,\cdots, \end{cases} \tag{6.1}$$

  where $\mathrm{E}[.]$ is denoted as the mathematical expectation and the overbars represent averaging with respect to time.

- Choose τ_m such that;

$$\tau_m = \min\left\{ \tau_y \, , \tau_{y^{2'}} \right\} \tag{6.2}$$

  where τ_y and $\tau_{y^{2'}}$ are the first minimums of $\Phi_{yy}(\tau_c)$ and $\Phi_{y^{2'}y^{2'}}(\tau_c)$ respectively. For systems that are explicitly known to be linear $\tau_m = \tau_y$ can be used directly.

- Finally, an appropriate sampling time can be chosen in the range;

$$\frac{\tau_m}{20} \le T_s \le \frac{\tau_m}{10} \tag{6.3}$$

- The above rule is a heuristic relation and not a precise mathematical one, as such the range shown in equation (6.3) can be often relaxed to [140];

$$\frac{\tau_m}{25} \le T_s \le \frac{\tau_m}{5} \tag{6.4}$$

6.3 Model term selection criterion and model building

The selection of appropriate model terms is of vital importance in order for the approximate dynamical reconstruction of a system from its input-output data [27], [146]. As pointed out in the previous section the sampling time, T_s, needs to be considered. Furthermore, the choice of maximum dynamic (lag) orders, n_y, n_u and n_c of the output $y(t)$, input $u(t)$ and the residuals $e(t)$ (also known as embedding dimensions), which will be used by a model structure determination algorithm such as the FRO is of significance, this has been pointed out in [26]. As discussed in Chapter 3 Section 3.6.2, two popularly used model term selection criteria are the ERR based FRO algorithm [109], [110] and the SRR based SEMP (Simulation Error Minimisation with Pruning) algorithm [106]. However, both these algorithms have shortcomings and are affected by the sampling time issue in the context of the approximate dynamical reconstruction of the true system dynamics. This section aims to formulate a System Identification methodology which will take into account the considerations of sampling time, dynamic order and model structure determination.

6.3.1 Choice of maximum dynamic order

Considering $n_y = n_u$, the choice of the maximum dynamic order n_y in the context of nonlinear System Identification is significant for the discrete dynamical reconstruction of the continuous time dynamics from the input-output data of the system. This is because the choice of n_y higher than a certain value has been reported to produce spurious dynamics in the case of chaotic systems [26] due to the occurrence of unnecessary Lyapunov exponents [146].

Aguirre and Billings in [27] introduced the concept of model structure space (MSS). It is the space in which all possible identified model structures can be characterised under. The MSS in [27] is defined in terms of the sampling time T_s, the dynamic order n_y and the total number of process terms n_p in the polynomial model. The authors demonstrated that the appropriate model structures resulting in the best-estimated models in the MSS lie within certain bounds. The best estimated models are with regard to dynamical reconstruction. Thus the sub region $\wp$ in the MSS in which these best model structures lies is in relation to the bounds of T_s, n_y and n_p, in which $\wp(n_y, n_p, T_s)$. Mendes and Billings in [147] expanded the initial concept of MSS and the subregion $\wp$ and revealed that $\wp$ should also be defined using the data length L used, the noise variance and the number of noise terms.

In considering the above and the usual approach that initially the process model structure is to be determined first before the noise model is considered, to avoid bias in the process model structure selection [24], [72]. The initial choice of T_s, n_y ($n_y = n_u$) and n_p is thus significant. The choice of T_s can be done using the approach introduced in

Section 6.2. For the initial determination of the maximum dynamic orders n_y and n_u, the method of obtaining a reduced set of candidate terms proposed by Wei *et al.* in [148] can be used. This method is introduced in the following section.

6.3.2 Reduced set of candidate model terms

Wei and Billings in [148] proposed an effective method of obtaining a reduced set of candidate model terms for the identification of nonlinear systems. This is based on the idea of fitting a locally linear model to the input-output data of a nonlinear system using the FRO algorithm. The set of input and output lagged terms or regressors of this local linear model, $\mathbf{\Phi}_{lin}$, is then used to compose the set of nonlinear model terms (regressors) $\mathbf{\Phi}_{nl}$. The reduced set of candidate model terms $\mathbf{\Phi}_s = \{\mathbf{\Phi}_{lin}, \mathbf{\Phi}_{nl}\}$ is then used for the identification of the nonlinear model. The authors demonstrated the effectiveness of this method and showed that this can be used in various linear-in-parameter model types such as polynomial, fuzzy logic, neural network and wavelet-based models. Using a reduced set of candidate model terms improves the computational time for the evaluation of the nonlinear models. This is because the identification algorithm must only consider a much lesser number of terms than an overall full set that includes all possible linear terms and the respective nonlinear combination of these.

The authors of [148] pointed out that if a certain lagged term, with respect to the output of a nonlinear system, is significant, thus it is significant in a linearized model as well. However, it should be noted that this method does not attempt to construct a linearized model representation. It is an initial step of selecting suitable model terms (regressors) to represent the linear dynamics of the system present within the data [148].

6.3.3 PEM and SEM approach to model term selection

The SRR based SEMP algorithm inherently is computationally intensive because of the need for running simulations in order to access the importance of each candidate regressor or model term [106]. This is a significant issue in the context of nonlinear System Identification as the number of candidate model terms is extremely large (see Chapter 3 Section 3.6). Conversely, the SEMP algorithm, since it is based on the SEM approach is reported to be more robust than the PEM counterparts such as the FRO algorithm and produces models that have the ability for long term prediction [80], [106]. Furthermore, the SEMP algorithm has the capability of removing any terms, which are added in previous iterations that become redundant because of the addition of new terms at subsequent iterations. Therefore, SEMP is a stepwise regression algorithm and this avoids the addition of spurious terms. A major advantage of the SEMP algorithm is that it can guarantee a stable model since it minimisers a simulation error based cost function [106]. For the specifics of the SEMP algorithm and its variants the reader is directed towards [106], [111], [149]–[151].

The OLS-ERR based FRO algorithm is a commonly used model term selection algorithm based on the forward selection approach. It is much faster and efficient at evaluating significant model terms than the SEMP algorithm because of its PEM based OLS-ERR framework. The recently introduced iterative FRO (iFRO) algorithm [83] has the ability to take several different orthogonalisation paths to produce competing models. This ability of iFRO algorithm overcomes one of the major drawbacks of the original FRO algorithm. From these competing models, the best performing model can then be chosen. This process can be completed in relatively low time and the iFRO algorithm has a higher possibility of achieving a global optimum solution in a PEM sense than the original FRO [83]. For specifics on the FRO and the iFRO algorithms, the reader is directed towards [83], [109], [110].

A PEM approach to System Identification aims at finding the optimum one-step ahead predictor, $\hat{y}(t \mid t-1)$, of the output data [24], [72] where;

$$\hat{y}(t \mid t-1) = f(\, y(t-1), \cdots, y(t-n_y), u(t-1), \cdots, u(t-n_u)\,) \tag{6.5}$$

in which for the NARX case f is a nonlinear mapping usually of the polynomial form (see Chapter 3 Section 3.4.2). The PEM approach asymptotically tends to the correct model depending on the amplitude and frequency content of the input excitation $u(t)$ [24], [72]. However, for the identified model to be able to reconstruct the actual dynamics of the system, its ability for long term prediction, i.e. simulation performance, needs to be considered as this shows the dynamical features of the model more directly [80], [152].

Sjöberg *et al.* in [88] pointed out that on the basis of the optimal predictor model, the optimal simulation model can be evaluated by setting $y(t) = \hat{y}_s(t)$ and $\hat{y}(t \mid t-1) = \hat{y}_s(t)$ in equation (6.5). Therefore,

$$\hat{y}_s(t) = f(\, \hat{y}_s(t-1), \cdots, \hat{y}_s(t-n_y), u(t-1), \cdots, u(t-n_u)\,) \tag{6.6}$$

where $\hat{y}_s(t)$ is the model predicted output or the simulated output of the model. This is the essence behind the SEMP algorithm. Furthermore, when considering multi-step ahead or k – steps ahead predictor models, the PEM criterion tends to the SEM criterion as k and the number of observations increases [79], [153], [154]. Thus, the optimal PEM model tends to the optimal SEM when considering longer prediction horizons.

6.4 A new method to System Identification based on SEM and iFRO

The iFRO algorithm [83] has the ability to search several orthogonalisation paths in order to achieve an optimal solution in a PEM sense. Each term in a given set of candidate model terms, $\mathbf{\Phi}_s = \{\phi_{s_1}, \phi_{s_2}, \cdots, \phi_{s_m}\}$, will be used as a starting point for the orthogonalisation process and several orthogonalisation paths will be searched

simultaneously resulting in m competing models. The best model is chosen based on parsimony and the sum of ERR ($SERR$) values of all terms contained within the corresponding models. The simplest models with high $SERR$ values are considered to be the most optimum. The search on each orthogonalisation path will be done using a pre-defined stopping criterion $(1-\rho)$, where ρ is a certain $SERR$ tolerance the model in the search path should not attain any higher.

In the iFRO algorithm, the initial term set $\mathbf{\Phi}_s$ is chosen from a larger term set $\mathbf{\Phi}_D$. The original FRO algorithm is applied to $\mathbf{\Phi}_D$ with a pre-defined tolerance ρ to obtain $\mathbf{\Phi}_s$. Thus applying the iFRO algorithm on $\mathbf{\Phi}_s$, the term set of the best performing model $\mathbf{\Phi}_{op}$ is obtained. Further iterations can be performed where each term in $\mathbf{\Phi}_{op}$ is selected as the first starting point and thus several orthogonalisation paths will be searched using all the terms in $\mathbf{\Phi}_s$. The best model from this iteration is then chosen as the new best model. Setting $\mathbf{\Phi}_s = \mathbf{\Phi}_{op}$ and the set of terms in the new best model as $\mathbf{\Phi}_{op}$. The process is then repeated. It should be noted that the best model obtained in the subsequent iteration will be less suboptimal than the model obtained in the previous iteration if the stopping criterion $(1-\rho)$ is kept unchanged [83]. However, as pointed out by Guo *et al.* in [83], often no further iterations are needed after the first iteration. Therefore, in the iFRO algorithm, the forward selection method based on the OLS-ERR can be directed towards a certain optimal orthogonalisation path. Furthermore, the most significant feature of the iFRO algorithm is that it has been demonstrated it can be used in System Identification even in the presence of inadequate inputs that do not persistently excite the system [83]. Thus, its potential in the System Identification strategy proposed in this chapter, specifically for Condition Monitoring and Fault Diagnosis. For in detail specifics on the iFRO algorithm the reader is directed to [83].

In this section, an extension to the iFRO algorithm is proposed in which the orthogonalisation path taken is directed towards minimising the simulation error of the model produced. As such this algorithm will be called the S-iFRO (Simulation error minimising iFRO) algorithm.

Guo *et al.* in [83] highlighted some important properties of the iFRO algorithm considering its iterative process of obtaining a model, these are;

1. If a correct model term is selected as the first term in the orthogonalisation path the algorithm will reach the stopping criterion, $(1-\rho)$, relatively faster thus resulting in a more parsimonious model.

2. Incorrect terms may contain information of more than one correct term thus obtaining a higher ERR value. However, if a correct term is forced to be selected as the first, the ERR value of such incorrect terms drops as its contribution to the output variance becomes less significant. Therefore, it is much unlikely for an incorrect term to be selected in the subsequent steps of term selection.

3. All correct terms will be significant, from an ERR point, on the correct orthogonalisation path.

Considering the above properties of the iFRO algorithm, the choice of the best model from a set of m competing models $\mathbb{M} = \{\mathcal{M}_1, \cdots, \mathcal{M}_m\}$ is done explicitly by using the respective simulation performance of each model $\mathcal{M}_k$, $k = 1, \cdots, m$. Thus, yielding the best performing simulation model. This is because more than one competing models in $\mathbb{M}$ may have the same number of terms. In such an instance comparison with one-step ahead prediction errors, $e_p(t) = y(t) - \hat{y}(t \mid t-1)$, and the $SERR$ might not yield a satisfactory model. This is because some of these models might perform poorly when simulated and even be unstable [106]. Thus, the model with the least simulation errors, $e_s(t) = y(t) - \hat{y}_s(t)$, should be considered. Therefore, the models $\mathcal{M}_k$, $\mathcal{M}_k \in \mathbb{M}$ for $k = 1, \cdots, m$ should be compared against the mean squared simulation errors of each model, $MSSE(\mathcal{M}_k)$, and the model with the least $MSSE$, i.e. $\overline{\mathcal{M}} = \min\{MSSE(\mathcal{M}_k) \mid \mathcal{M}_k \in \mathbb{M}, k = 1, \cdots, m\}$ is chosen as the best model.

Recalling that the model which is found in the subsequent iteration will not be worse than the model in the previous iterations, given the stopping criterion is kept unchanged. Thus, in consideration of the properties of the iFRO algorithm, mentioned earlier, and the iterative procedure of directing the iFRO algorithm to follow an optimum orthogonalisation path. The iFRO algorithm can be made to follow an orthogonalisation path directed towards an optimum SEM search path. This can be achieved by making the choice of the best model throughout the iFRO algorithm using the $MSSE$, such that;

$$\overline{\mathcal{M}_i} = \min\left\{ MSSE(\mathcal{M}_{k_i}) \mid \mathcal{M}_{k_i} \in \mathbb{M}_i, k_i = 1, \cdots, m_i \right\} \tag{6.7}$$

where i denotes the respective iteration. $\overline{\mathcal{M}_i}$ is the respective best model, $\mathbb{M}_i$ is the set of competing models and m_i is the total number of competing models in the i^{th} iteration. It should be strictly followed that for $i \geq 2$ the competing models, $\mathcal{M}_{k_i}$, in $\mathbb{M}_i$ are under the condition that;

$$MSSE(\mathcal{M}_{k_i}) < MSSE(\overline{\mathcal{M}_{i-1}}) \tag{6.8}$$

As such in the i^{th} iteration if the set of competing models $\mathbb{M}_i = \varnothing$, where $\varnothing$ denotes a null or an empty set, then the final model is taken as $\overline{\mathcal{M}_{i-1}}$. This is the essence behind the S-iFRO algorithm.

The models obtained in using the S-iFRO algorithm will tend to obtain the optimal simulation model of the system in relation to the input-output data. At each iteration *i*, $\overline{\mathcal{M}_i}$ obtained is the best simulation model in $\mathbb{M}_i$. Thus, the terms that compose $\overline{\mathcal{M}_i}$ will

be the best combination of terms that can reconstruct the dynamics of the actual system among all the competing models. This is because as mentioned in Section 6.3.3, simulation performance shows the dynamical features of the model more directly. Hence as iterations progress, better models in a dynamical sense will be obtained. Furthermore, $\overline{\mathcal{M}_i}$ is more likely to have a higher number of correct terms.

It should be highlighted that given a certain maximum dynamic order, where $n_y = n_u$, and that the sampling time T_s is set appropriately. In the perspective of the MSS (see Section 6.3.1), in the S-iFRO algorithm, the iFRO part will produce possible models that lie in the space of the MSS because of the several orthogonal paths taken. The selection of the best model $\overline{\mathcal{M}_i}$ is done using the minimum $MSSE$, subjected to the condition in equation (6.8). This implies that as the iterations progress, $\overline{\mathcal{M}_i}$ will contain more terms that would reconstruct the actual dynamics of the system more accurately. Thus further implying that some of the terms in $\overline{\mathcal{M}_i}$ would actually be a part of the model structure in the sub-region $\wp$ of the MSS. Recalling that $\wp$ is the region in which the best model structures that could reconstruct the system dynamics well thus attaining the best simulation performances. $\overline{\mathcal{M}_i}$ would tend to be in this region as the iterations progress. Because of the efficiency of the iFRO to search several orthogonal paths [83], this would mean that $\overline{\mathcal{M}_i}$ will tend to this region efficiently. Thus, the S-iFRO algorithm can obtain models that can reconstruct the actual system dynamics present in the data effectively.

The S-iFRO algorithm is much more efficient than the SEMP algorithm because of the much lesser number of simulations needed to be carried out. In the SEMP algorithm model terms are selected in a stepwise regression fashion in which case simulations are needed to be carried out every time a term is added or removed. Conversely, in the S-iFRO algorithm simulations are carried out on the already formed models in the set of competing models. However, naturally, the S-iFRO algorithm requires more computational effort than the iFRO algorithm. Nevertheless, because of the superior efficiency inherently present within the iFRO algorithm in obtaining optimum models and the unlikely possibility of requiring a higher number of iterations [83], the number of simulations that needed to be conducted will mainly depend on the size of the initial set of model terms $\mathbf{\Phi}_s$ used. Thus, using a reduced set of candidate model terms, obtained using the method introduced in Section 6.3.2, would increase the efficiency of the S-iFRO algorithm. It should be noted that because of the SEM nature of the S-iFRO algorithm the models produced are robust and often could produce unbiased estimates [80], [152], [155].

In the following subsection, a method of obtaining a reduced set of candidate model terms based on the method introduced in Section 6.3.2 but using the S-iFRO algorithm is presented.

6.4.1 Obtaining a reduced set of candidate model terms using the S-iFRO algorithm

The total number of candidate model terms for a nonlinear system can be a large number depending on the maximum dynamic order ($n_y = n_u$) used and the highest polynomial nonlinearity N_p considered. Using a reduced set of candidate model terms significantly reduces the computational effort of identifying a nonlinear model such as a NARX model (Section 6.3.2).

The significant model terms (regressors) of the locally linear model, $\mathbf{\Phi}_{lin}$, can be obtained and a reduced set of linear ($\mathbf{\Phi}_{lin}$) and nonlinear ($\mathbf{\Phi}_{nl}$) candidate terms, $\mathbf{\Phi}_D = \left\{\mathbf{\Phi}_{lin}, \mathbf{\Phi}_{nl}\right\}$, can be composed. By using the S-iFRO algorithm to obtain $\mathbf{\Phi}_{lin}$, because of the SEM nature, the linear model terms obtained will be robust and often unbiased [80], [152], [155]. Furthermore, the process can be even done if the system is not persistently excited. The reduced set of candidate terms $\mathbf{\Phi}_D$ is then composed using these robust linear terms. It should be noted that robustness is in relation to the data and the local dynamics present within the data. Furthermore, because of the SEM nature of the S-iFRO algorithm and considering that the simulation performance is a direct measure of the model dynamics (see Section 6.3.3). The linear model terms (regressors) $\mathbf{\Phi}_{lin}$ chosen will describe the true locally linear dynamics. As discussed in Section 6.3.2 a model term that is significant in the original nonlinear system will be significant in the linearized model. Thus, since the terms in $\mathbf{\Phi}_{lin}$ are robust, some of these terms should describe the nonlinear terms and thus the nonlinear dynamics sufficiently.

The detailed steps involved in the S-iFRO algorithm including the pre-selection of the reduced set of candidate terms are as follows;

1. Setting an appropriate maximum dynamic order n_y and $n_y = n_u$. Obtain a full set of linear input and output lagged terms (regressors) $\mathbf{\Phi}_{D,lin}$.

2. Setting a certain tolerance ρ, perform the iFRO algorithm on $\mathbf{\Phi}_{D,lin}$. In each iteration of the algorithm, select the best model using the simulation performance in a SEM sense using equation (6.7) along with the condition in equation (6.8) to produce the best simulation model.

3. The terms in the best simulation model are taken as $\mathbf{\Phi}_{lin}$. Thus compose all the nonlinear terms arising from the nonlinear combinations of the terms in $\mathbf{\Phi}_{lin}$ until a certain degree N_p to form $\mathbf{\Phi}_{nl}$. Thus $\mathbf{\Phi}_D = \left\{\mathbf{\Phi}_{lin}, \mathbf{\Phi}_{nl}\right\}$.

4. Perform the iFRO procedures in which the best model $\overline{\mathcal{M}_i}$ in each iteration i, is chosen in accordance with equation (6.7) subjected to the condition in equation (6.8) to produce the final model.

One approach of selecting the maximum dynamic order in step 1 above is such that, determine the value of n_y, $n_y = n_u$, from a range of values. This would produce several locally linear models in following through steps 1 and 2. The locally linear model with the least $MSSE$ is then chosen and the corresponding model terms are selected as $\mathbf{\Phi}_{lin}$ in step 3.

Example of a nonlinear System Identification using the S-iFRO algorithm

The performance of the S-iFRO algorithm in the case of nonlinear System Identification in the presence of a disturbance is shown here. The nonlinear system that is to be identified is shown in equation (6.9) below.

$$\ddot{y}(t) + 0.2\,\dot{y}(t) + y(t) + K_1\,y(t) + 5\,y^3(t) = u(t) \tag{6.9}$$

The nonlinear system in equation (6.9) is subjected to an input $u(t)$ where;

$$u(t) = A(\sin(2\pi f_1 t) + \sin(2\pi f_2 t)) \tag{6.10}$$

in which $f_1 = 10\,Hz$, $f_2 = 25\,Hz$ and $A = 50$.

The S-iFRO algorithm was used with a reduced set of candidate terms in the following manner;

- A locally linear model was first fitted to the data using the S-iFRO algorithm to obtain a set of linear model terms $\mathbf{\Phi}_{D,lin}$. A reduced set of candidate model terms $\mathbf{\Phi}_D = \{\mathbf{\Phi}_{lin}, \mathbf{\Phi}_{nl}\}$ was formed where $\mathbf{\Phi}_{nl}$ is the set of nonlinear candidate terms composed using $\mathbf{\Phi}_{D,lin}$ up to a nonlinear polynomial order $N_p = 3$. The stopping criteria $(1-\rho) = 10^{-4.6}$.

- The S-iFRO algorithm was then used along with $\mathbf{\Phi}_D$ to obtain the final system model. The stopping criterion at this stage was used as $(1-\rho)$ where $\rho = SERR_{D,lin} + \min(ERR_{D,lin})$, in which $SERR_{D,lin}$ is the sum of $SERR$ values of the terms in $\mathbf{\Phi}_{D,lin}$ and $\min(ERR_{D,lin})$ is the corresponding minimum ERR value the term set $\mathbf{\Phi}_{D,lin}$.

The system shown in equation (6.9) was subjected to the input in equation (6.10) with sampling time $T_s = 360\,Hz$. A step disturbance was added to the output as shown in Figure 6.1 before the identification process.

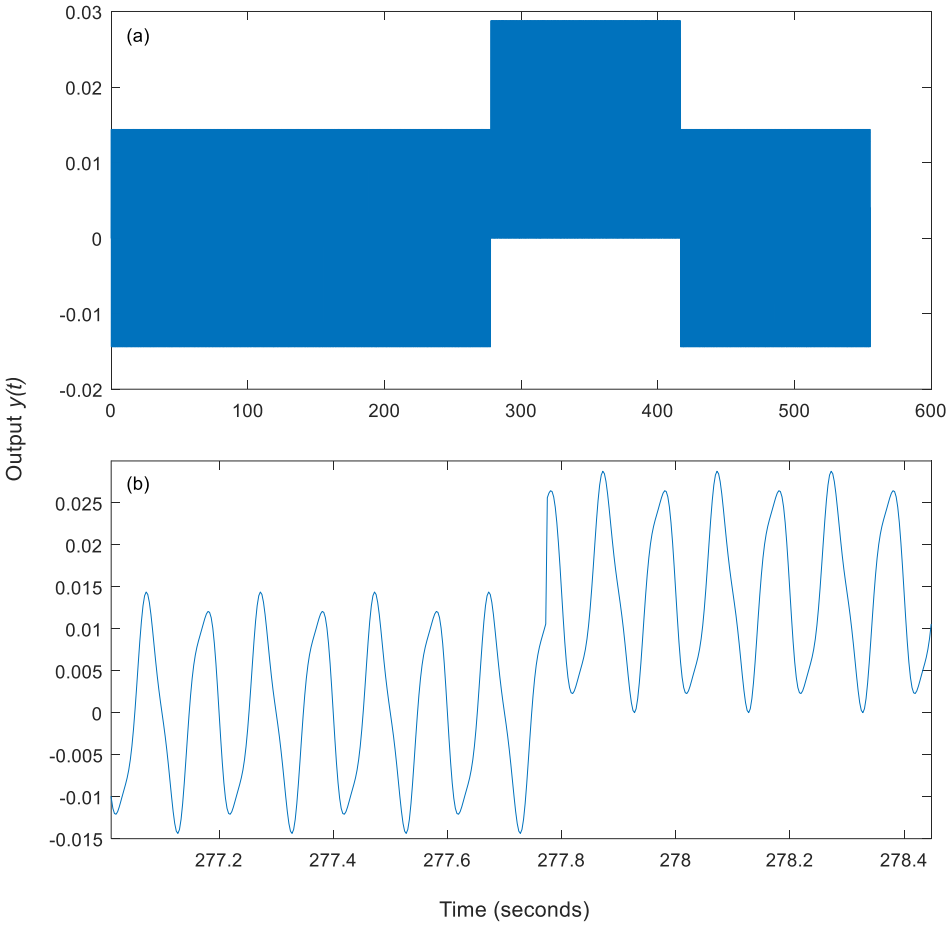

Figure 6.1: Output *y(t)* of the system with added step disturbance. (a) shows the complete time series of the output. (b) shows the section of the time series in which the disturbance is added.

System Identification was performed using the S-iFRO algorithm as mentioned above. Figure 6.2 illustrates the model predicted output or the simulation output against the actual output of the system with the added disturbance. Table 5 shows the corresponding ERR values of the final model along with the parameter values.

Table **6** shows the corresponding model with the lowest $MSPE$ (mean square of the prediction error) value. It is seen from Table 5 and

Table **6** that the best simulation model has a four times higher $MSSE$ than the lowest $MSPE$ model. However, the $MSPE$ values of both the models are approximately the same even though the $MSSE$ values are significantly different. This indicates the model selected using the $MSSE$ is more dynamically accurate. The frequency components generated by the nonlinearity of the system is very minute compared to the complete output signal which is dominated by the frequencies f_1 and f_2. Thus, selecting the best model using the $MSSE$ rather than the $MSPE$ produces models that are more dynamically accurate. This is significant in the case of CM-FD as the System Identification process needs to be able to capture the dynamics of the system present in the data well. However, it should

be noted that it is foremost the iFRO part of the algorithm that produces these competing models. This indicates the significant ability of the iFRO to produce dynamically correct models. The S-iFRO being an extension of the iFRO selects the most dynamically correct model from the competing models produced.

Table 5: Specifics on the best simulation model

Model term	***ERR***
$y(t-1)^2\, y(t-5)$	*0.56279*
$y(t-1)$	*0.4169*
$y(t-5)$	*0.0168*
$u(t-2)$	*0.0035*
$u(t-5)$	$6.6345e^{-7}$
$u(t-4)$	$7.8074e^{-6}$
$\boldsymbol{MSSE = 1.0348e^{-4}}$	$\boldsymbol{MSPE = 2.5729e^{-9}}$

Table 6: Specifics on the least MSPE model

Model term	***ERR***
$y(t-1)^3$	*0.6373*
$y(t-1)$	*0.3417*
$y(t-5)$	*0.0174*
$u(t-2)$	*0.0035*
$u(t-5)$	$6.2330e^{-7}$
$u(t-4)$	$7.8273e^{-6}$
$\boldsymbol{MSSE = 4.0667e^{-4}}$	$\boldsymbol{MSPE = 2.5727e^{-9}}$

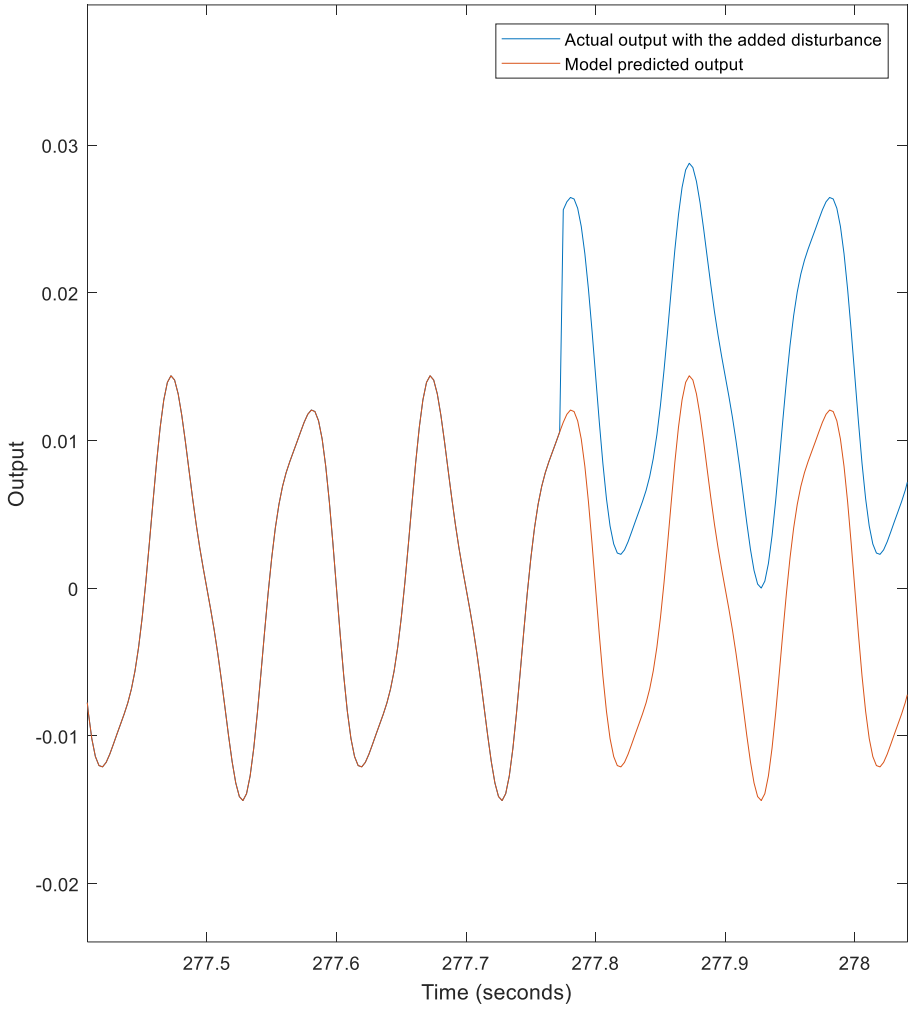

Figure 6.2: Actual output (blue) against the model predicted or the simulation output (orange) at the start of the disturbance. It is seen clearly that the model predicted output performs well in comparison to the actual output.

6.5 CM-FD methodology based on SI and FRA optimised for practical implementation

The S-iFRO algorithm proposed in this chapter can address the concerns mentioned in Section 6.1 which is part of the main motivations of the current study (see Chapter 1 Section 1.2). Because of the SEM nature of the S-iFRO algorithm and the inherent efficiencies present within the iFRO method. The task of System Identification can be conducted even in the presence of inadequate inputs which does not persistently excite the system. This, however, will be to a certain degree. The matter of accurate dynamical reconstruction is addressed because of the SEM nature of the S-iFRO algorithm. Therefore, the models identified will be robust and would be able to reconstruct the actual system dynamics present within the data.

The issues of numerical accuracy present within the original LS method for the evaluation of NOFRFs has been addressed by the proposed M-LS in Chapter 5. It has been shown that the NOFRFs can now be applied, using the M-LS method, to locally approximate a nonlinear system that exhibits severe nonlinearities. This enables the use of the NOFRFs for CM-FD of nonlinear systems of the severe nonlinear type. Thus, with the improvements to the NOFRFs presented in Chapter 5 and the proposed S-iFRO method for System Identification, the first three objectives of this study (see Section 1.3) have been achieved. Consequently, a new methodology for System Identification and Frequency Response Analysis of nonlinear systems will be as follows;

1. Select an appropriate sampling time using the method introduced in Section 6.2.

2. Identify the model that fits the data using the S-iFRO algorithm with pre-selection of the reduced set of candidate terms, steps 1 – 4 in Section 6.4.1.

3. Evaluate the NOFRFs of the model using the M-LS method.

The above methodology proposed for SI and FRA of nonlinear systems is then used with the previously proposed framework in [15] for a complete data-driven FDI framework for CM-FD of nonlinear systems. The same framework can be used in the case of linear systems in which instead of the NOFRFs the linear systems FRF is used in step 3 above.

6.6 Summary

In this chapter, a new System Identification algorithm called the S-iFRO is proposed. This along with the strategies mentioned for selection of sampling time and maximum dynamic order, a complete System Identification methodology is presented which addresses the practical concerns of using System Identification in CM-FD. The concept of MSS was explained in detail. Thus, the importance of sampling time, nonlinearity detection and the selection of the maximum dynamic order were discussed extensively using the concept of MSS. The significance of achieving a dynamically correct model in the System Identification stage of the SI and FRA approach is critical. Accurate dynamical reconstruction of a system using input-output data was discussed extensively with regard to PEM and SEM approaches. It was pointed out how a SEM approach to System Identification produces more dynamically accurate models. However, PEM approaches are much more computationally efficient. Therefore, a System Identification algorithm that combines the efficiency of PEM and the dynamical accuracy of SEM was considered. Thus, the extension proposed to the iFRO algorithm, the S-iFRO, makes certain that the model produced in the identification stage is the most dynamically accurate model according to the input-output data of the system. A detail discussion of the S-iFRO algorithm was presented in order to explain how the algorithm will produce dynamically accurate models with regard to the concept of MSS. An example of identifying a system with an external disturbance in the output data was shown to highlight the capabilities of the proposed algorithm. The inclusion of the M-LS method to the evaluation of NOFRFs

further improves the complete CM-FD methodology based on System Identification and Frequency Response Analysis. Thus, facilitating the practicality of applying this approach.

Chapter 7

Low-Frequency RFID Based Eddy Current Probing and Defect Characterisation Using System Identification and Frequency Response Analysis

7.1 Introduction

LF (Low Frequency) RFID (Radio Frequency IDentification) technology based NDE&T (Non-Destructive Evaluation and Testing) or non-invasive technique for SHM has been recently proposed [32], [33]. In [32], [33], the respective authors used features from the time-series signal of the RFID system to distinguish between different stages of corrosion and different progressions of cracks.

Most RFID reader and tag systems function, according to the principles of inductive coupling. Thus, the procedures of power and data transfer are governed by the physical principles of magnetic phenomena [35]. The basic theories and details behind the working principles of RFID tags can be found in [35]. RFID systems comprise of a reader (primary coil) and tag/transponder (secondary coil) and use electromagnetic induction for power and data transfer. The reader and the tag are inductively coupled. During which the reader transfers power via magnetic induction (the carrier wave) to activate the tag and receives data which is stored in the tag memory and also communicates with it. Due to the reader coil and tag coil being magnetically coupled, the magnetic field of the tag is reflected upon the reader coil as an imaginary impedance. Hence, any variation in the tag magnetic field is reflected on the reader through this imaginary impedance (carrier and tag signal). The voltage reading taken around the reader coil is a differential voltage which is the result of the tag magnetic field inducing currents on the reader coil, that are opposite in direction (Lenz's law) to reader coil currents.

Considering when a RFID tag is attached to a metal, the electromagnetic coupling between the metal and the tag will cause certain changes to the magnetic field produced by the RFID tag. This depends on the electrical properties of the metal attached. Since these changes are observable from the reader, any changes in the electrical properties of the metal will be reflected in the tag magnetic field. Consequently, any changes to the

electrical properties of the metal will be observable from the reader. Various defects in metals result in changes in its electrical properties. This is the essence behind the concept of using RFID for defect characterisation. The viability and effectiveness of this concept were illustrated by the authors of [33] and [32]. Essentially the RFID reader tag system acts as a wireless probing and sensing mechanism in NDE&T for the purpose of SHM.

In [33] and [32] the tag response was obtained by filtering the output signal (comprising the carrier wave and the tag response) and then applying amplitude modulation. The tag response was analysed using traditional signal processing techniques of extracting features such as peak amplitude, signal height etc. The authors of [33] presented in their results a clear distinction of corrosion characterization and the potential of using RFID tags for defect detection in metal structures. Popularly like in other eddy current based NDE&T techniques, the features are extracted and the analysis is conducted only by way of observing the output response of the probing mechanism. This indirectly brings about the assumption that the response signal, that is to be compared with a reference signal, is measured not only under the same or similar conditions, but also the same input or excitation signal to the probing device. Therefore, this implies that even though the features extracted are defect specific to a degree, these features also to a certain significance depends on other factors as well. Hence with the type of signal processing techniques used and basing the analysis only on the output response results in several disadvantages which have to be mitigated for practical implementation. These disadvantages are briefly mentioned below [4], [6].

- Due to the effect of noise and other disturbances, fault features such as; amplitude and phase gets affected.
- Dynamic interrelationship lacks between the fault and signal. Therefore, a comprehensive Fault Diagnosis might not be able to be carried out.
- Fault features depend on the input signal, other system loads and disturbances and other background effects. Therefore, many other factors could influence fault features.
- Many pre-processing steps are to be taken before feature extraction which could distort useful information.

For detecting structural defects such as corrosion, crack etc. and its severity, utilizing RFID tags as a sensor, a good Condition Monitoring method should be used which could differentiate and determine the defects when multiple defects occur. Furthermore, the Condition Monitoring method should be robust against noise, disturbances and other uncertainties. Thus, in this chapter, the FDI method proposed in the previous chapter is used to characterise defects, in particular; crack length, crack depth and corrosion. The LF RFID based eddy current probing method coupled with SI and FRA presented in this chapter is novel implementation for SHM.

7.2 Experimental rig used for LF RFID based SHM

The experimental rig that was used to collect data from a LF RFID based NDE&T system was a setup used in an EPSRC funded project in collaboration with Network rail, the University of Newcastle and the University of Sheffield for rail track defect detection. The University of Newcastle has set up the rig for collection of data from different corrosion and crack samples using LF RFID based wireless eddy current method. The rig was inspected and data was collected to begin preliminary investigations into RFID based NDE&T method in a systems perspective for corrosion and crack characterization. Data were obtained from different corrosion samples, crack length samples and crack depth samples. Figure 7.1 illustrates the experimental setup that was used.

The RFID tag used is a passive low-frequency ATMEL ATA577 tag that is tuned to 125 KHz. Both the reader and the tag are tuned to resonate at 125 KHz, hence the input voltage to the RFID reader was a square wave with a frequency of 125KHz. RFID tags produce a load modulation sequence once it is powered by the carrier wave [35]. This is how each tag is uniquely identified when it is used in its usual commercial applications [35]. The LF RFID tag is programmed to produce a load modulation sequence of 1's and 0's once it is powered. This sequence will be embedded in the carrier signal through amplitude modulation [35]. The experimental setup is the same as the one used by authors of [33]. Except the data is not pre-processed after being sampled and digitised. The data is directly used for System Identification and Frequency Response Analysis.

The LF RFID tag when placed on the metal sample, becomes a part of the RFID tag antenna. This is because of the mutual inductance that is created between the tag and the metal sample. Thus the metal sample acts as a pseudo inductor connected in parallel to the tag antenna [33]. Hence the resonant frequency of the tag becomes lower. The RFID tag and the metal sample collectively will be called the Tag-Metal system or simply Tag-Metal. Because of the mutual inductance between the Tag-Metal and the reader coil, the Tag-Metal acts as a pseudo inductance on the reader coil. Consequently, any changes in the electrical properties of the metal sample due to defects will be embedded in the carrier and tag signal or simply the carrier-tag signal. It should be noted that, even though there is a magnetic coupling (mutual inductance) between the reader coil and the metal sample, the magnetic coupling between the RFID tag and the metal sample is much greater. Also, the distance between the reader and the coil is placed such that this is true and thus the RFID tag and the metal sample can be approximated as one isolated system [32], [33]. The complete setup of the reader coil, LF RFID tag and the metal sample can be considered as one system and will be called the Reader-Tag-Metal system. This is because the reader coil and the Tag-Metal are dynamically interrelated to each other via mutual inductance. Figure 7.2 illustrates this dynamical interrelationship.

The Reader-Tag-Metal system has one main input and one main output as shown in bold lettering in Figure 7.2. The input voltage to the reader system is the main input which will produce the carrier signal while the voltage measurement around the reader coil is the main output (carrier-tag signal). This point of view of the complete setup can be

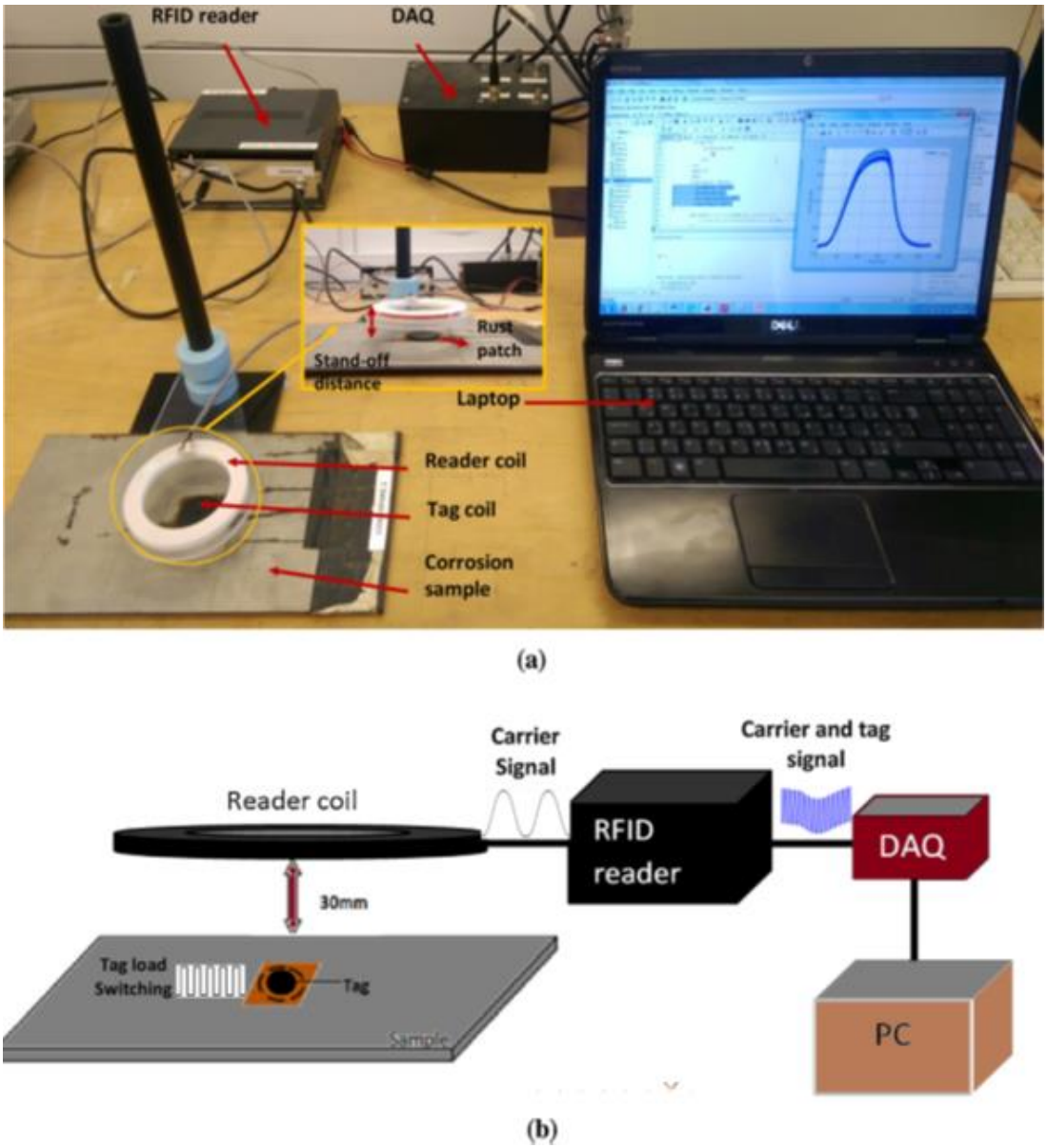

Figure 7.1: (a) Experimental Rig used by The University of Newcastle (b) Diagram of the setup [33]

considered as observing the RFID reader system, LF RFID tag and the metal sample in a systems perspective.

In the same systems perspective viewpoint it should be noted that the modulation sequence, which varies the tag antenna resistance [33], and the distance between the RFID reader system and the Tag-Metal (Stand-off distance [33]), can be considered as either internal system disturbances or as varying internal parameters or even as main inputs to the system. This is an important observation as both of these, the load modulation sequence and the Stand-off distance affects the whole Reader-Tag-Metal

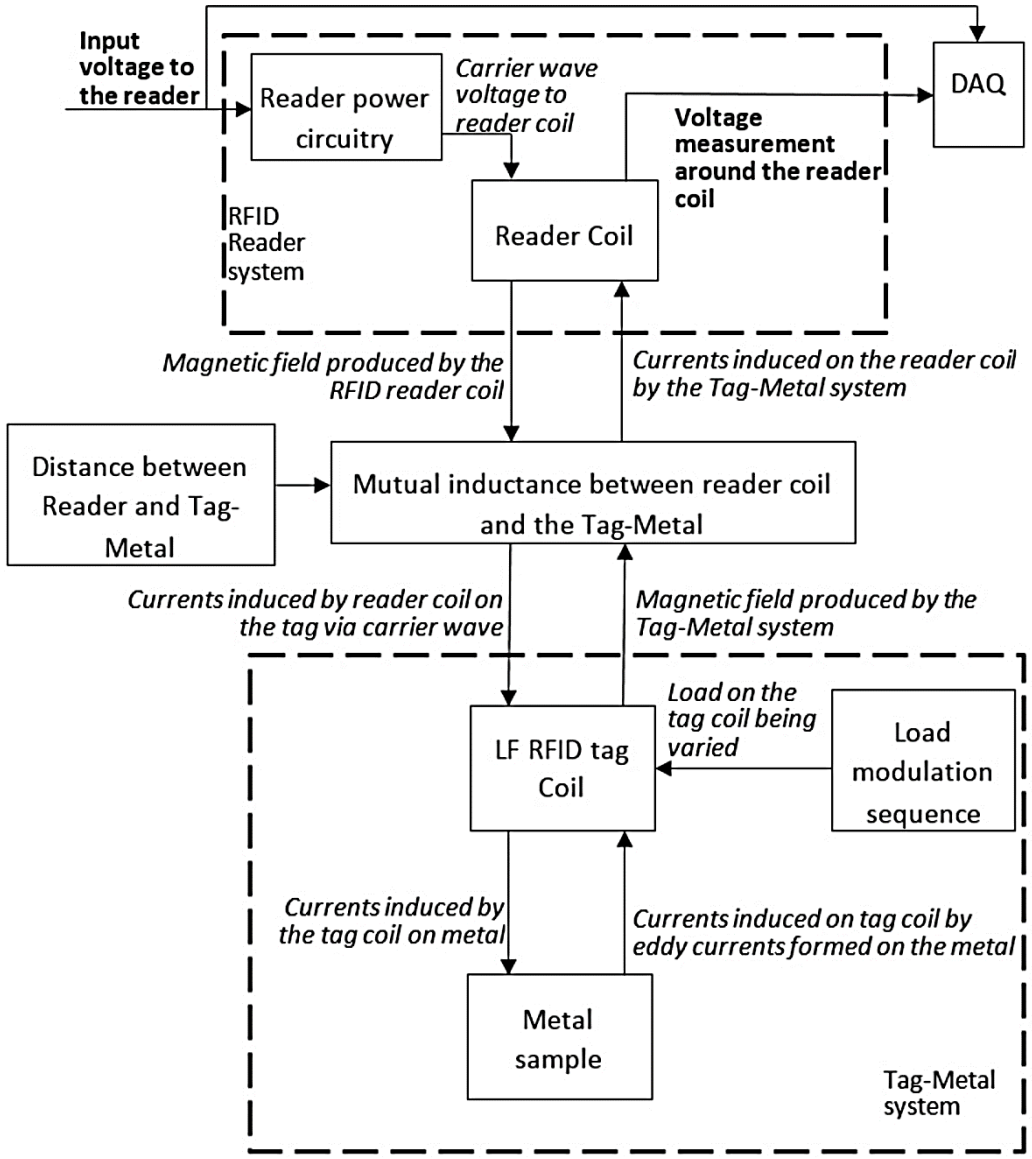

Figure 7.2: Systems perspective to the Reader-Tag-Metal system. The Tag-Metal system and the RFID reader system is shown separated outlined by a dashed box. The main input (**Input voltage to the reader**) and the output (**Voltage measurement around the reader coil**) are shown in bold lettering. The distance between the Reader and Tag-Metal can be regarded as internal disturbances.

system dynamics in a similar manner. Both these internal disturbances influence the current induced by the RFID reader on the Tag-Metal and vice versa but by different means;

- The Stand-off distance directly affects the mutual inductance between the RFID reader and the Tag-Metal system. This will affect the current induced by the Tag-Metal system on the Reader coil and vice versa. The

Stand-off distance and its effects on the mutual inductance is a considerable factor [33], [35].

- The load modulation effects the resistance of the tag coil. Which in turn affects the current produced in the RFID tag. Hence the magnetic field produced by the tag. It can be shown by the reader coil voltage readings that the effects of load modulation on the main output is much smaller considering the Reader-Tag-Metal system output as a whole. This will be illustrated in a later part of this section.

Taking the above factors into account the positions of the tag and the reader were kept at a constant distance at all times. This was such that the reader coil does not have a significant influence on the metal sample however, not too far from the LF RFID tag. This is because the mutual coupling between the reader and the tag has to be significant. The tag was placed directly on top of the defect region of the metal sample, see Figure 7.1. The data collected was sampled at a frequency of 10 MHz and 50,000 data points were collected and six such input-output data sets were obtained for each metal sample that was used.

7.3 The Reader-Tag-Metal system

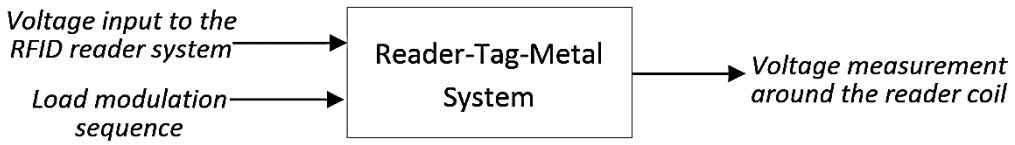

Figure 7.3: Simple representation of the Reader-Tag-Metal system in terms of inputs and outputs. The effect of the stand-off distance is not considered as it is kept constant.

Figure 7.3 above is a less abstract view of the Reader-Tag-Metal system. Given that the stand-off distance is kept constant the effect of it on the wider Reader-Tag-Metal system can be disregarded and does not need to be considered in the analysis.

In order to understand the effect of the modulation sequence on the system output, just the RFID reader and the LF RFID tag without the metal sample (Reader-Tag system) was examined. Figure 7.4 – (b) shows the voltage measurement around the reader coil (output) of just the Reader-Tag system. Figure 7.4 – (c) illustrates a longer time sequence of the same output and Figure 7.4 – (d) shows a zoomed in version of Figure 7.4 – (c) around the top region of the output signal. It can be clearly observed from Figure 7.4 – (d), the binary sequence is embedded by the modulation sequence of the RFID tag on the output signal. However, it is noticeable that the actual size of the amplitude of the

embedded modulation sequence is significantly smaller compared to the complete amplitude span of the signal. When a metal sample without any defects is placed and the output of the Reader-Tag-Metal system is observed. The amplitude modulation seems to be very insignificant to the fact that it can be hardly examined without filtering the output signal, this is shown in Figure 7.5. This may be because the effect of the metal sample on the tag antenna coil, as a pseudo impedance, is much more significant than the change in resistance of the antenna coil produced by the modulation sequence. Hence the resulting amplitude modulation on the output cannot be observed. Thus, from these observations, it can be deduced that the effect of the load modulation of the RFID tag antenna coil has a very insignificant effect on the output of the Reader-Tag-Metal system as a whole and can be disregarded. Therefore, the complete Reader-Tag-Metal system can be approximated as single input single output system (SISO) with the main input as the voltage input to the RFID reader system and the main output as the voltage measurement around the reader coil as shown in Figure 7.6.

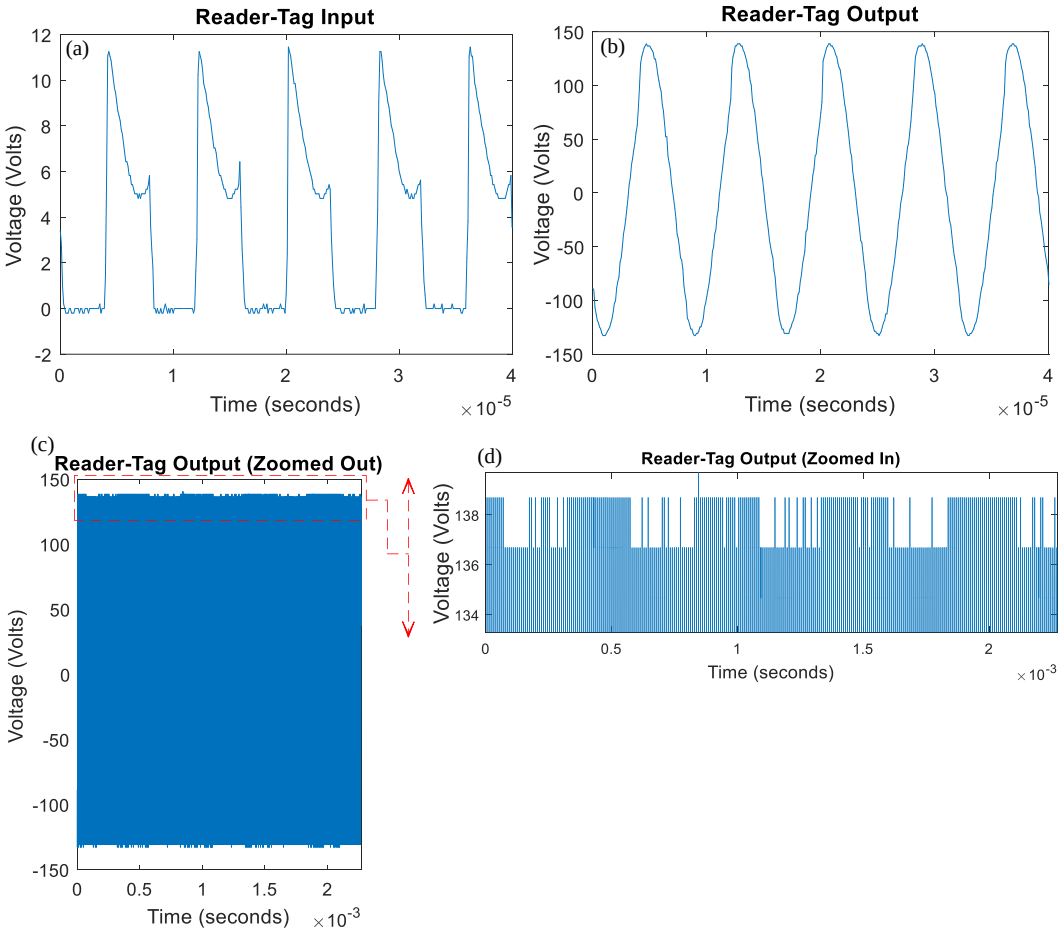

Figure 7.4: (a) and (b) Input and Output time-series of the Reader-Tag system (without a metal sample) respectively. (c) Longer time sequence of (b). (d) Zoomed in version of the top part of the output signal in (c).

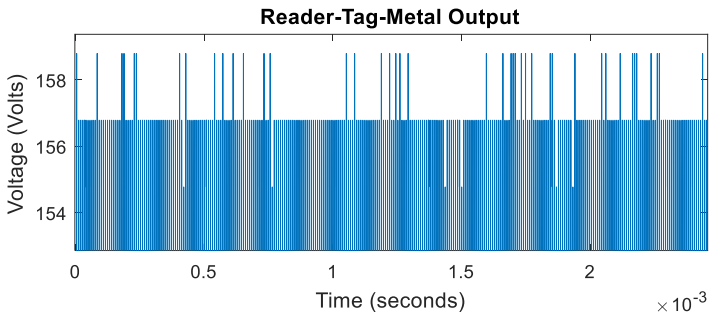

Figure 7.5: Reader-Tag-Metal (Metal sample without any defects) output signal which is zoomed in on the top region. It is seen that the effect of the modulation sequence of the RFID tag is no longer visible in the output.

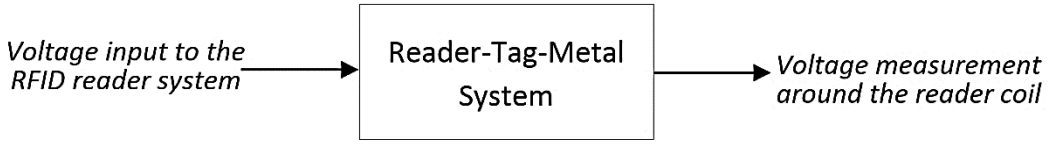

Figure 7.6: Reader-Tag-Metal system approximated as a SISO system.

7.4 Analysis of the Reader-Tag-Metal system using the SI and FRA approach with metal samples of various defects

The analysis of the Reader-Tag-Metal system using System Identification and Frequency Response Analysis was done through linear System Identification and the FRF. The linear model structure that was used is the ARX model structure. This was in reason that a linear ARX model was adequate to explain the system input-output relationship exhibiting good simulation results. The metal samples analysed were of three different kinds of defects, each sample with one kind of defect. The three types of defects being corrosion, crack depth and crack length. Under these three types of defects were samples of different severities of each defect were analysed. Table 7 below shows the damages on each sample used and the corresponding severities of the damage on different samples.

The models identified were set to be of the same maximum dynamic order, where the input-output dynamic orders were set to $n_y = n_u = 20$. This choice was made such this was the respective dynamic order in which all models obtained showed good simulation performance and passed the cross-correlation test between in the input and the residuals which lied between the 95% confidence interval. It should be noted that none of the models passed the auto-correlation test thus the residuals produced from any of the models from all the candidate model orders are not white. This was because of the

effect of the modulation sequence which is embedded on the output was not considered in the modelling process. The Reader-Tag-Metal system was approximated as a SISO system when ideally it should be a Multiple Input Single Output (MISO) system as discussed in the previous section. Although the effect of the modulating sequence cannot be clearly seen on the output signal when a metal sample is placed, Figure 7.5, traces of the modulating sequence will be yet embedded in the Reader-Tag-Metal output. Therefore, since it is not considered in the modelling process, the model output will not contain this feature which is present in the actual system output. Thus, the residuals will contain some traces of the modulation sequence. Consequently, the residuals will not be white noise. The ACF (Auto-Correlation Function) of the residuals will hence contain a periodicity and this approximately matches to the periodicity of the amplitude modulation of the Reader-Tag system in Figure 7.4 – (d). This is illustrated in Fig xx below.

Table 7: Metal samples and the respective defects of each sample used in the analysis

Corrosion metal samples (corrosion measured in months of exposure)	Crack depth samples (depth measured in mm)	Crack length samples (length measured in mm)
0 (No corrosion)	0 (No cracks)	0 (No cracks)
1	2	4
3	5	8
6	7	12
10	9	16
12		20
		24
		28
		32

Frequency features obtained from the FRFs of the identified models were used for comparing the metal samples of the same defect and the progression of the features in relation to the severity of each defect. The magnitude values of the FRFs were used as features, in particular since the input signal is 125 KHz, the FRF magnitudes at this particular frequency was used. This is because of the identified model would only be accurate around this frequency. As mentioned earlier in Section 7.2, six sets of input-output data were collected from each sample thus six different ARX models were identified for each sample. Therefore, six different FRFs and resulting in six FRF magnitude features at 125 KHz. An average value of the respective FRF magnitudes at 125 KHz was then used to compare each sample with the same defect against the different severities to observe the progress of the features. The following subsections will look into the different defects on metal samples that were examined using the LF RFID NDE&T method

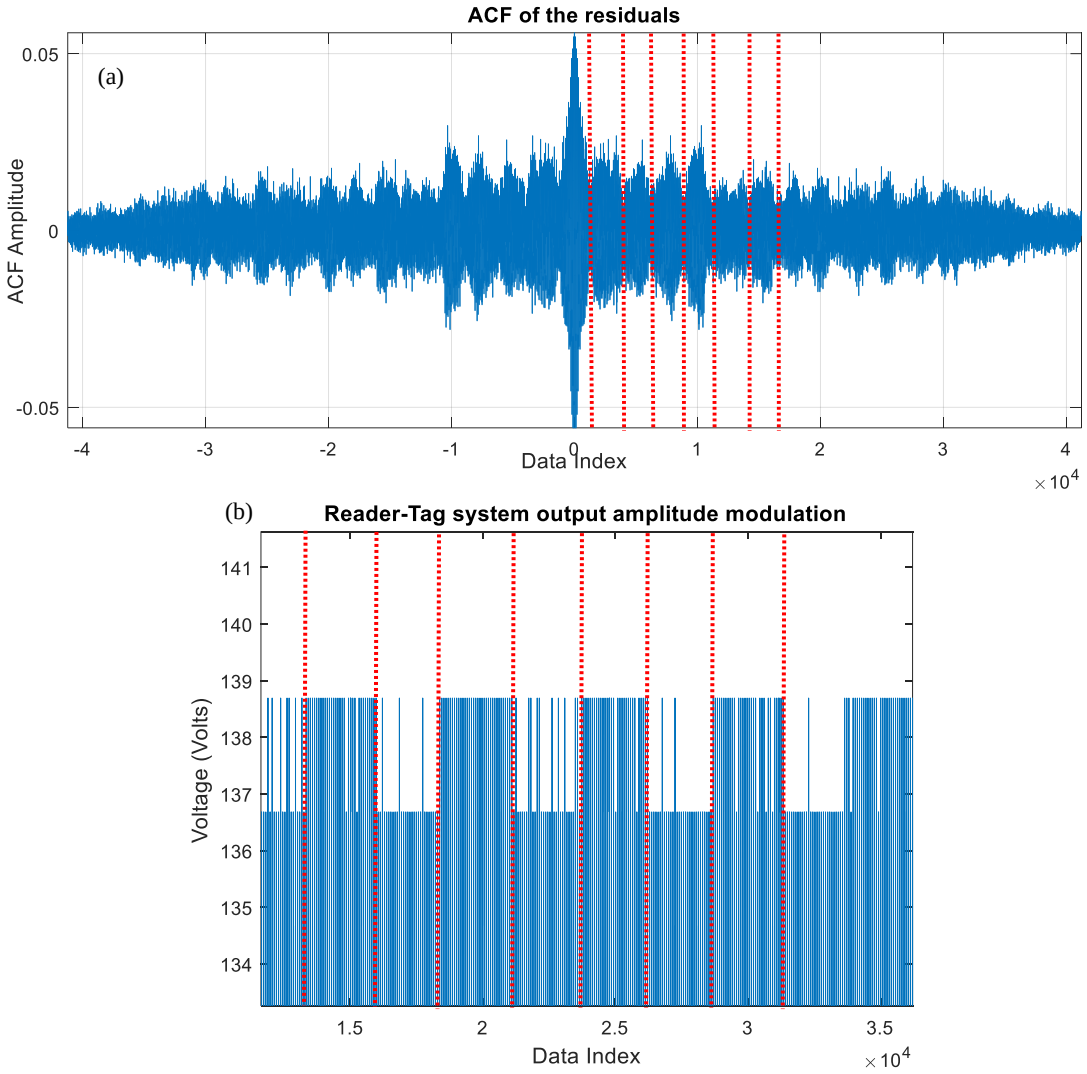

Figure 7.7: Periodicity of the residual ACF and Reader-Tag output amplitude modulation. The periodicity of the ACF of the residual signal (a) is marked with the red dotted lines. The periodicity of the square wave embedded due to the modulating sequence (b) is marked with the red dotted lines. Both periods approximately match.

and the data obtained analysed using a control systems analysis approach via FRF features.

7.4.1 Corrosion characterisation

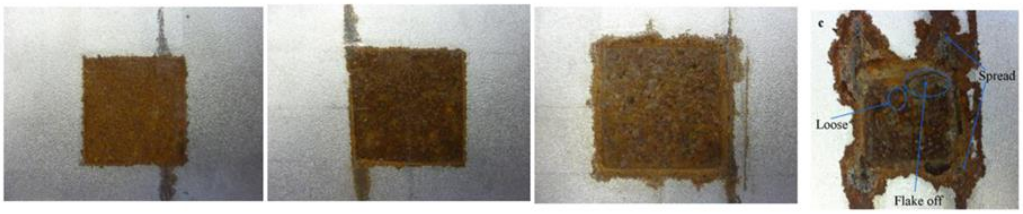

Figure 7.8: Corrosion samples: (a) 1 month, (b) 3 months, (c) 6months and (d) 10 months exposure. 12 months exposure sample is not shown. This image is taken from [33] has these are the same samples used in this research as well.

To investigate the progress of corrosion using LF RFID technology base NDE&T method the SI and FRA method was applied to the input-output data that was collected from six corrosion samples of metal. Each sample having different levels of corrosion.

- Corrosion samples examined: 0 months, 1 month, 3 months, 6 months, 10 months and 12 months.

Figure 7.9 below illustrates how the FRF magnitude features appear when plotted against the number of months each corroded metal sample is exposed to. It can be clearly observed from Figure 7.9 that between each sample there is a clear variation with overlapping of standard deviations of each feature. Essentially an increasing trend can be observed as corrosion increases. This is because of the decrease in conductivity and permeability of the metal in the area of corrosion [33]. As the conductivity and the permeability reduces the inductance of the metal reduces. Because of the magnetic coupling between the metal sample and the RFID tag, the sample acts as a pseudo inductance connected in parallel to the tag antenna coil. Thus, resulting in an overall increase in the inductance of the parallel combination of the tag coil and the metal. Hence the magnetic coupling between the tag and the reader decreases. Thus, increasing the overall Tag-Metal magnetic coupling with the reader coil. It should be noted that these results are comparable and the trend of the features matches to the result of Ali Imam Sunny *et al.* in [33].

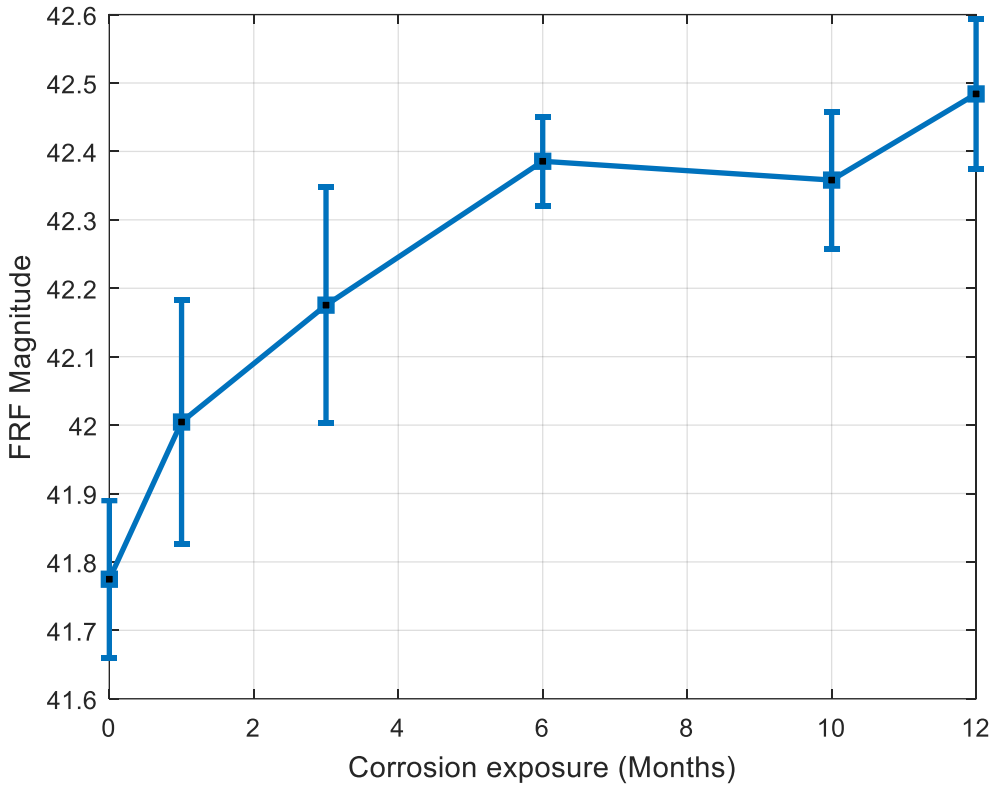

Figure 7.9: Comparison of different averaged FRF magnitude features for corrosion samples against the amount of corrosion the samples were exposed to. An increasing trend is observed in the features as the corrosion progresses. However, large overlaps of features are seen resulting from the standard deviation of each respective feature.

7.4.2 Crack length and crack depth progressions

Analysis of the progression of crack length and crack depth applying the SI-FRA method was done in the exact same manner to the analysis done in corrosion.

Crack length

To simulate the effects of crack length, a long slit was cut into a metal sheet and the crack was incrementally moved into the RFID tag to mimic the progression of a crack, Figure 7.11 illustrates this process. The LF RFID tag was moved in 4mm increments after each reading was taken, hence nine different crack lengths were examined.

- Lengths of cracks examined: 0mm, 4mm, 8mm, 12mm, 16mm, 20mm, 24mm, 28mm and 32mm.

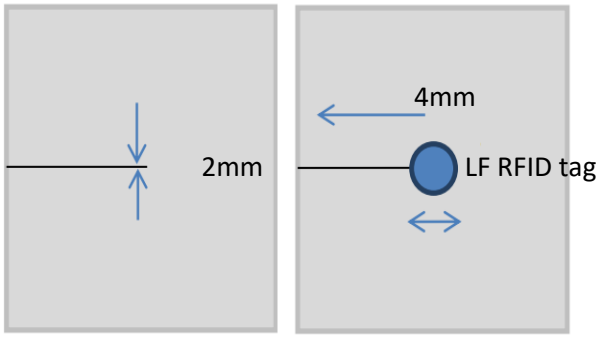

Figure 7.11: Mimicking crack length progression. The RFID tag was moved along the crack in 4mm increments to simulate crack growth

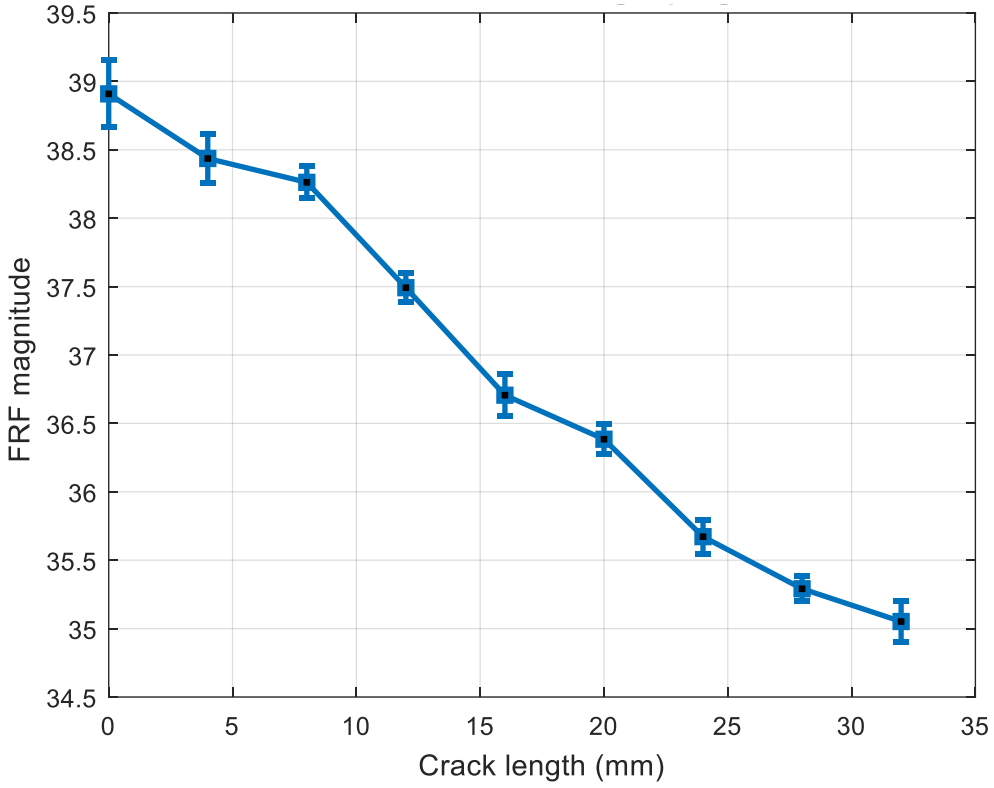

Figure 7.10: Comparison of different FRF magnitude features for crack length samples against the length of the crack. A decreasing monotonic like trend is seen between the FRF features as the crack length progresses. Some overlap between the features are seen.

The variations of the FRF magnitude features according to different crack lengths are illustrated below in Figure 7.10. The features vary approximately in a monotonic manner, therefore the values of the FRF magnitude features are inversely proportional to the length of the crack. It can be argued that as the crack length increases, a relatively larger part of the magnetic field gets trapped within the crack. This is because of the field getting

reflected within the crack walls. Hence reducing the magnetic coupling between the tag antenna coil and the metal sample. Thus, reducing the inductance of the Tag-Metal as a whole, which reduces the magnetic coupling between the Tag-Metal and the reader coil resulting in a lower FRF feature magnitude.

Crack depth

Figure 7.12: Crack depth samples. Slits of different depths cut into the metal is used to mimic the effect of a crack at different depths

The LF RFID tag was placed directly on top of different crack depths in the sample shown in Figure 7.12 to take the readings. Five crack depths were examined.

- The depths of cracks examined: 0mm, 2mm, 5mm, 7mm, 9mm.

The procedures followed to examine and extract FRF features were exactly the same as for crack length samples as well as corrosion samples. Figure 7.13 illustrates the FRF feature variation in various crack depths. An increase in depth decreases the feature value. This is due to part of the magnetic field bouncing off between the crack walls, thus the field gets trapped within the crack. Therefore, the deeper the crack is a larger portion of the field gets trapped within the crack. This will result in a decrease in the magnetic coupling between the reader and Tag-Metal.

Observing the FRF feature variations for both the crack length and crack depth it can be said that, as the overall dimensions of a crack increases, the FRF feature index would decrease, due to the magnetic field being trapped within the crack walls.

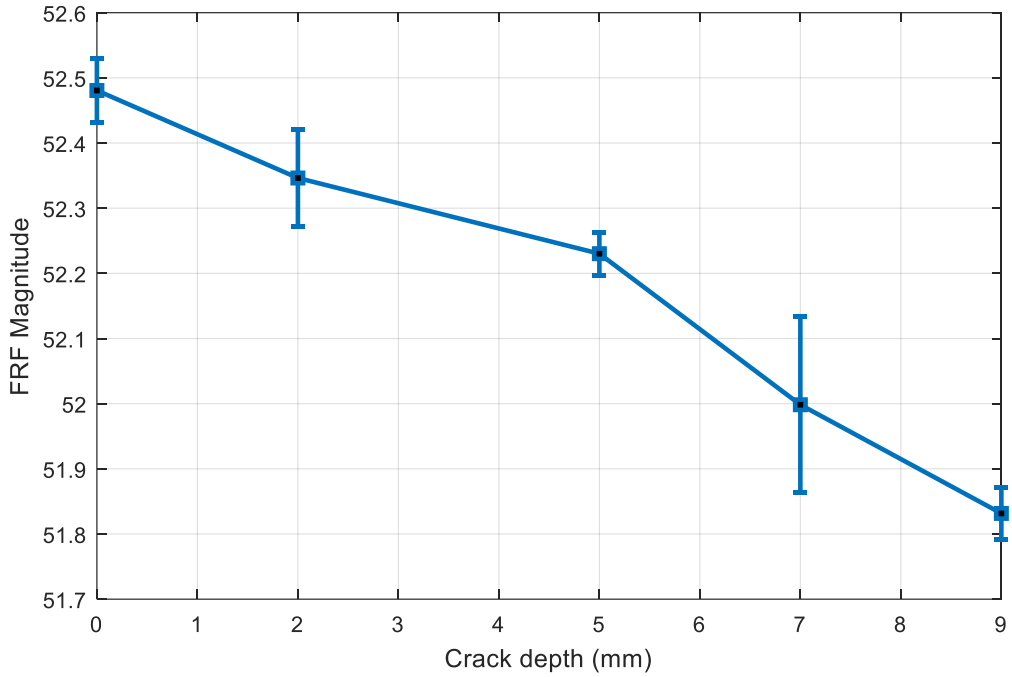

Figure 7.13: Comparison of different FRF magnitude features for crack depth samples against the depth of the crack. A decreasing monotonic like trend is seen between the FRF features as the crack depth progresses. Some overlaps between the features are observed.

From the above inspection of different defects using FRF magnitude based features, there are many overlaps between the features due to the high standard deviations. However, by changing the order of the fixed ARX model structure (note that the model order was fixed for all the models that were extracted) the overlapping of features could be reduced. This is because the parameters of all the models extracted are biased to a certain degree because of not taking into consideration the effect of the modulation sequence. Thus, as observed in Figure 7.7, the ACF of the residuals are not white and is actually periodic in nature. Hence the model parameters are biased. As such a noise model is required to be fitted. Fitting such a noise model would reduce the biasness of the parameters estimated in the model used and may even reduce the standard deviation of the features thus reducing the overlap. It should be emphasised that the SI and FRA method was applied directly to the raw without any pre-processing. Furthermore, the models fitted were extracted using the simple least squares method with input and output lagged terms in the order of $n_y = n_u = 20$. Even using such a simple method, however, resulted in substantial results which attests to the significant potential of using System Identification and Frequency Response Analysis as a CM-FD method. Furthermore, physical interpretations of the results were given to the variation of the FRF features in relation to the defect and the behaviour of the electromagnetic system. This is significant as this demonstrates that the SI and FRA approach to CM-FD can be used to actually

interpret the fault features to the physical characteristics of the fault and the wider system considered. This is because FRA is an analysis method used in control systems analysis to understand the dynamical behaviour of systems in the frequency domain.

7.5 Summary

The chapter presents a novel implementation of a System Identification and frequency response approach to LF RFID technology based wireless eddy current probing method for the non-invasive characterising of defects in metal samples. Even though a simple System Identification method is used, the results presented show the significant potential of the approach. Different levels of exposure to corrosion and crack length and depth progression is characterised in relation to variations in FRF magnitude features as the severity of the defect increases. A clear physical interpretation of the FRF feature variations in relation to each defect type and its corresponding severities were given. This attests to the advantage of using a control systems analysis approach to CM-FD in which physical interpretation of fault features can be made. Further refinement is however needed in order to use this method as a complete SHM tool in practical applications. The internal workings of a LF RFID tag was discussed in detail. It was shown that the complex Reader-tag-metal system can be approximated as a SISO system. The feasibility and the assumptions required were pointed out in a systems perspective. It should be noted that the SI and FRA were conducted on the raw data from the RFID reader and no pre-processing was done on the data. Thus, emphasising that from the results presented, the novel implementation of SI and FRA approach to LF RFID based wireless eddy current probing is an initial step towards a potential new SHM technology.

Chapter 8

Conclusions

8.1 Conclusions and summary

Previous studies on the controls systems analysis approach to CM-FD have been conducted however, the concerns mentioned in considering the System Identification aspect has been overlooked. Furthermore, the numerical inaccuracies of the original least-squares based method of evaluating NOFRFs have not been addressed.

In the present study, the numerical inaccuracy aspect of the LS method has been addressed and a Modified-Least-Squares method is proposed. In the M-LS method, the information matrix for the LS operation at each frequency is constructed according to the contributions made by the respective orders of system nonlinearity to the output response at the corresponding frequency. The effectiveness of the new method was demonstrated under general band limited and harmonic inputs. Because of the accuracy attained by the M-LS method the possibility of local approximation of nonlinear systems in the regions of severe nonlinear behaviour has been demonstrated using NOFRFs. Hence for the first time, the convergence of a Volterra series based method around the regions of severe nonlinear behaviour has been demonstrated. This type of convergence of the Volterra series has only been theoretically argued because of the requirement of a very high order nonlinearities. Because of the multi-dimensional nature of the Volterra series and methods based on it such as the GFRFs, such an achievement was deemed impossible or impractical. However, because of the one-dimensional nature of the Volterra series based NOFRFs and the significant numerical accuracy of the M-LS method to evaluating NOFRFs. The existence of such convergence at regions of severe nonlinear behaviour has been practically demonstrated using the M-LS method of evaluating NOFRFs. This is potentially an initial step for the investigation of severe nonlinear behaviour in the frequency domain leading to the analysis, design and Fault Diagnosis of such nonlinear systems. In consequence to evaluating NOFRFs accurately using the M-LS method, the potential and the ease of use of the NOFRFs in analysis and design of a wider class of nonlinear systems in the frequency domain has been facilitated significantly.

The concerns in regard to System Identification in the controls systems analysis approach to CM-FD has been addressed in the present study. Inadequate inputs that do not persistently excite the system is a major concern. As CM-FD often needs to be carried out without disrupting the normal operations nothing can be done about this. Thus, a CM-FD method needs to able to identify faults even in such scenarios. Furthermore, in the CM-FD approach investigated in the present study observes the dynamic changes of the system induced by fault and off-spec conditions using the Frequency Response Analysis

of the identified model of the system. System Identification is used as a method of capturing the dynamics present within the input-output data. Thus, reconstruction of the system dynamics present within the input-output data from System Identifications methods needs to be attained to a certain degree of accuracy. The iFRO algorithm has been demonstrated to be able to identify the system in the presence of inadequate inputs. Since the simulation error is a more direct manner in which to assess the dynamical correctness of the identified model, an extension to the iFRO algorithm, the S-iFRO is proposed. In the S-iFRO algorithm, the best model from a set of competing models produced in every iteration of the iFRO part is explicitly chosen using only the mean square of the simulation error performance of the models. As such the iFRO algorithm will be directed towards an orthogonalisation path that leads to a dynamically optimum model. However, because of the SEM nature of the S-iFRO algorithm searching large initial term sets requires considerable computational effort. However, using a reduced set of candidate model terms resolves this issue to a certain degree. A method previously proposed for the FRO algorithm in obtaining a reduced set of candidate terms is used for the S-iFRO. Using the S-iFRO the concerns mentioned earlier related to System Identification is mitigated and dynamically optimum models can be obtained.

In the final chapter of this thesis a novel implementation of control systems analysis approach to defect characterisation using LF RFID based wireless eddy current probing is implemented. Several sets of data obtained from each defect sample were used to identify models thus obtaining several FRFs for each sample. The variation of the average FRF magnitudes of each sample along with the standard deviation was compared with respect to each defect sample of the same defect type. Clear physical interpretations were made in relation to the feature variations of the defects as the severity of the defect increases. The SI and FRA analysis was conducted on the raw data without any pre-processing. This novel implementation along with the results presented shows clear potential in the application of SI and FRA approach to LF RFID wireless eddy current probing method as new NDT&E tool for SHM.

8.2 Future work

Potential improvements and limitations to the work undertaken in this thesis are addressed in this section. Several future direction and interests resulting from the work are also discussed.

- **Extension of the M-LS method to the MIMO instance and the NOFRFs analysis using multi-tone inputs**.

  The M-LS method of evaluating NOFRFs currently can only be applied to the case of Single Input Single Output (SISO) systems. Thus, the method needs to be extended into the Multiple Input Multiple Output (MIMO) instance in order to extend to the general application of all types of nonlinear systems. Furthermore, the M-LS method was studied under the harmonic and general band limited instance. However, the new method can also be used with

multi-toned inputs, which as not possible before. In order to achieve this an algorithm that evaluates the possible output frequencies of a nonlinear system under multi-toned inputs need to be used in order to construct the information matrix in the M-LS method appropriately. Such algorithms have been proposed in the literature and can be used with ease. Analysis of nonlinear systems under multi-toned inputs gives significant insight into the various dynamical behaviour of the system. Thus, extending the M-LS method to the analysis under these kinds of inputs will be substantial for the frequency domain analysis of nonlinear systems design and Fault Diagnosis.

- **Development of new convergence criteria for the local approximation of several nonlinear systems.**

  The convergence of the NOFRFs around severe nonlinear systems behaviour draws in new avenues of research into these types of systems. Although it has been shown that these types of systems can now be analysed using Frequency Response Analysis methods, no clear theoretical convergence bounds or criteria have been investigated. Furthermore, only the case of the jump phenomena has been studied. Other severe nonlinear behaviours in which the Volterra series was not able to converge needs to be investigated.

- **Condition Monitoring and Fault Diagnosis of fast sampled systems.**

  The identification methodology proposed suggests downsampling of data in order for the system to be properly identified and avoid numerical issues. However, at times this might not be possible in terms of fast sampled systems. A natural suggestion to this would be to formulate the identification framework using the delta-domain identification technique. The delta domain identification method to NARX model identification has been demonstrated to be accurate even at highly sampled instances. The delta domain formulation of the ARX/NARX models can be easily formulated into a simulation approach in order to be used with the S-iFRO algorithm. Thus, this would further extend the control systems analysis approach to Fault Diagnosis to the instance of fast sampled systems. One such example of fast sampled systems is electronic circuitry in the communications field.

- **Fault tolerant control**

  Fault tolerant control systems aim to optimise control strategies in real-time in order for safe operations under faulty conditions. Incorporating the CM-FD approach into these applications has significant potential. Since the CM-FD methodology is based on the control systems analysis approach, it can be integrated with fault tolerant control applications in a more natural way. The information provided by the identified model and the Frequency Response

Analysis conducted not only can be used for the diagnosing of fault but also to provide dynamic changes that have occurred to appropriately modify the control strategies applied to the system.

- **LF RFID wireless eddy current probing with SI and FRA**

  The initial investigations on the potential of using LF RFID wireless eddy current probing along with SI and FRA show the clear potential of this new technique being used as NDT&E method for SHM. However, the results presented only shows that the technology is applicable. In order for this technique to be used in practical applications, further investigations are required. In practical applications, the RFID data will be subjected to higher levels of noise and other disturbances. Thus, the SI and FRA approach has to be applied such that these considerations are taken into account. It should be noted that the samples used in this investigation were of only one defect per sample. However, in the real-world scenarios, there will be occurrences of more than one defect with different levels of severity in the area under inspection. This would mean more complexities and nonlinearities may start to appear in the RFID data. Thus, the use of NARX models and NOFRFs based analysis. Hence, further investigations with more complex defect samples would be the next step towards developing this technique.

References

[1] V. Venkatasubramanian, R. Rengaswamy, S. N. Kavuri, K. Yin, S. N. Kavuri, and K. Yin, "A review of process fault detection and diagnosis Part III: Process history based methods," *Comput. Chem. Eng.*, vol. 27, no. 3, pp. 327–346, Mar. 2003.

[2] C. W. De Silva, *Vibration and shock handbook*. CRC press, 2005.

[3] V. Palade, C. D. Bocaniala, and L. C. Jain, *Computational Intelligence in Fault Diagnosis*. London: Springer-Verlag, 2006.

[4] E. Sobhani-Tehrani and K. Khorasani, *Fault Diagnosis of nonlinear systems using a hybrid approach*, vol. 383, Boston, MA: Springer US, 2009.

[5] J. Korbicz, J. M. Koscielny, Z. Kowalczuk, and W. Cholewa, *Fault Diagnosis*. Berlin, Heidelberg: Springer Berlin Heidelberg, 2004.

[6] S. X. Ding, *Data-driven Design of Fault Diagnosis and Fault-tolerant Control Systems*. London: Springer London, 2014.

[7] S. X. Ding, *Model-based Fault Diagnosis Techniques*. Berlin, Heidelberg: Springer Berlin Heidelberg, 2008.

[8] S. Simani, C. Fantuzzi, and R. J. Patton, *Model-based Fault Diagnosis in dynamic systems using identification techniques*, vol. 67. London: Springer London, 2003.

[9] S. Tripakis, "A Combined On-Line/Off-Line Framework for Black-Box Fault Diagnosis," in *Runtime Verification. RV 2009. Lecture Notes in Computer Science*, 2009, vol. 5779, pp. 152–167.

[10] S. Simani and R. J. Patton, "Fault Diagnosis of an industrial gas turbine prototype using a System Identification approach," *Control Eng. Pract.*, vol. 16, no. 7, pp. 769–786, Jul. 2008.

[11] L. B. Palma, F. V. Coito, and R. N. Silva, "Fault Diagnosis based on black-box models with application to a liquid-level system," in *EFTA 2003. 2003 IEEE Conference on Emerging Technologies and Factory Automation. Proceedings (Cat. No.03TH8696)*, 2003, vol. 2, no. 1, pp. 739–746.

[12] L. Ljung, "Black-box models from input-output measurements," *IMTC 2001. Proc. 18th IEEE Instrum. Meas. Technol. Conf. Rediscovering Meas. Age Informatics (Cat. No.01CH 37188)*, vol. 1, no. 2, pp. 138–146, 2001.

[13] Z. K. Peng, Z. Q. Lang, and S. A. Billings, "The Nonlinear Output Frequency Response Function and its Application to Fault Detection," in *Fault Detection, Supervision and Safety of Technical Processes 2006*, 2007, vol. 39, no. 13, pp. 36–41.

[14] S. D. Fassois, J. S. Sakellariou, S. D. Fassois, and J. S. Sakellariou, "Time series methods for fault detection and identification in vibrating structures," *Philos. Trans. R. Soc. Math. Phys. Eng. Sci.*, vol. 365, no. 1851, pp. 411–448, Feb. 2007.

[15] R. S. Bayma and Z. Q. Lang, “Fault Diagnosis methodology based on nonlinear system modelling and frequency analysis,” *IFAC Proc. Vol.*, vol. 47, no. 3, pp. 8278–8285, 2014.

[16] X. Xia, J. Zhou, C. Li, and W. Zhu, “A novel method for Fault Diagnosis of hydro generator based on NOFRFs,” *Int. J. Electr. Power Energy Syst.*, vol. 71, pp. 60–67, Oct. 2015.

[17] Z. Q. Lang *et al.*, “Transmissibility of non-linear output Frequency Response Functions with application in detection and location of damage in MDOF structural systems,” *Int. J. Non. Linear. Mech.*, vol. 46, no. 6, pp. 841–853, 2011.

[18] R. Yusof and U. Teknologi, “Fault Diagnosis Based on the NARX Model in the Frequency Domain for Rotary Machine,” *Int. J. Innov. Manag. Inf. Prod.*, vol. 2, no. July, pp. 71–77, 2016.

[19] Z. K. Peng, Z. Q. Lang, C. Wolters, S. A. Billings, and K. Worden, “Feasibility study of structural damage detection using NARMAX modelling and Nonlinear Output Frequency Response Function based analysis,” *Mech. Syst. Signal Process.*, vol. 25, no. 3, pp. 1045–1061, Apr. 2011.

[20] R. Isermann, *Fault-diagnosis systems: An introduction from fault detection to fault tolerance*. Springer-Verlag Berlin Heidelberg, 2006.

[21] J. Chen and R. J. Patton, *Robust Model-Based Fault Diagnosis for Dynamic Systems*, vol. 3, no. 1. Boston, MA: Springer US, 1999.

[22] V. Venkatasubramanian, R. Rengaswamy, K. Yin, and S. N. Kavuri, “A review of process fault detection and diagnosis Part I: Quantitative model-based methods,” *Comput. Chem. Eng.*, vol. 27, no. 3, pp. 293–311, Mar. 2003.

[23] V. Venkatasubramanian, R. Rengaswamy, and S. N. Kavuri, “A review of process fault detection and diagnosis part II: Qualitative models and search strategies,” *Comput. Chem. Eng.*, vol. 27, no. 3, pp. 313–326, Mar. 2003.

[24] S. A. Billings, *Nonlinear System Identification: NARMAX methods in the time, frequency, and spatio-temporal domains*, vol. 13, no. 4. Chichester, UK: John Wiley & Sons, Ltd, 2013.

[25] R. Isermann, *Fault-Diagnosis Applications*, vol. 1. Berlin, Heidelberg: Springer Berlin Heidelberg, 2011.

[26] L. A. Aguirre and S. A. Billings, “Discrete Reconstruction of Strange Attractors of Chua’S Circuit,” *Int. J. Bifurc. Chaos*, vol. 04, no. 04, pp. 853–864, Aug. 1994.

[27] L. A. Aguirre and S. A. Billings, “Dynamical effects of over parametrization in nonlinear models.,” *Phys. D*, vol. 80, pp. 26–40, 1995.

[28] S. A. Billings and L. A. Aguirre, “Effects of the sampling time on the dynamics and identification of nonlinear models,” *Int. J. Bifurc. Chaos*, vol. 05, no. 06, pp. 1541–1556, Dec. 1995.

[29] Z. Q. Lang and S. A. Billings, “Energy transfer properties of non-linear systems in the frequency domain,” *Int. J. Control*, vol. 78, no. 5, pp. 345–362, 2005.

[30] H. Zhang, Z. Q. Lang, and Y. P. Zhu, “A comparative study on the evaluation of Nonlinear Output Frequency Response Functions (NOFRFs) of nonlinear systems,” in *2016 22nd International Conference on Automation and Computing (ICAC)*, 2016, pp. 323–328.

[31] L. M. Li and S. A. Billings, “Analysis of nonlinear oscillators using Volterra series in the frequency domain,” *J. Sound Vib.*, vol. 330, no. 2, pp. 337–355, Jan. 2011.

[32] M. Alamin, G. Y. Tian, A. Andrews, and P. Jackson, “Corrosion detection using low-frequency RFID technology,” *Insight Non-Destructive Test. Cond. Monit.*, vol. 54, no. 2, pp. 72–75, Feb. 2012.

[33] A. I. Sunny, G. Y. Tian, J. Zhang, and M. Pal, “Low frequency (LF) RFID sensors and selective transient feature extraction for corrosion characterisation,” *Sensors Actuators, A Phys.*, vol. 241, pp. 34–43, 2016.

[34] C. W. De Silva, A. Borbely, J. F. Kreider, A. Bejan, J. S. Cundiff, and L. R. Davis, *Vibration Monitoring, Testing, and Instrumentation*. CRC Press. 2007.

[35] K. Finkenzeller, *RFID Handbook*. Chichester, UK: John Wiley & Sons, Ltd, 2010.

[36] R. Isermann, “Model-based fault-detection and diagnosis - Status and applications,” *Annu. Rev. Control*, vol. 29, no. 1, pp. 71–85, Jan. 2005.

[37] M. Nyberg, “Criterions for detectability and strong detectability of faults in linear systems,” *Int. J. Control*, vol. 75, no. 7, pp. 490–501, Jan. 2002.

[38] L. Jain and X. Wu, *Advanced Information and Knowledge Processing*. Springer, London. 2005.

[39] X. Zhang, T. Parisini, and M. M. Polycarpou, “Adaptive fault-tolerant control of nonlinear uncertain systems: An information-based diagnostic approach,” *IEEE Trans. Automat. Contr.*, vol. 49, no. 8, pp. 1259–1274, 2004.

[40] B. Mnassri, E. M. El Adel, and M. Ouladsine, “Generalization and analysis of sufficient conditions for PCA-based fault detectability and isolability,” *Annu. Rev. Control*, vol. 37, no. 1, pp. 154–162, Apr. 2013.

[41] R. Martinez-Guerra and J. L. Mata-Machuca, *Fault Detection and Diagnosis in Nonlinear Systems*. Cham: Springer International Publishing, 2014.

[42] S. Yin, S. X. Ding, X. Xie, S. Member, and H. Luo, “A Review on Basic Data-Driven Approaches for Industrial Process Monitoring,” vol. 61, no. 11, pp. 6418–6428, 2014.

[43] R. J. Patton, P. M. Frank, and R. N. Clark, *Issues of Fault Diagnosis for Dynamic Systems*, vol. 1. London: Springer London, 2000.

[44] L. H. Chiang, E. L. Russell, R. D. Braatz, and E. L. Russell, *Fault Detection and Diagnosis in Industrial Systems*, vol. 3, no. 2. London: Springer London, 2001.

[45] C. Fantuzzi and S. Simani, *Parametric Identification for Robust Fault Detection*, vol. 35, no. 1. IFAC, 2002.

[46] S. J. Qin, “Survey on data-driven industrial process monitoring and diagnosis,” *Annu. Rev. Control*, vol. 36, no. 2, pp. 220–234, 2012.

[47] H. Ferdowsi, “Model based Fault Diagnosis and prognosis of nonlinear systems,” 2013.

[48] H. Ferdowsi and S. Jagannathan, “A unified model-based Fault Diagnosis scheme for nonlinear discrete-time systems with additive and multiplicative faults,” *Proc. IEEE Conf. Decis. Control*, pp. 1570–1575, 2011.

[49] S. X. Ding, P. Zhang, A. Naik, E. L. Ding, and B. Huang, “Subspace method aided data-driven design of fault detection and isolation systems,” *J. Process Control*, vol. 19, no. 9, pp. 1496–1510, 2009.

[50] M. Schwabacher, “A Survey of Data-Driven Prognostics,” in *Infotech@Aerospace*, 2005, no. September, pp. 1–5.

[51] R. Ghimire *et al.*, “Integrated model-based and data-driven fault detection and diagnosis approach for an automotive electric power steering system,” in *AUTOTESTCON (Proceedings)*, 2011, vol. 1001445, pp. 70–77.

[52] Aishe Shui, Weimin Chen, Peng Zhang, Shunren Hu, and Xiaowei Huang, “Review of Fault Diagnosis in control systems,” *2009 Chinese Control Decis. Conf.*, pp. 5324–5329, 2009.

[53] P. M. Frank, “Fault Diagnosis in dynamic systems using analytical and knowledge-based redundancy. A survey and some new results,” *Automatica*, vol. 26, no. 3, pp. 459–474, 1990.

[54] S. Simani and C. Fantuzzi, “Dynamic System Identification and model-based Fault Diagnosis of an industrial gas turbine prototype,” *Mechatronics*, vol. 16, no. 6, pp. 341–363, Jul. 2006.

[55] S. Simani, “Identification and Fault Diagnosis of a Simulated Model of an Industrial Gas Turbine,” *IEEE Trans. Ind. Informatics*, vol. 1, no. 3, pp. 202–216, Aug. 2005.

[56] D. G. Dimogianopoulos, J. D. Hios, and S. D. Fassois, “FDI for aircraft systems using stochastic pooled-NARMAX representations: Design and assessment,” *IEEE Trans. Control Syst. Technol.*, vol. 17, no. 6, pp. 1385–1397, 2009.

[57] M. Yang and V. Makis, “ARX model-based gearbox fault detection and localization under varying load conditions,” *J. Sound Vib.*, vol. 329, no. 24, pp. 5209–5221, 2010.

[58] L. Yin and L. Guo, “Fault detection for NARMAX stochastic systems using entropy optimization principle,” *2009 Chinese Control Decis. Conf. CCDC 2009*, pp. 859–864, 2009.

[59] B. Abichou, D. Flórez, M. Sayed-mouchaweh, H. Toubakh, B. François, and N. Girard, “Fault Diagnosis Methods for Wind Turbines Health Monitoring : a Review,” *19th Int. Conf. Electr. Mach. ICEM 2010*, pp. 1–8, 2013.

[60] D. Bernal, D. Zonta, and M. Pozzi, “ARX residuals in damage detection,” *Struct. Control Heal. Monit.*, vol. 19, no. 4, pp. 535–547, Jun. 2012.

[61] S. X. Ding, “Data-driven design of monitoring and diagnosis systems for dynamic processes: A review of subspace technique based schemes and some recent results,” *J. Process Control*, vol. 24, no. 2, pp. 431–449, 2014.

[62] S. Yin, G. Wang, and H. R. Karimi, “Data-driven design of robust fault detection system for wind turbines,” *Mechatronics*, vol. 24, no. 4, pp. 298–306, 2014.

[63] S. Lu and B. Huang, *Fault Detection, Supervision and Safety of Technical Processes 2006*, 1st ed., vol. 1. IFAC, Elsevier, 2007.

[64] G. Bloch, M. Ouladsine, and P. Thomas, “On-line Fault Diagnosis of dynamic systems via robust parameter estimation,” *Control Eng. Pract.*, vol. 3, no. 12, pp. 1709–1717, Dec. 1995.

[65] G. C. Luh and W. C. Cheng, “Identification of immune models for fault detection,” *Proc. Inst. Mech. Eng. Part I J. Syst. Control Eng.*, vol. 218, no. 5, pp. 353–367, 2004.

[66] Z. Q. Lang, A. Agurto, G. Y. Tian, and A. Sophian, “A System Identification based approach for pulsed eddy current non-destructive evaluation,” *Meas. Sci. Technol.*, vol. 2083, no. April 2016, pp. 2083–2091, Jul. 2007.

[67] D. L. J. Kauffman, *Systems One : An Introduction to Systems Thinking*. Pegasus Communications, 1980.

[68] K. J. Keesman, *System Identification*. London: Springer London, 2011.

[69] C. Q. G. Munoz, R. R. D. Gonzalez-Carrato, J. R. T. Arenas, and F. P. G. Marquez, “A Novel Approach to Fault Detection and Diagnosis on Wind Turbines,” *Glob. Nest J.*, vol. 16, no. 6, pp. 1029–1037, 2014.

[70] V. Krishnaswami, G. Luh, and G. Rizzoni, “Nonlinear parity equation based residual generation for diagnosis of automotive engine faults,” *Control Eng. Pract.*, vol. 3, no. 10, pp. 1385–1392, Oct. 1995.

[71] G. E. P. Box, G. M. Jenkins, G. C. Reinsel, and G. M. Ljung, *Time series analysis: forecasting and control*, 5th ed. Hoboken, New Jersey: John Wiley & Sons, Inc, 2015.

[72] L. Ljung, *System Identification: Theory for the User*, 2nd ed. Prentice Hall, 1997.

[73] C. Ho, Z. Q. Lang, and S. A. Billings, “A frequency domain analysis of the effects of nonlinear damping on the Duffing equation,” *Mech. Syst. Signal Process.*, vol. 45, no. 1, pp. 49–67, 2014.

[74] W. R. Jacobs *et al.*, “Control-focused, nonlinear and time-varying modelling of dielectric elastomer actuators with Frequency Response Analysis,” *Smart Mater. Struct.*, vol. 24, no. 5, p. 055002, May 2015.

[75] R. C. Dorf and R. H. Bishop, *Modern Control Systems*, 12th ed. Upper Saddle River, New Jersey: Pearson Education, Inc, 2011.

[76] J. J. E. Slotine and W. Li, *Applied Nonlinear Control*, 1st ed., vol. 199, no. 1. Englewood Cliffs, NJ: Prentice Hall, 1991.

[77] I. D. Landau and Z. Gianluca, *Digital control systems: design, identification and implementation*. Springer Science & Business Media, 2005.

[78] R. K. Pearson, “Selecting nonlinear model structures for computer control,” *J. Process Control*, vol. 13, no. 1, pp. 1–26, Feb. 2003.

[79] M. Farina and L. Piroddi, “Approximate SEM identification of polynomial input-output models,” in *Proceedings of the 2010 American Control Conference*, 2010, pp. 7040–7045.

[80] L. A. Aguirre, B. H. G. Barbosa, and A. P. Braga, “Prediction and simulation errors in parameter estimation for nonlinear systems,” *Mech. Syst. Signal Process.*, vol. 24, no. 8, pp. 2855–2867, Nov. 2010.

[81] W. J. Rugh, *Nonlinear system theory The Volterra/Wiener Approach*, vol. 1981. Johns Hopkins University Press, 1981.

[82] P. J. Fleming and R. C. Purshouse, “Evolutionary algorithms in control systems engineering: A survey,” *Control Eng. Pract.*, vol. 10, no. 11, pp. 1223–1241, 2002.

[83] Y. Guo, L. Z. Guo, S. A. Billings, and H. L. Wei, “An iterative orthogonal forward regression algorithm,” *Int. J. Syst. Sci.*, vol. 46, no. 5, pp. 776–789, Apr. 2015.

[84] M. Farina and L. Piroddi, “An iterative algorithm for simulation error based identification of polynomial input–output models using multi-step prediction,” *Int. J. Control*, vol. 83, no. 7, pp. 1442–1456, Jul. 2010.

[85] K. Li, J. X. Peng, and G. W. Irwin, “A fast nonlinear model identification method,” *IEEE Trans. Automat. Contr.*, vol. 50, no. 8, pp. 1211–1216, Aug. 2005.

[86] S. A. Billings and K. Z. Mao, “Model Identification and Assessment based on Model Predicted Output,” 1998.

[87] K. Rodríguez-Vázquez, and P. J. Fleming, “Multi-objective genetic programming for nonlinear System Identification,” *Electron. Lett.*, vol. 34, no. 9, p. 930, 1998.

[88] J. Sjöberg *et al.*, “Nonlinear black-box modeling in System Identification: a unified overview,” *Automatica*, vol. 31, no. 12, pp. 1691–1724, Dec. 1995.

[89] O. Nelles, *Nonlinear System Identification*. Berlin, Heidelberg: Springer Berlin Heidelberg, 2001.

[90] I. J. Leontaritis and S. A. Billings, “Input-output parametric models for non-linear systems Part I: deterministic non-linear systems,” *Int. J. Control*, vol. 41, no. 2, pp. 303–328, Feb. 1985.

[91] G. Zito and I. D. Landau, “Narmax model identification of a variable geometry turbocharged diesel engine,” in *Proceedings of the 2005, American Control Conference, 2005.*, 2005, pp. 1021–1026.

[92] B. A. Foss and T. A. Johansen, “Parallel nonlinear decoupling for process control — A NARMAX approach,” *Annu. Rev. Autom. Program.*, vol. 17, pp. 49–54, 1992.

[93] S. K. Pradhan and B. Subudhi, “NARMAX modeling of a two-link flexible robot,” *Proc. - 2011 Annu. IEEE India Conf. Eng. Sustain. Solut. INDICON-2011*, no. 3, pp. 1–5, 2011.

[94] S. L. Kukreja, H. L. Galiana, and R. E. Kearney, “NARMAX representation and identification of ankle dynamics,” *IEEE Trans. Biomed. Eng.*, vol. 50, no. 1, pp. 70–81, 2003.

[95] F. He, H. L. Wei, and S. A. Billings, “Identification and frequency domain analysis of non-stationary and nonlinear systems using time-varying NARMAX models,” *Int. J. Syst. Sci.*, vol. 46, no. 11, pp. 2087–2100, 2013.

[96] J. S. H. Tsai, W. T. Hsu, L. G. Lin, S. M. Guo, and J. W. Tann, “A modified NARMAX model-based self-tuner with fault tolerance for unknown nonlinear stochastic hybrid systems with an input–output direct feed-through term,” *ISA Trans.*, vol. 53, no. 1, pp. 56–75, Jan. 2014.

[97] N. Chiras, C. Evans, and D. Rees, “Global Nonlinear Modeling of Gas Turbine Dynamics Using NARMAX Structures,” *J. Eng. Gas Turbines Power*, vol. 124, no. 4, pp. 817–826, 2002.

[98] O. M. Boaghe, S. A. Billings, L. M. Li, P. J. Fleming, and J. Liu, “Time and frequency domain identification and analysis of a gas turbine engine,” *Control Eng. Pract.*, vol. 10, no. 12, pp. 1347–1356, 2002.

[99] S. Chen and S. A. Billings, “Representations of non-linear systems: the NARMAX model,” *Int. J. Control*, vol. 49, no. 3, pp. 1013–1032, Mar. 1989.

[100] L. Ljung, “Recursive identification algorithms,” *Circuits, Syst. Signal Process.*, vol. 21, no. 1, pp. 57–68, Jan. 2002.

[101] L. Ljung, “Theory and Practice of Recursive Identification.pdf,” *Cambridge, MA MIT Press*, vol. 21, no. 4, pp. 499–501, 1983.

[102] P. C. Young, *Recursive Estimation and Time-Series Analysis*, vol. 28, no. 3. Berlin, Heidelberg: Springer Berlin Heidelberg, 2011.

[103] T. Baldacchino, S. R. Anderson, and V. Kadirkamanathan, “Computational System Identification for Bayesian NARMAX modelling,” *Automatica*, vol. 49, no. 9, pp. 2641–2651, 2013.

[104] K. Rodriguez-Vazquez, and P. J. Fleming “A genetic programming/NARMAX approach to nonlinear System Identification,” in *Second International Conference on Genetic Algorithms in Engineering Systems*, 1997, vol. 1997, no. 446, pp. 409–414.

[105] S. A. Billings, S. Chen, and M. J. Korenberg, “Identification of MIMO non-linear systems using a forward-regression orthogonal estimator,” *Int. J. Control*, vol. 49, no. 6, pp. 2157–2189, Jun. 1989.

[106] L. Piroddi and W. Spinelli, “An identification algorithm for polynomial NARX models based on simulation error minimization,” *Int. J. Control*, vol. 76, no. 17, pp. 1767–1781, Nov. 2003.

[107] S. A. Billings and W. S. F. Voon, “A prediction-error and stepwise-regression estimation algorithm for non-linear systems,” *Int. J. Control*, vol. 44, no. 3, pp. 803–822, Sep. 1986.

[108] M. Korenberg, S. A. Billings, Y. P. Liu, and P. J. McIlroy, “Orthogonal parameter estimation algorithm for non-linear stochastic systems,” *Int. J. Control*, vol. 48, no. 1, pp. 193–210, Jul. 1988.

[109] S. Chen, S. A. Billings, and W. Luo, “Orthogonal least squares methods and their application to non-linear System Identification,” *Int. J. Control*, vol. 50, no. 5, pp. 1873–1896, 1989.

[110] S. A. Billings, M. J. Korenberg, and S. Chen, “Identification of non-linear output-affine systems using an orthogonal least-squares algorithm,” Sheffield, Jan. 1987.

[111] L. Piroddi, “Simulation error minimisation methods for NARX model identification,” *Int. J. Model. Identif. Control*, vol. 3, no. 4, p. 392, 2008.

[112] X. Hong, R. J. Mitchell, S. Chen, C. J. Harris, K. Li, and G. W. Irwin, “Model selection approaches for non-linear System Identification: a review,” *Int. J. Syst. Sci.*, vol. 39, no. 10, pp. 925–946, Oct. 2008.

[113] A. V. Oppenheim, R. W. Schafer, and J. R. Buck, *Discrete-time Signal Processing*, 2nd ed. Prentice Hall, 1999.

[114] Z. K. Peng, Z. Q. Lang, and S. A. Billings, “Resonances and resonant frequencies for a class of nonlinear systems,” *J. Sound Vib.*, vol. 300, no. 3–5, pp. 993–1014, Mar. 2007.

[115] E. J. Powers, “Application of Higher Order Spectral Analysis to Cubically Nonlinear System Identification,” *IEEE Trans. Signal Process.*, vol. 42, no. 7, pp. 1746–1765, 1994.

[116] Z. Q. Lang and S. A. Billings, “Output frequencies of nonlinear systems,” *Int. J. Control*, vol. 67, no. 5, pp. 713–730, Jan. 1997.

[117] Z. Q. Lang and S. A. Billings, “Output frequency characteristics of nonlinear systems,” *Int. J. Control*, vol. 64, no. 6, pp. 1049–1067, Aug. 1996.

[118] X. Xia, W. Ni, and Y. Sang, “A novel analysis method for Fault Diagnosis of hydro-turbine governing system,” *Proc. Inst. Mech. Eng. Part O J. Risk Reliab.*, vol. 231, no. 2, pp. 164–171, Apr. 2017.

[119] Z. K. Peng, Z. Q. Lang, and S. A. Billings, “Crack detection using nonlinear output Frequency Response Functions,” *J. Sound Vib.*, vol. 301, no. 3–5, pp. 777–788, Apr. 2007.

[120] D. A. George, “Continuous nonlinear systems,” CAMBRIDGE, MASSACHUSETTS, 1959.

[121] J. C. Peyton Jones and S. A. Billings, “Interpretation of non-linear Frequency Response Functions,” *Int. J. Control*, vol. 52, no. 2, pp. 319–346, Aug. 1990.

[122] Z. K. Peng, Z. Q. Lang, S. A. Billings, and Y. Lu, “Analysis of bilinear oscillators under harmonic loading using nonlinear output Frequency Response Functions,” *Int. J. Mech. Sci.*, vol. 49, no. 11, pp. 1213–1225, 2007.

[123] M. Y. Chen, J. Q. Zhai, Z. Q. Lang, F. Sun, and G. Hu, “A nonlinear frequency analysis based approach for power cable insulation fault detection,” *COMPEL - Int. J. Comput. Math. Electr. Electron. Eng.*, vol. 31, no. 2, pp. 369–386, Mar. 2012.

[124] H. Huang *et al.*, "Study of cumulative fatigue damage detection for used parts with nonlinear output Frequency Response Functions based on NARMAX modelling," *J. Sound Vib.*, vol. 411, pp. 75–87, Dec. 2017.

[125] J. Cao, L. Chen, J. Zhang, and W. Cao, "Fault Diagnosis of complex system based on nonlinear frequency spectrum fusion," *Measurement*, vol. 46, no. 1, pp. 125–131, 2013.

[126] T. Volterra, W. Approach, and W. J. Rugh, "Nonlinear System Theory by Volterra," vol. 1981, 2002.

[127] C. M. Cheng, Z. K. Peng, W. M. Zhang, and G. Meng, "Volterra-series-based nonlinear system modeling and its engineering applications: A state-of-the-art review," *Mech. Syst. Signal Process.*, vol. 87, no. November 2016, pp. 340–364, 2017.

[128] A. Novak, "Identification of Nonlinear Systems: Volterra Series Simplification," *Acta Polytech. J. Adv. Eng.*, vol. 47, no. 4–5, 2007.

[129] J. M. T. Thompson, M. Thompson, and H. B. Stewart, *Nonlinear Dynamics and Chaos*, 2nd ed. John Wiley & Sons, 2002.

[130] L. M. Li, S. A. Billings, "Discrete time subharmonic modelling and analysis," *Int. J. Control*, vol. 78, no. 16, pp. 1265–1284, Nov. 2005.

[131] Z. Xiao, X. Jing, and L. Cheng, "Parameterized convergence bounds for volterra series expansion of NARX models," *IEEE Trans. Signal Process.*, vol. 61, no. 20, pp. 5026–5038, Oct. 2013.

[132] A. Chatterjee and N. S. Vyas, "Convergence analysis of volterra series response of nonlinear systems subjected to harmonic excitation," *J. Sound Vib.*, vol. 236, no. 2, pp. 339–358, Sep. 2000.

[133] F. Thouverez, "A new convergence criteria of Volterra series for harmonic inputs," in *Proceedings of the 16th International Modal Analysis Conference*, 1998, vol. 1, pp. 723–727.

[134] G. R. Tomlinson, G. Manson, and G. M. Lee, "A simple criterion for establishing an upper limit to the harmonic excitation level of the duffing oscillator using the volterra series," *J. Sound Vib.*, vol. 190, no. 5, pp. 751–762, Mar. 1996.

[135] Z. K. Peng and Z. Q. Lang, "On the convergence of the Volterra-series representation of the Duffing's oscillators subjected to harmonic excitations," *J. Sound Vib.*, vol. 305, no. 1–2, pp. 322–332, Aug. 2007.

[136] I. Kovacic and M. J. Brennan, *The Duffing equation: Nonlinear oscillators and their behaviour*. John Wiley & Sons, Ltd, 2011.

[137] S. A. Billings and O. M. Boaghe, "The Response Spectrum Map, A Frequency Domain Equivalent To The Bifurcation Diagram," *Int. J. Bifurc. Chaos*, vol. 11, no. 07, pp. 1961–1975, Jul. 2001.

[138] Z. K. Peng, Z. Q. Lang, S. A. Billings, and G. R. Tomlinson, "Comparisons between harmonic balance and nonlinear output Frequency Response Function in nonlinear system analysis," *J. Sound Vib.*, vol. 311, no. 1–2, pp. 56–73, Mar. 2008.

[139] L. A. Aguirre, “Some Remarks On Structure Selection For Nonlinear Models,” *Int. J. Bifurc. Chaos*, vol. 04, no. 06, pp. 1707–1714, Dec. 1994.

[140] L. A. Aguirre, “A nonlinear correlation function for selecting the delay time in dynamical reconstructions,” *Phys. Lett. A*, vol. 203, no. 2–3, pp. 88–94, Jul. 1995.

[141] J. Escobar and M. Enqvist, “On the Detection of Nonlinearities in Sampled Data,” in *IFAC Proceedings Volumes*, 2012, vol. 45, no. 16, pp. 1587–1592.

[142] T. Buzug and G. Pfister, “Comparison of algorithms calculating optimal embedding parameters for delay time coordinates,” *Phys. D Nonlinear Phenom.*, vol. 58, no. 1–4, pp. 127–137, Sep. 1992.

[143] K. Worden, P. K. Stansby, G. R. Tomlinson, and S. A. Billings, “Identification of nonlinear wave forces,” *J.\ Fluids Struct.*, vol. 8, no. 1, pp. 19–71, Jan. 1994.

[144] M. T. Rosenstein, J. J. Collins, and C. J. De Luca, “Reconstruction expansion as a geometry-based framework for choosing proper delay times,” *Phys. D Nonlinear Phenom.*, vol. 73, no. 1–2, pp. 82–98, May 1994.

[145] H. D. I. Abarbanel, R. Brown, and J. B. Kadtke, “Prediction in chaotic nonlinear systems: Methods for time series with broadband Fourier spectra,” *Phys. Rev. A*, vol. 41, no. 4, pp. 1782–1807, Feb. 1990.

[146] E. M. A. M. Mendes and S. A. Billings, “On Overparametrization of Nonlinear Discrete Systems,” *Int. J. Bifurc. Chaos*, vol. 08, no. 03, pp. 535–556, Mar. 1998.

[147] E. M. A. M. Mendez and S. A. Billings, “An alternative solution to the model structure selection problem,” *IEEE Trans. Syst. Man, Cybern. - Part A Syst. Humans*, vol. 31, no. 6, pp. 597–608, 2001.

[148] H. L. Wei, S. A. Billings, and J. Liu, “Term and variable selection for non-linear System Identification,” *Int. J. Control*, vol. 77, no. 1, pp. 86–110, Jan. 2004.

[149] M. Bonin, V. Seghezza, and L. Piroddi, “NARX model selection based on simulation error minimisation and LASSO,” *IET Control Theory Appl.*, vol. 4, no. 7, pp. 1157–1168, 2010.

[150] W. Spinelli, L. Piroddi, and M. Lovera, “A two-stage algorithm for structure identification of polynomial NARX models,” in *2006 American Control Conference*, 2006, p. 6 pp.

[151] M. Bonin, V. Seghezza, and L. Piroddi, “LASSO-enhanced simulation error minimization method for NARX model selection,” *Proc. 2010 Am. Control Conf.*, pp. 4522–4527, Jun. 2010.

[152] P. Connally, K. Li, and G. W. Irwin, “Prediction and simulation-error based perceptron training: Solution space analysis and a novel combined training scheme,” *Neurocomputing*, vol. 70, no. 4–6, pp. 819–827, Jan. 2007.

[153] M. Farina and L. Piroddi, “Some convergence properties of multi-step prediction error identification criteria,” in *2008 47th IEEE Conference on Decision and Control*, 2008, pp. 756–761.

[154] M. Farina and L. Piroddi, “Simulation error minimization identification based on multi-stage prediction,” *Int. J. Adapt. Control Signal Process.*, vol. 25, no. 5, pp. 389–406, May 2011.

[155] T. Söderström and P. Stoica, “Some properties of the output error method,” *Automatica*, vol. 18, no. 1, pp. 93–99, Jan. 1982.